HYGRO-THERMO-MECHANICAL BENDING BEHAVIOR OF ADVANCED FUNCTIONALLY GRADED CERAMIC METAL PLATES RESTING ON VISCOELASTIC FOUNDATIONS

BY

ISMAIL MOHAMMED MUDHAFFAR

A Thesis Presented to the

DEANSHIP OF GRADUATE STUDIES

KING FAHD UNIVERSITY OF PETROLEUM & MINERALS

DHAHRAN, SAUDI ARABIA

In Partial Fufillment of the
Requirements for the Degree of

MASTER OF SCIENCE

In

CIVIL & ENVIRONMENTAL ENGINEERING

April 2021

KING FAHD UNIVERSITY OF PETROLEUM & MINERALS

DHAHRAN- 31261, SAUDI ARABIA

DEANSHIP OF GRADUATE STUDIES

This thesis, written by **Ismail Mohammed Mudhaffar** under the direction of his thesis advisor and approved by his thesis committee, has been presented and accepted by the Dean of Graduate Studies, in partial fulfillment of the requirements for the degree of **MASTER OF SCIENCE IN CIVIL AND ENVIRONMENTAL ENGINEERING.**

Dr. Mohammed A. Al-Osta
(Advisor)

Dr. Salah U. Al-Dulaijan
Department Chairman

Chair. Prof. Abdelouahed Tounsi
(Member)

Prof. Suliman Saleh Al-Homidan
Dean of Graduate Studies

Dr. Mesfer Al-Zahrani
(Member)

Date: April 2021

عمادة الدراسات العليا
DEANSHIP OF GRADUATE STUDIES

This work is dedicated to my beloved family.

ACKNOWLEDGMENT

I am grateful to Almighty Allah for providing me the knowledge, time, and health to successfully conduct this work. My gratitude is expressed to King Fahd University of Petroleum and Minerals (KFUPM) for offering me the precious scholarship opportunity in an environment of motivation and support. Thanks are expressed to the Civil and Environmental Engineering department in which I did my undergraduate and graduate studies. Thanks to all the instructors and staff.

I would like to convey my deepest gratitude to my advisor Dr. Mohammed Ali Al-Osta. He has been extremely supportive and helpful and guided me toward more success and productivity. I am also grateful to my committee members Chair. Prof. Abdelouahed Tounsi and Dr. Mesfer Al-Zahrani for their support and guidance.

In addition, I acknowledge the support of the Deanship of Graduate Studies (DSR) for giving me the opportunity and funding the research project. Appreciation extends to Dr. Abdelbaki Chikh, and Mr. Saeed Tahir, and Mr. Mohammed Zitoun for their time, effort, and encouragement during tens of meetings.

My deepest thanks to my parents, brothers, and sisters for their prayers, support, and love. Thanks to my wife and son for their love and encouragement. I would like also to thank my friends and colleagues who were always beside me.

TABLE OF CONTENTS

LIST OF TABLES

LIST OF FIGURES

LIST OF ABBREVIATIONS

FGM	:	Functionally Graded Material
HOSDT	:	Higher-Order Shear Deformation Theory
CPT	:	Classical Plate Theory
FOSDT	:	First-Order Shear Deformation Theory
SIPRE	:	Snow, Ice and Permafrost Research Establishment

ABSTRACT

Full Name : Ismail Mohammed Mohammed Mudhafar

Thesis Title : Hygro-Thermo-Mechanical Bending Behavior of Advanced Functionally Graded Ceramic Metal Plates Resting on Viscoelastic Foundation

Major Field : Civil and Environmental Engineering

Date of Degree : April 2021

Multi-layered materials are utilized in various structures. Layers in the conventional laminated structures are bonded together to enhance their mechanical-thermal properties. Such assembly caused major inconvenience, which is the stress concentration along the interfaces, especially at elevated temperatures leading to delamination, cracks, and other damage mechanisms. Functionally graded materials (FGMs) overcome this problem by continuously varying the material constituents along the thickness. This research focuses on studying the hygro-thermo-mechanical bending behavior of advanced functionally graded ceramic-metal plates resting on viscoelastic foundation using a simple higher-order integral shear deformation theory with only four unknowns. The power-law function in terms of volume fraction is used to vary the elastic material constituents through the plate's thickness. The in-plane displacement field uses a sine shape function that changes linearly through the plate thickness to calculate the out-of-plane shear deformation. Both the linear and nonlinear influence of temperature and moisture concentration on the bending response is investigated. For the first time, a three-

parameter viscous foundation model is used to study the bending response utilizing the damping coefficient in addition to Winkler’s and Pasternak’s parameters. The governing equations are derived using the principle of virtual displacement, and the analytical solution is obtained by the Navier method. Non-dimensional numerical results are validated with existing results in the literature. A parametric investigation is established to discuss the effect of the power-law gradient index, temperature rise and moisture concentration, elastic foundation coefficients, and the viscoelastic damping coefficient on the FGM plate's bending response.

ملخص الرسالة

الاسم الكامل: إسماعيل محمد محمد مظفر

عنوان الرسالة: الإجهاد الميكانيكي-الحراري-الرطوبي لصفائح السيراميك المعدنية المتدرجة وظيفيا والمستندة على قاعدة لزجة ومرنة

التخصص: هندسة مدنية وبيئية

تاريخ الدرجة العلمية: ابريل 2021

يتم استغلال المواد المركبة المكونة من عدة طبقات في أنواع مختلفة من الهياكل والصفائح الإنشائية وتُربط هذه الطبقات ببعضها لتعزيز الخصائص الميكانيكية الحرارية، لكن هذا الترابط يركز قوى الضغط في أماكن تلاقيها خاصة عند درجات الحرارة العالية ما يسبب حدوث شقوق وانفصال للطبقات عن بعضها. تتغلب المواد المتدرجة وظيفيا (FGM) على هذه المشكلة من خلال التغيير المستمر لمكونات المواد خلال سماكة الصفيحة الإنشائية. يُركز هذا البحث على دراسة الإجهاد الميكانيكي-الحراري-الرطوبي لصفائح السيراميك المعدنية المتدرجة وظيفيا والمستندة على قاعدة لزجة ومرنة بإستخدام نظرية الإزاحة بقوى القص ذات الرتبة العليا والمعتمدة على أربعة مجاهيل فقط. أُستعملت دالة قانون القوى والمعتمدة على النسب الحجمية لأجل توزيع نسبة المواد خلال سماكة الصفيحة الإنشائية. يستغل مجال الإزاحة الأفقية دالة جيبية مثلثية لحساب مجال الإزاحة الرأسية بقوى القص. تم دراسة تأثير عوامل الحرارة والرطوبة الخطية وغير الخطية على الإجهادات داخل الصفيحة. لأول مرة، تم استعمال نموذج قاعدة لزجة ومطاطية ذا ثلاثة عوامل لدراسة قوى الإجهادات في الصفيحة مع الأخذ بعين الإعتبار تأثير عامل التثبيط بالإظافة الى عومل "وينكلر" و"باستيرناك". تم إستخدام مبدأ الإزاحة الإفتراضية لإشتقاق المعادلة التفاضلية الحاكمة، وتم التوصل الى الحل التحليلي بإستخدام طريقة "نافيير". تم مقارنة النتائج القياسية مع نتائج الدراسات المتوفرة في المجال للتحقق من صحتها. تم إجراء تحقق معياري لمناقشة تأثير مؤشر التدرج لقانون القوى، تركيز الحرارة والرطوبة، معاملات القاعدة، بالإضافة الى تأثير عامل التثبيط في القاعدة المرنة ذات اللزوجة.

CHAPTER 1

INTRODUCTION

1.1 Background

The need for efficient structural materials is increasing in many engineering fields such as civil, aerospace, ship-building industry, nuclear, optical, automotive, biochemical, chemical, mechanical, electronics, and other industries, etc. [1]. The increased demand led to the emergence of functionally graded materials (FGMs) which pose strength in terms of stiffness and temperature resistance. The smooth varying of material properties significantly enhanced the resistance to the temperature gradient, wear resistance, and at the same time led to the reduction of thermal stress residual. It is known that metals such as iron and copper pose high strength and elasticity under normal temperatures, but they are weak under high temperatures. Ceramic on the other hand has high-temperature resistance but low elasticity. Therefore, functionally graded materials are made of both ceramic and metal to have high stiffness, elasticity, and high-temperature resistance under different types of loadings.

Many theories were used in the analysis of plates. The first is the classical plat theory [2], which gives good results for thin plates. However, thick plates require the use of higher-order shear deformation theories such as the first-order shear deformation theory [3] and the third-order shear deformation theory (HSDT) [4]. In this study, a higher-order shear deformation theory will be used to study the effect of temperature, moisture, and mechanical loading on

FGM plates resting on viscoelastic foundations. This work will give insight about main concepts needed in the derivation of the governing differential equations and state the methodology for the analytical and numerical solution.

1.2 Thesis Objectives

This thesis aims to study the "hygro-thermo-mechanical" bending behavior of advanced FGM ceramic-metal structures using new thermoelastic "shear deformation theories". The variational principle and principle of virtual work will be used to obtain the "governing differential equations". The objectives of this study are:

1. Employing a simple HSDT with few variables to study the bending behavior of functionally graded ceramic-metal plates resting on a viscoelastic foundation.

2. The effects of viscoelastic foundations parameters on the bending behavior of the FGM plate will be investigated.

3. The influences of moisture concentration, temperature, structure aspect ratio, side to thickness ratio, and volume fraction variation on the bending behavior of FGM structures will be also investigated.

1.3 Significance of the Research

This thesis has great value for the Kingdom as it will be a first-of-its-kind breakthrough multidisciplinary project at the interface of material and mathematical sciences. The hygro-thermo-mechanical effects on structures made of advanced functionally graded materials become important topics for scientists and researchers. Nowadays, FGMs are classified as novel composite materials that are extensively used in many industries such as civil, aerospace, ship building industry, etc. The smooth varying of material properties significantly enhanced the resistance to the temperature gradient, wear resistance, and at the same time led to the reduction of thermal stress residual. In this study, new shear deformation theories will be developed to study the bending of advanced FGM structures subjected to hygro-thermal environments.

1.4 Thesis organization

The body of the thesis contains six chapters. It starts with the introduction about the topic in general and the statement of the problem while defining the objectives of the study. The second chapter presents the literature done about the topic, explaining important concepts needed for understanding the approach to solving the problem. Chapter three contains a full published journal article about the 2D theory addressing the solution to the problem, while chapter four presents another journal article regarding the more accurate quasi-3D theory. The thesis concludes in chapter five by summarizing the important points of the study and suggesting future work on the area of functionally graded plates.

CHAPTER 2

LITERATURE REVIEW

2.1 Plate Theories

In this section, the theories used in studying plates and the method of varying the material constituents along the plate thickness will be described as shown in Figure 1[5]. It can be seen that the bottom surface of the plate is metal, while the top surface is ceramic, and the in-between is FGM with gradation described in the coming subsection.

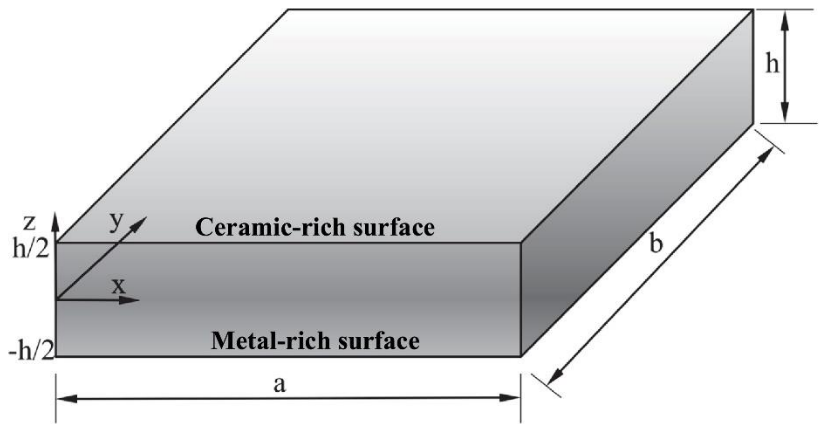

Figure 1 Typical Functionally Graded Plate

Plate analysis started with the classical plate theory [6] in which it neglects the shear effect leading to errors in the results especially when dealing with thick plates. The first-order shear deformation theory [3] came after, and included the shear effect and provided appropriate results, but it requires a shear correction factor to ensure zero shear stress at the boundaries.

After that, many researchers suggested higher-order shear deformation theories without the need to shear correction factors [7]–[12]. The following chart summarizes the classification of the plate theories. The original theory is the 3D elasticity, and the rest are reduced by assuming certain kinematics to change the analysis from 3D to 2D.

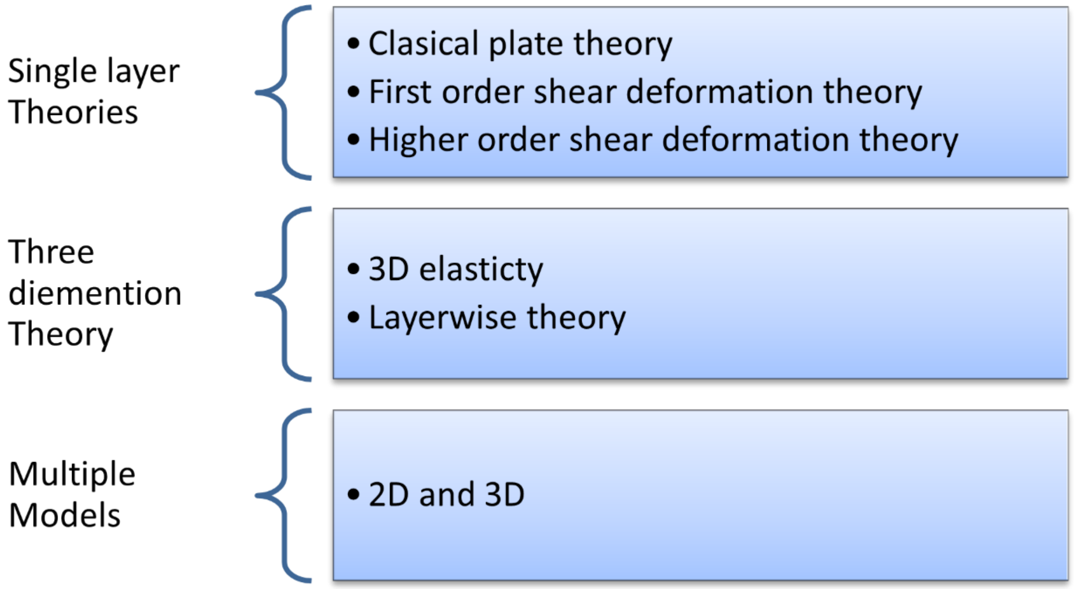

2.2 Material Gradation of FGM Plates

Functionally graded materials are produced by varying the material constituents throughout the thickness so that it starts with a certain material type, say metal, and end with another type, say ceramic and the middle is varying by percentage according to the volume fraction. The variation could be also for a sandwich plate where the plate is composed of three layers one of them is FGM and the other is of a certain material. Researchers use one of the following for describing the volume fraction: Power-law function, Exponential or Sigmoid function.

Calculating the volume fraction by the power law is widely used among researchers. It is described as follows [13]:

$$V(z) = \left(\frac{z}{h} + \frac{1}{2}\right)^{p} \tag{1}$$

where p is the material parameter and h is the plate thickness. The plate properties such as Young's modulus are then defined by the rule of mixture described in equation (2)

$$P(z) = P_1 V_1 + P_2\, V_2 \tag{2}$$

where P_1 and V_1 refer to the first material property and volume respectively whereas P_2 and V_2 refer to the property and volume of the second material, respectively.

The Young's modulus can be described as follows:

$$E(z) = V(z)\, E_1 + [1 - V(z)]\, E_2 \tag{3}$$

$E(z)$ is the Youngs modulus for the two composing materials and across the thickness of the plate. Figure 2 [13] shows the plot of $E(z)$ with $-\frac{h}{2} < z < \frac{h}{2}$. It can be observed that the two edges of the plates are of two separate materials while the middle portion is a mix of the two making it functionally graded plate. Also, increasing the p value results in increasing the portion material 2.

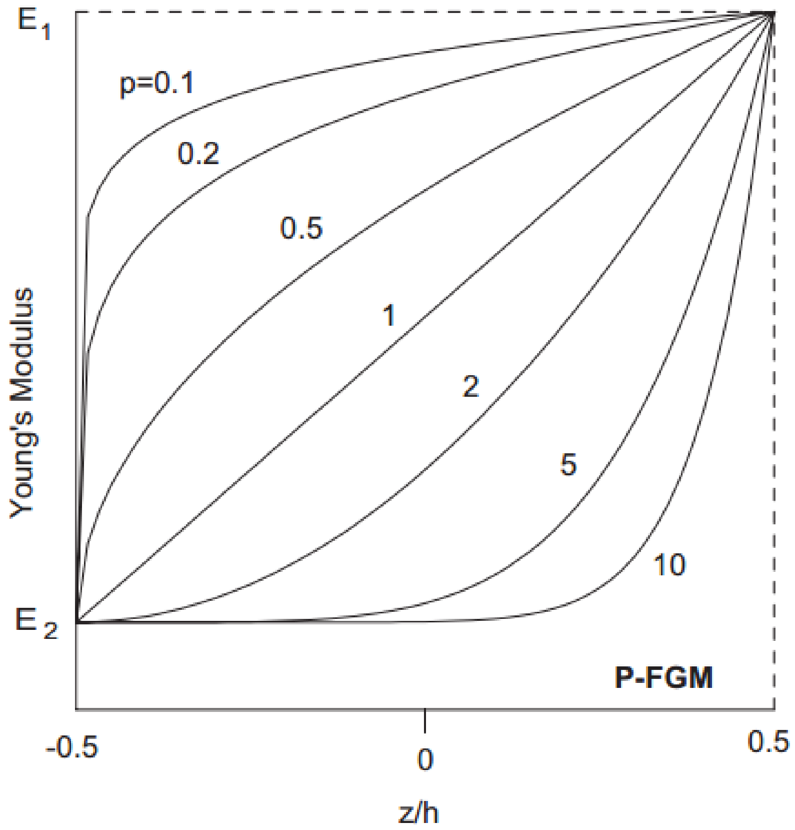

Figure 2 Young's modulus variation along the plate thickness

2.3 Plate Foundations

There are three famous foundations models available to support plates.

2.3.1 Winkler's Model

Winkler [14] proposed the first foundation model. In this model, the foundation was assumed to be closely spaced springs, where the loaded beam or plate is resting on them as shown in Figure 3-a [15]. The relation between the applied load and the resulting deflection curve is shown in equation (4).

$$p(x, y) = k\, w(x, y) \tag{4}$$

Winkler’s model suggests that deflection happens only to springs of direct contact with the surface. In reality, deflection happens also to the neighboring springs, but the effect decreases with increasing the horizontal distance between the load and the springs.

2.3.2 Pasternak’s Model

Pasternak in 1954 modified Winkler’s model by adding a shear layer over the springs as shown in Figure 3-b to distribute the load and cause deflection even to those springs, not in contact with the loaded surface. The modified relation is shown in equation (5)

$$P = kw - G\nabla^2 w \tag{5}$$

where the additional term $G\nabla^2 w$ accounts for Pasternak shear layer. This model is referred to as an elastic foundation.

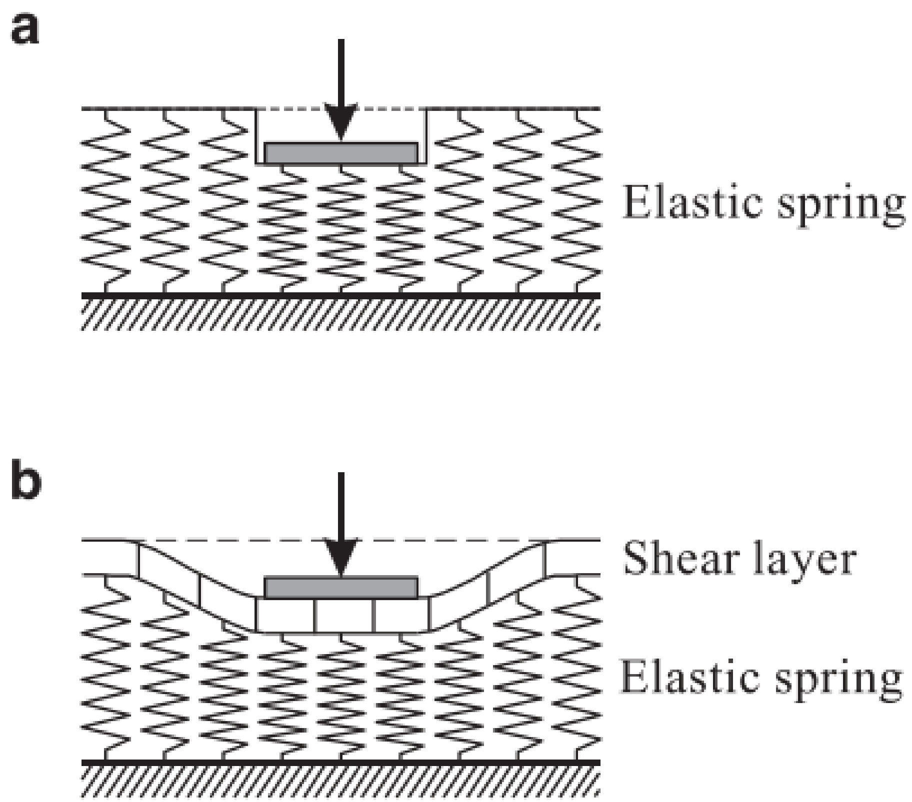

Figure 3 a) Winkler model b) Pasternak Model

2.3.3 Viscoelastic Pasternak Foundation

In the Pasternak model, the deflection was assumed to happen immediately after applying the load. However, there is a considerable creep effect in the foundation. A footing load test was done by the Snow Ice and Permafrost Research Establishment (SIPRE), U. S. Army in 1959 showed the creep effect to increase linearly with time in days as shown in Figure 4 [16]. The Pasternak elastic model formula is modified to take into account deflection caused by creep as in equation (6).

$$R_f = \left(k_w - k_s\nabla^2 + c_t\frac{\partial}{\partial t}\right)w \tag{6}$$

where $k_w$is the Winkler parameter, k_s is Pasternak shear model, and $c_t \frac{\partial}{\partial t}$ is the viscoelastic medium coefficient.

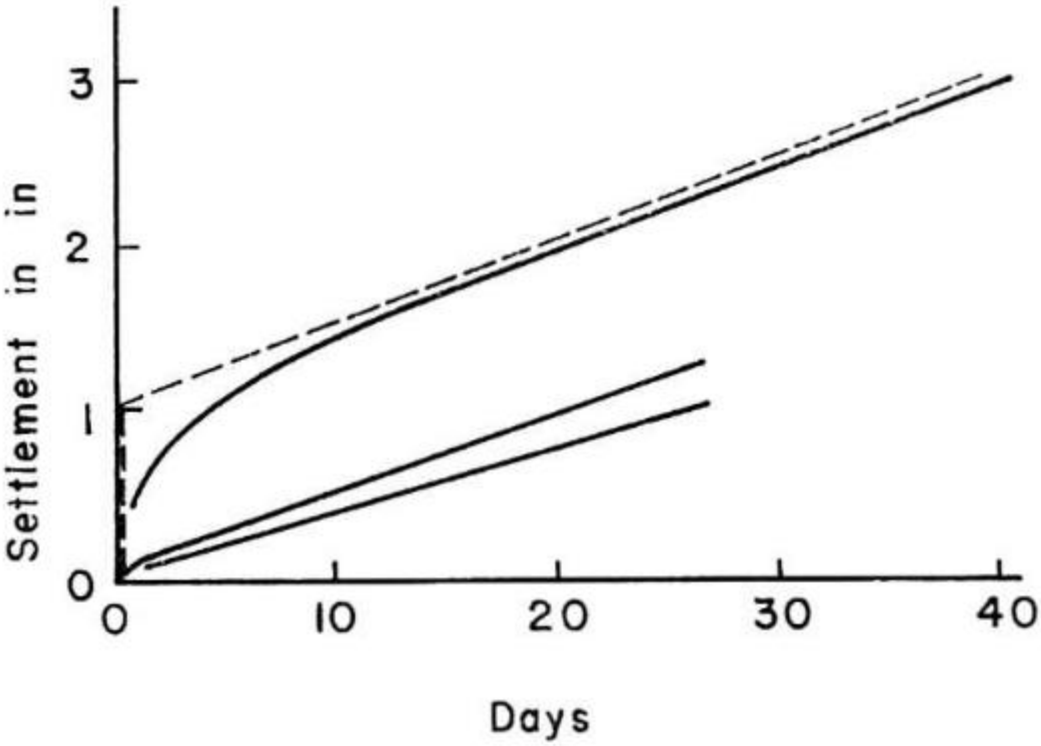

Figure 4 Creep of loaded Ice foundation

2.4 Applications of Functionally Graded Materials

In FGMs, the material particles are gradually distributed through the thickness according to the intended usage, hence called functionally graded. As Figure 6 [17] indicates, Many engineering fields utilize FGMs for example, in civil engineering, they are utilized to manufacture fiber-reinforced polymers (FRP) used for reinforcing bridge concrete materials which enhance resistance to corrosion [18], while the aerospace and automotive industries use them in the production of external and internal parts of aircrafts, rockets, and engines [19], examples are shown in Figure 5. Some types of FGMs include compositional gradients which are applied in defense, porosity gradients used in filters and dental, while other types of FGMs include microstructural gradients used in armory [20]. For this importance, researchers extensively studied the static and dynamic responses of these materials under various loading conditions.

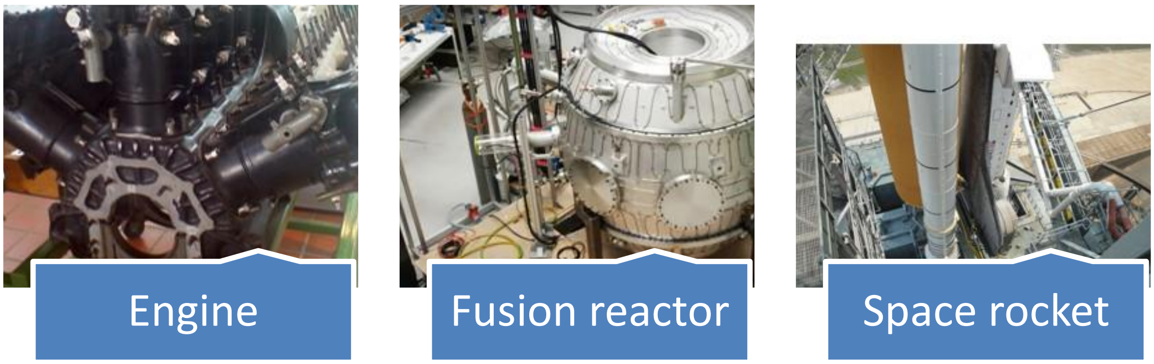

Figure 5 Examples of FGM Applications

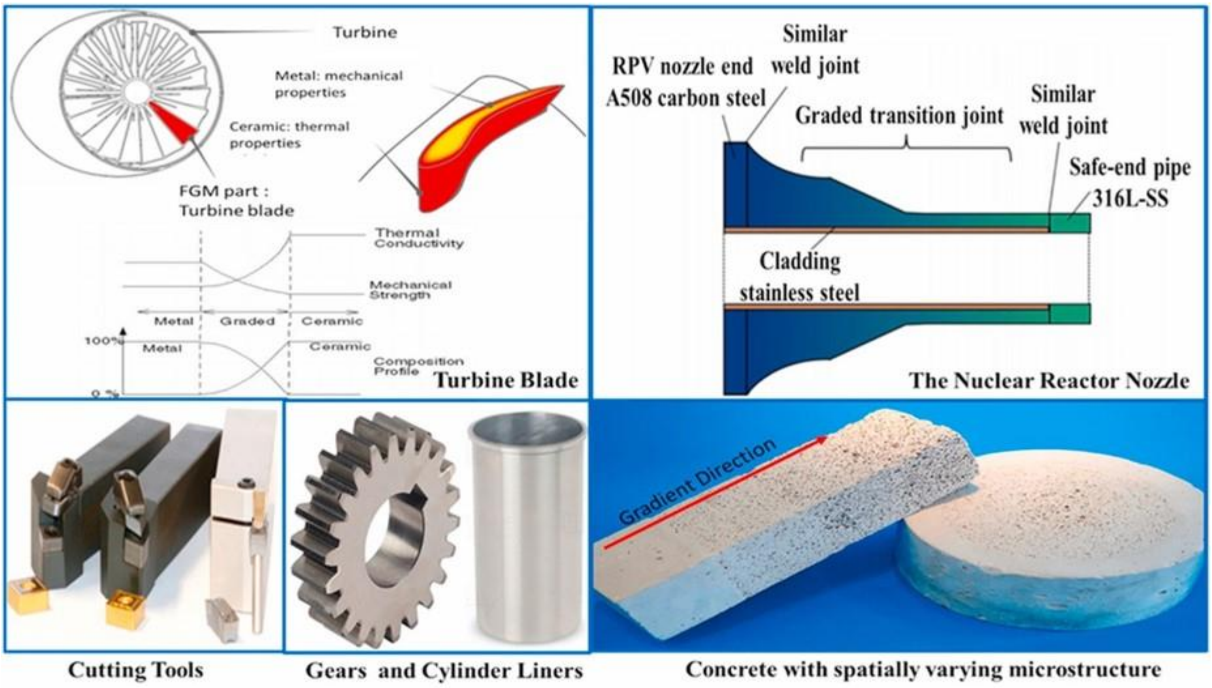

Figure 6 Various fields Utilize FGMs.

2.5 Manufacturing of FGMs

The fabrications process is challenging in the field of FGMs. This is because it involves mixing two solid materials at the atom level. Some of the famous manufacturing methods are shown in Figure 7 [17]. The centrifugal force method is widely used in the industry followed by the powder metallurgy method.

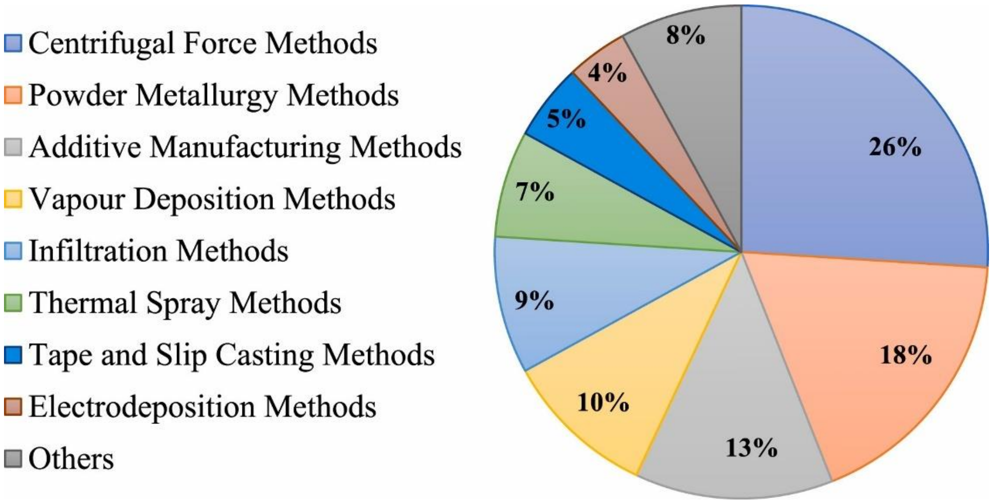

Figure 7 Famous FGMs Fabrication methods

The centrifugal manufacturing method shown in Figure 8 [17] mixes the two melted materials utilizing a spinning force. The particles are then casted into a sand form to produce the needed shape.

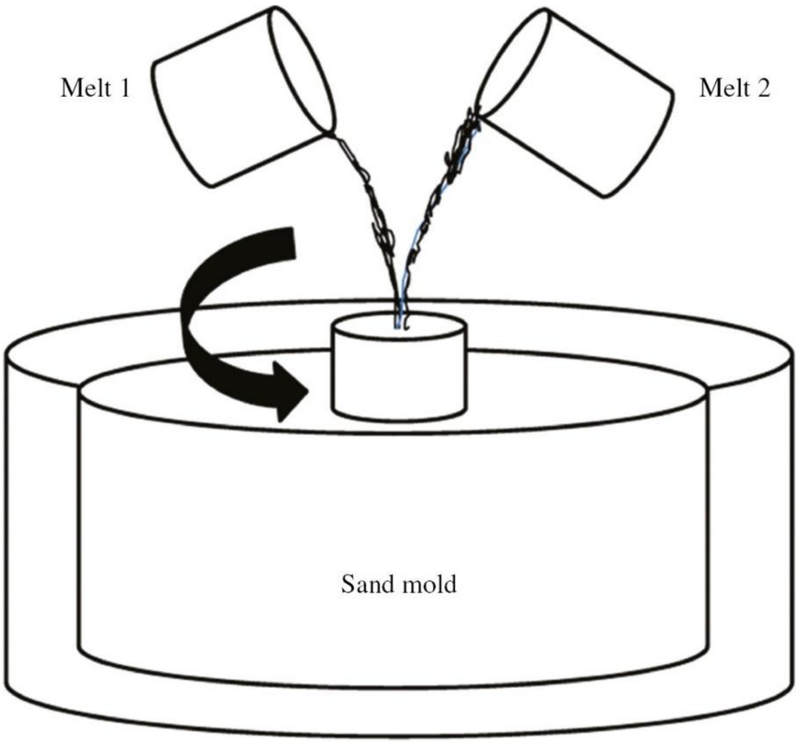

Figure 8 The Centrifugal FGMs Manufacturing Method

Another famous method is the powder metallurgy process in which the two materials are mixed, stacked, then pressed employing high pressures and temperature with the sequence shown in the diagram of Figure 9 [17].

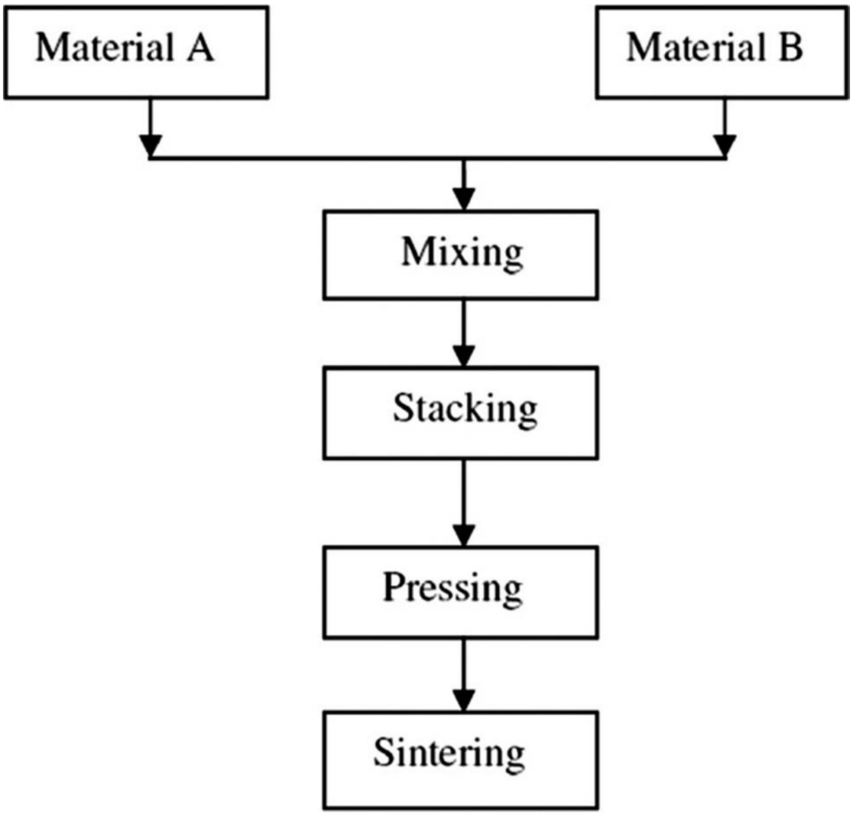

Figure 9 Powder Metallurgy process

2.6 Kinematics and Constitutive Equations

2.6.1 Displacement field

The displacement field is composed of four variables u, v, w, θ. The first order and many high order shear deformation theories use more than five unknowns. The following relations show the unknown integral term that reduced the variables into four unknowns.

$$\mathrm{U}(\mathrm{x,y,z,t}) = \mathrm{u}_0(x,y,t) - z\frac{\partial\, \mathrm{W}_0(x,y,t)}{\partial x} + \mathrm{K}_1\, f(z) \int \theta(x,y,t)\, \mathrm{d}x \qquad (7)$$

$$V(\mathrm{x,y,z,t}) = v_0(x,y,t) - z\frac{\partial\, \mathrm{W}_0(x,y,t)}{\partial y} + \mathrm{K}_1\, f(z) \int \theta(x,y,t)\, \mathrm{d}x \qquad (8)$$

$$W(\mathrm{x,y,z,t}) = w_0(x,y,t) \qquad (9)$$

u_0, v_0, w_0 are the middle surface displacements in the x, y, z directions respectively K_1, K_2 are parameters related to the plate's geometry, $f(z\ )$ is the shape function of the shear strain to be used in this research.

$$f(z) = \frac{h}{\pi} sin\left(\frac{\pi z}{h}\right) \qquad (10)$$

Other types of function utilize exponential and others utilize the hyperbolic function. The current shape function in equation (10) utilizes the sine function to predict the shear strain.

2.6.2 Strain Tensor

The strain tensor can be found by taking the derivative of the displacement field with respect to the corresponding direction as shown in equation (11)

$$\epsilon_{\mathrm{ij}} = \frac{1}{2}\left(\frac{\partial u_i}{\partial x_j} + \frac{\partial u_j}{\partial x_i}\right) \qquad (11)$$

For $i = 1 \ldots 3, j = 1 \ldots 3$ then the strain tensor is shown in equation (12)

$$\begin{Bmatrix} \epsilon x \\ \epsilon y \\ \gamma xy \\ \gamma xz \\ \gamma yz \end{Bmatrix}$$

$$= \begin{Bmatrix} \frac{\partial \mathrm{u}\,0(x,y,t)}{\partial x} - z\frac{\partial^2 \mathrm{w}\,0(x,y,t)}{\partial x^2} - \frac{\mathrm{k1}\,f(z)\frac{\partial^2\,\theta(x,y,t)}{\partial x^2}}{\lambda^2} \\ \frac{\partial \mathrm{v}\,0(x,y,t)}{\partial y} - z\frac{\partial^2 \mathrm{w}\,0(x,y,t)}{\partial y^2} - \frac{\mathrm{k2}\,f(z)\frac{\partial^2\,\theta(x,y,t)}{\partial y^2}}{\mu^2} \\ \frac{\partial \mathrm{u}\,0(x,y,t)}{\partial y} + \frac{\partial \mathrm{v}\,0(x,y,t)}{\partial x} - 2z\frac{\partial^2 \mathrm{w}\,0(x,y,t)}{\partial x\,\partial y} - \frac{\mathrm{k1}\,f(z)\frac{\partial^2\,\theta(x,y,t)}{\partial x\,\partial y}}{\lambda^2} - \frac{\mathrm{k2}\,f(z)\frac{\partial^2\,\theta(x,y,t)}{\partial x\,\partial y}}{\mu^2} \\ -\frac{\mathrm{k1}\frac{\partial\,\mathrm{f}(z)}{\partial z}\frac{\partial\,\theta(x,y,t)}{\partial x}}{\lambda^2} \\ -\frac{\mathrm{k2}\frac{\partial\,\mathrm{f}(z)}{\partial z}\frac{\partial\,\theta(x,y,t)}{\partial y}}{\mu^2} \end{Bmatrix} \quad (12)$$

2.6.3 Stress Tensor

The stress tensor is derived from the strain tensor in equation (13).

$$\sigma = \begin{Bmatrix} \sigma x \\ \sigma y \\ \tau xy \\ \tau yz \\ \tau xz \end{Bmatrix} = \begin{bmatrix} C_{11} & C_{12} & 0 & 0 & 0 \\ C_{12} & C_{22} & 0 & 0 & 0 \\ 0 & 0 & C_{44} & 0 & 0 \\ 0 & 0 & 0 & C_{55} & 0 \\ 0 & 0 & 0 & 0 & C_{66} \end{bmatrix} . \begin{Bmatrix} \epsilon x - \alpha\Delta T - \beta\Delta C \\ \epsilon y - \alpha\Delta T - \beta\Delta C \\ \gamma xy \\ \gamma yz \\ \gamma xz \end{Bmatrix} \quad (13)$$

The parameters $C_{ij}$are as follow:

$C_{11} = C_{22} = \frac{E}{1-v^2}$, $C_{12} = \frac{v\,E}{1-v^2}$, $C_{44} = C_{55} = C_{66} = \ C_{12} = \frac{v\,E}{2(1-v^2)}$

α and β are the temperature and humidity coefficients respectively, $\Delta T\ and\ \Delta C$ are the temperature and humidity gradients through the thickness and are described in equation (14)

$$\Delta \mathrm{T}(x,y,z) = T_1(x,y) + \frac{z}{h} T_2(x,y) + \frac{f(z)}{h} T_3(x,y)$$

(14)

$$\Delta \mathrm{C}(x,y,z) = C_1(x,y) + \frac{z}{h} C_2(x,y) + \frac{f(z)}{h} C_3(x,y)$$

2.6.4 Principal of Virtual Work

After setting the strain and the stress tensors, we use the principle of virtual work to generate the governing differential equations. The principle is stated in equation (15).

$$\int_{\frac{-h}{2}}^{\frac{h}{2}} \int_{\Omega} [\sigma_x \delta\epsilon_x + \sigma_y \delta\epsilon_y + \tau_{\mathrm{xy}} \delta\gamma_{\mathrm{xy}} + \tau_{\mathrm{xz}} \delta\gamma_{\mathrm{xz}} + \tau_{\mathrm{yz}} \delta\gamma_{\mathrm{yz}}] \, \mathrm{d}\Omega \, \mathrm{d}z$$

(15)

$$- \int_{\Omega} (q - f_e) \, \delta w \, \mathrm{d}\Omega = 0$$

q is the mechanical load applied on the plate along the z direction and f_e is the force coming from the foundation. The force is described according to the Winkler-Pasternack model as in equation (16).

$$K_w \, \mathrm{w}(x,y) - k_{\mathrm{p1}} \frac{\partial^2 \mathrm{w}\, 1(x,y)}{\partial x^2} - k_{\mathrm{p2}} \frac{\partial^2 \mathrm{w}(x,y)}{\partial y^2} \tag{16}$$

k_{p1} *and* k_{p2} are the shear parameters and K_w is the Winkler parameter. It is noticed that the principal applies the integral for the product of the stress and the variation of the strain along the xy domain first, and then integrate along the plate thickness.

The governing equations will be generated in the research by substituting the parameters in equation (15) and integrating them by parts, then the analytical solution will be generated using the Naiver method.

CHAPTER 3

Journal Article 1

Hygro-Thermo-Mechanical Bending Behavior of Advanced Functionally Graded Ceramic Metal Plate Resting on a Viscoelastic Foundation

Ismail M. Mudhaffar[1], Abdelouahed Tounsi*[1,2,3], Abdelbaki Chikh[3,4], Mohammed A. Al-Osta[1], Mesfer M. Al-Zahrani[1] and Salah U. Al-Dulaijan[1]

1Department of Civil and Environmental Engineering, King Fahd University of Petroleum & Minerals, 31261 Dhahran, Eastern Province, Saudi Arabia
2YFL (Yonsei Frontier Lab), Yonsei University, Seoul, Korea
3Material and Hydrology Laboratory, University of Sidi Bel Abbes, Faculty of Technology, Civil Engineering Department, Algeria
4Université Ibn Khaldoun, BP 78 Zaaroura, 14000 Tiaret, Algérie

3.1 Abstract

In this work, the bending behavior of an advanced functionally graded ceramic-metal plate subjected to a hygro-thermo-mechanical load and resting on a viscoelastic foundation is studied using a simple higher-order integral shear deformation theory. The power-law function in terms of volume fraction is used to vary the elastic material constituents through the plate's thickness. The in-plane displacement field uses a sine shape function that changes linearly through the plate thickness to calculate the out-of-plane shear deformation. Both the linear and nonlinear influence of temperature and moisture concentration on the bending response are investigated. For the first time, a three-parameter viscous foundation model is used to study the bending response utilizing the damping coefficient in addition to Winkler's and Pasternak's parameters. The governing equations are derived using the principle of virtual displacement, and the analytical solution is obtained by the Navier method. Non-dimensional numerical results are validated by existing results in the literature. A parametric investigation

is established to discuss the effects of the power-law gradient index, temperature rise and moisture concentration, elastic foundation coefficients, and the viscoelastic damping coefficient on the FGM plate's bending response.

Keywords: Functionally graded plates; bending response; viscoelastic foundation; hygro-thermo-mechanical loading; higher-order shear deformation theory.

3.2 Nomenclature

FGMs	Functionally Graded Materials
CLPT	Classical Plate Theory
HSDT	Higher-Order Shear Deformation Theory
SIPRE	Snow, Ice, and Permafrost Research Establishment
u_0, v_0	The middle surface displacements in the x, y, z directions, respectively
w_0, θ	Vertical displacements due to bending and shear, respectively.
a, b	Length and width of the plate, respectively
p	Power law gradient index
K_1, K_2	Plate's geometry parameters
ε	Strain
α	Temperature coefficient
β	Humidity coefficient
ΔT	Temperature gradient
ΔC	Humidity gradients
q	Applied mechanical load
$k_{\mathrm{p1}}, k_{\mathrm{p2}}$	Pasternak shear parameters in x, y, respectively.
K_w	Winkler parameter
C_t	The damping coefficient
$\delta u_0, \delta v_0, \delta w_0, \delta\theta$	The first variation of u_0, v_0, w_0, θ, respectively.

3.3 Introduction

The need for efficient structural materials is increasing in many engineering fields. Multilayered materials are utilized in numerous structures [21], [22]. Layers in conventional laminated structures are bonded together to enhance their mechanical-thermal properties. However, this type of assembly produces stress concentration at the ply's interfaces, especially under elevated temperatures, leading to delamination, cracks, and other damage mechanisms [11], [21], [23]. Functionally graded materials (FGMs), which were first proposed in 1984 by a Japanese material scientist in Sedni [24], overcome these problems by continuously varying the material constituents along the plate's thickness. Nowadays, FGMs are classified as novel composite materials [25] that are used extensively in various fields such as civil engineering, aerospace, and the shipbuilding industry, along with the following industries: nuclear, optical, automotive, biochemical, chemical, mechanical, electronics, etc. [1], [26]. In a recent review article, Njim et al. [20] described the use of FGMs by application areas. Compositional gradient FGMs are utilized in defense, energy, and aerospace. Porosity gradient FGMs are used in filters, orthopedic, and dental. Microstructural gradient FGMs are utilized in defense and armory. This need comes from the point that FGMs came to solve problems in composite structures. Due to their importance, researchers have focused their studies on the behavior of these materials and their bending response under various load combinations.

FGMs exhibit strength in terms of their stiffness and temperature resistance [27]. The smooth varying of the material properties significantly enhance the resistance to the impact of the temperature gradient and the wear resistance while at the same time cutting down the thermal stress residual [28]. It is known that metals such as iron and copper have high strength and elasticity under normal temperatures, but they are weak under high temperatures. Ceramic, on the other hand, has great resistance to temperature but low elasticity. Therefore, functionally graded materials are made of both ceramic and metal to combine high stiffness, elasticity, and high-temperature resistance under different types of loadings [29]. The concept of functionally grading is implemented with various materials to give improved properties. For example, the Carbone nanotubes are functionally graded to give functionally graded nano carbons reinforced composites (FG-CNTRCS) [30]–[32].

There are three famous foundation models available to support the plate. The first is Winkler [14], in which the foundation was assumed to have closely spaced springs supporting the loaded structure. Winkler's model suggests that deflection happens only to springs in direct contact with the surface. In reality, deflection also occurs with the neighboring springs, but the effect decreases with increasing the horizontal distance between the load and the springs. Pasternak [33] modified Winkler's model by adding a shear layer over the springs to distribute the load and cause deflection, even to those springs not in contact with the loaded surface. In the Pasternak model, the deflection was assumed to happen immediately after applying the load. However, there is a considerable creep effect in the foundation. A footing load test was done by the Snow Ice and Permafrost Research Establishment (SIPRE). In 1959 the U.S. Army showed that the creep effect increases linearly with time in days [16]. Therefore, the Pasternak elastic model formula is modified to consider deflection caused by creep through a damping parameter [16].

Several theories have been used in the analysis of plates [28]. The first is the classical plate theory [2], which gives good results for thin plates. However, thick plates require higher-order shear deformation theories such as the first-order shear deformation theory by Mindlin [3] and the third-order shear deformation theory by Reddy [4].

Plates, in general, have been investigated heavily, and the focus increases on the plates with functionally graded materials. Zenkour [34] presented a two-dimensional solution for the bending behavior of a metal-ceramic sandwich plate having simply-support boundary conditions. The study assumed the top and bottom faces of the plate to be an isotropic material comprised of two constituents distributed through the thickness according to the power-law function in terms of the volume fraction. Zghal, Frikha, and Dammak [35] used the extended rule of the mixture to study the static response of carbon nanotubes-reinforced FGM plates, in which they considered five types of reinforcement distributions. Zenkour [36] studied FGM's static response to transverse loading using generalized shear deformation theory, which was simplified by implementing traction-free boundary conditions at the plate faces. M. Li et al. [37] Conducted a static analysis of FGM plates using a five variable plate theory. An exponential function was utilized to predict the transverse shear strain and to satisfy the zero-shear strain at the plate's top and bottom without shear correction factors. Tu, Quoc, and Van Lon [38] developed a new eight-unknown theory based on a twelve-unknown theory to investigate the bending response of FGM plates. The same theory is used to investigate the vibration response of plates in thermal environments [39]. The investigation found that the natural plate frequency decreases by increasing the temperature or the volume fraction index.

Reddy [4] developed a simple high order theory for laminated plates with the same number of unknowns as the first-order theory by Whitney and Sun [40]. A theory for the static and dynamic isotropic plates was developed by Levinson [8]. The plate here was considered to have a uniform thickness. Touratier [9] developed a standard plate theory that considers a cosine shear stress distribution. The number of unknowns is similar to the first-order shear deformation theory but does not require a shear correction factor. Wang et al. [41] discussed the three-order shear theory and studied the bending response. Finally, a comprehensive analysis of FGM plates under mechanical load was presented by Chi and Chung [13].

The bending analysis of imperfect FGM plates under hygro-thermo-mechanical loading was investigated by Daouadji et al. [42]. The plate's imperfection comes from technical problems during fabrication that causes micro-voids and porosities inside the plate. The even and uneven voids were investigated using the modified rule of mixture and the porosity volume fraction.

The effect of nonlinear hygro-thermo-mechanical loading on an FGM plate resting on the elastic foundation was investigated by Sayyad and Ghugal [43] using a four-unknown plate theory. The in-plane displacement field incorporates an exponential function through the thickness coordinate to calculate the out-of-plane shear strains. Zghal, Frikha, and Dammak [44] studied the free vibration response of carbon nanotubes' FGM shell structures using three distributions of carbon nanotubes. The same response was investigated on improved finite shell elements [45]. A unified shear deformation theory was used by Sayyad and Ghugal [46] to study the bending of isotropic FGM laminated sandwich plates and beams. The theory included four types of shape functions: parabolic, trigonometric, hyperbolic, and exponential shape functions. The parabolic shape function gave results similar to Reddy’s theory, while the other shape functions were used for the first time. Zghal et al. [47] studied the nonlinear bending of nanocomposites reinforced by graphene-nanotubes using a double director shell model and membrane enhancements.

The research went beyond the regular foundation investigation. Bouderba [48] studied the FGM rectangular plate's bending analysis resting on a non-uniform elastic foundation under a thermal loading environment. The analysis used refined plate theory with a nonlinear variation of the in-plane displacement.

Aliaga and Reddy [40] developed a displacement finite element model to study the linear and nonlinear thermoelastic response of FGM plates subjected to static and dynamic loads using third-order shear deformation theory. The power-law index's parametric effect, surface temperature, and mechanical loads were studied using simply and clamped boundary conditions, and the model is valid for any boundary condition. A significant finding in the research was that the deflection values are not in the middle range of the pure ceramic or metal plates values because of the nonlinear coupling between the thermal and mechanical loading contributions. Van Long, Quoc, and Tu [49] studied the bending and free vibration of FGM plates using finite elements and incorporating an eight-unknowns shear deformation theory. Kim and Paulino [50] used a finite element methodology and a modified crack closure method to study the mixed-mode fracture of orthotropic functionally graded materials. The crack orientation was arbitrary to the direction of the principal axes of the material orthotropy.

Hellal et al. [51] studied the dynamic and stability analysis and buckling of FGM sandwich plates resting on an elastic foundation in a hygro-thermal environment using simple higher-order shear theory. The model uses a trigonometric distribution of the shear stress. The displacement equations incorporate an integral term that reduces the number of unknowns and necessary equations. A hyperbolic HSDT with Sin function was used by Neves et al. [52] to study the linear buckling of FGM sandwich plates. The boundary conditions and the governing equation were obtained using Carrera’s unified formulation and were interpolated by a radial basis function. Zghal, Frikha, and Dammak [30] studied the buckling response of power-based nanotubes functionally graded plates and curved panels using four types of carbon reinforcements through the thickness. Trabelsi et al. [53] extended Kirchhoff–Love model to discussed the thermo-elastic buckling and post-buckling of FG thin plates and shells. S. Trabelsi et al. [15] utilized the modified first-order shear deformation theory to study the thermal post-buckling of functionally graded structures. FGMs are further utilized in beams. Melaibari et al. [54] investigated the influence of axial load distribution on the FG beam buckling load using Reddy's higher-order shear deformation theory (HOSDT). The shear effect was considered for the first time as previous research studied only constant axial loads.

Guellil et al. [55] recently investigated the effect of porosity distribution in the FGM plates. The study assumed that porosity lowers the plate's strength. The model used a four-unknown theory and elastic foundation. Tran et al. [56] used a nonlocal four-unknowns theory to study the plate behavior. Uneven and logarithmic porosity distribution was introduced to the plate. The article discusses the effect of the assumed porosity on the static, dynamic, and buckling response of the plate. Daikh et al. [57] proposed a nonlocal strain gradient quasi-3D theory to study the bending of FGM sandwich plates. The study used the elastic foundation model and concluded that the static response of the plate is significantly affected by the volume fraction exponent. An inverse trigonometric shear theory was used by Sah and Ghosh [58] to study the dynamic and buckling behavior of FGM plates under various boundary conditions. They developed a methodology using a finite element to predict the plate behavior in various loadings and boundary conditions. Non-linear Large deflection investigation of nanocomposite plates and panels was investigated by Zghal et al. [59] using a finite element method.

The FGM plates' bending response was intensely studied using various theories and under different combinations of loadings. However, the FGM plates' response resting on a viscoelastic foundation under non-linear hygro-thermo-mechanical loads has not been investigated. Therefore, this study investigates the bending response of the FGM plates resting on viscoelastic foundations under hygro-thermo-mechanical loads by using a higher-order integral shear deformation theory with only four unknowns.

3.4 Functionally Graded Plate Construction

A rectangular functionally graded plate with a length, width, and thickness of $a, b,$ and h, respectively, as shown in Figure 10 is considered. The FG plate is produced by varying the material constituents throughout the thickness so that the bottom surface is metal-rich, and the top surface is ceramic rich while the middle is a mixture of both, which is varied using the power-law function, exponential, or Sigmoid function.

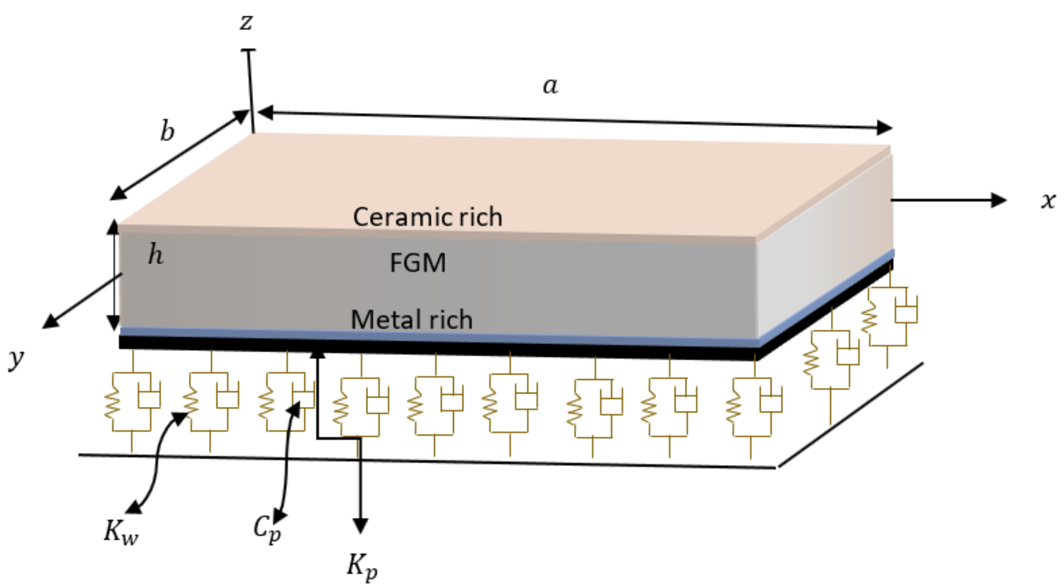

Figure 10 A typical AFG ceramic-metal plate resting on a viscoelastic foundation.

Calculating the volume fraction by the power law is widely used among researchers. It is described as follows [13]:

$$V(z) = \left(\frac{z}{h} + \frac{1}{2}\right)^{p} \tag{17}$$

p, h are the material index and plate thickness, respectively. Plate properties such as Young's modulus are then defined by the rule of mixture [51] described in equation (2)

$$P(z) = P_1 V_1 + P_2\, V_2 \tag{18}$$

where P_1 and V_1 refer to the first material property and volume respectively, whereas P_2 and V_2 refer respectively to the property and volume of the second material.

The Young's modulus can be described as follows:

$$E(z) = V(z)\, E_1 + [1 - V(z)]\, E_2 \tag{19}$$

$E(z)$ is Young's modulus for the two composting materials and across the thickness of the plate.

3.5 Theoretical Formulation

3.5.1 Kinematics

The displacement field can be expressed in the form of El-Haina et al. [60] shown in equation (20). The first order, along with many higher-order shear deformation theories, uses more than five unknowns. The field of the present model incorporates an integral term that reduces the number of unknowns to only four variables, namely, u, v, w, θ.

$$U(x,y,z,t) = u_0(x,y,t) - z\frac{\partial\, w_0(x,y,t)}{\partial x} + k_1\, f(z)\int \theta(x,y,t)\, dx$$

$$V(x,y,z,t) = v_0(x,y,t) - z\frac{\partial\, w_0(x,y,t)}{\partial y} + k_2\, f(z)\int \theta(x,y,t)\, dy \tag{20}$$

$$W(x,y,z,t) = w_0(x,y,t)$$

where u_0, v_0 are the x, y middle surface displacements, whilew_0, θ are the vertical displacements in the z direction due to bending and shear, respectively. k_1, k_2 are parameters related to the plate's geometry defined in equation (26), and $f(z\ )$ is the shape function. Many researchers use shape functions that utilize exponential or hyperbolic functions. This research uses a shape function incorporating the trigonometric $sine$ function which changes linearly through the plate thickness to predict the shear strain shown in equation (10).

$$f(z) = \frac{h}{\pi} sin\left(\frac{\pi z}{h}\right) \tag{21}$$

3.5.2 Constitutive Equations

3.5.2.1 Strain Tensor

The strain tensor is found by taking the derivative of the displacement field with respect to the corresponding direction, as shown in equation (22).

$$\varepsilon_{ij} = \frac{1}{2}\left(\frac{\partial u_i}{\partial x_j} + \frac{\partial u_j}{\partial x_i}\right) \tag{22}$$

where $i = 1 \ldots 3, j = 1 \ldots 3$

The total strain is expressed in the form of the pure middle plane strain and the strain effect coming from the bending and shear.

$$\begin{Bmatrix} \varepsilon_x \\ \varepsilon_y \\ \gamma_{xy} \end{Bmatrix} = \begin{Bmatrix} \varepsilon_x^0 \\ \varepsilon_y^0 \\ \gamma_{xy}^0 \end{Bmatrix} - z \begin{Bmatrix} \varepsilon_x^b \\ \varepsilon_y^b \\ \gamma_{xy}^b \end{Bmatrix} + f(z) \begin{Bmatrix} \varepsilon_x^s \\ \varepsilon_y^s \\ \gamma_{xy}^s \end{Bmatrix}, \qquad \begin{Bmatrix} \gamma_{xz} \\ \gamma_{yz} \end{Bmatrix} = g(z) \begin{Bmatrix} \gamma_{xz}^s \\ \gamma_{yz}^s \end{Bmatrix} \tag{23}$$

where $g(z) = \frac{df(z)}{dz}$. The strain vectors are related to displacement as follows:

$$\begin{Bmatrix} \varepsilon_x^0 \\ \varepsilon_y^0 \\ \gamma_{xy}^0 \end{Bmatrix} = \begin{Bmatrix} \dfrac{\partial u_0}{\partial x} \\ \dfrac{\partial v_0}{\partial y} \\ \dfrac{\partial u_0}{\partial y} + \dfrac{\partial v_0}{\partial x} \end{Bmatrix}, \qquad \begin{Bmatrix} \varepsilon_x^b \\ \varepsilon_y^b \\ \gamma_{xy}^b \end{Bmatrix} = \begin{Bmatrix} \dfrac{\partial^2 w_0}{\partial x^2} \\ \dfrac{\partial^2 w_0}{\partial y^2} \\ 2\dfrac{\partial^2 w_0}{\partial x \partial y} \end{Bmatrix},$$

$$\begin{Bmatrix} \varepsilon_x^s \\ \varepsilon_y^s \\ \gamma_{xy}^s \end{Bmatrix} = \begin{Bmatrix} k_1\, A'\, \theta \\ k_2\, B'\, \theta \\ k_1\, A' \displaystyle\int \frac{\theta}{\partial y} dx \ + k_2\, B' \int \frac{\theta}{\partial x} dy \end{Bmatrix} \tag{24}$$

$$\begin{Bmatrix} \gamma_{\mathrm{xz}}^{\mathrm{s}} \\ \gamma_{\mathrm{yz}}^{\mathrm{s}} \end{Bmatrix} = \begin{Bmatrix} \mathrm{k}_1\ \mathrm{A}' \displaystyle\int \theta\, \mathrm{dx} \\ \mathrm{k}_2\ \mathrm{B}' \displaystyle\int \theta\, \mathrm{dy} \end{Bmatrix}$$

Since the Navier solution is used, the four displacement components' solutions are expressed in terms of the trigonometric sine and the cosine functions. The constants λ and μ link their integrals and derivatives. Using this property, the integrals and the derivatives of the shear displacement θ are expressed in equation (25).

$$\frac{\partial}{\partial y}\int \theta\, dx = A'\frac{\partial^2\theta}{\partial x\partial y}\,, \qquad \frac{\partial}{\partial x}\int \theta\, dy = B'\frac{\partial^2\theta}{\partial x\partial y}\,,$$
$$\int \theta\, dx = A'\frac{\partial\theta}{\partial x}\,, \int \theta\, dy = B'\frac{\partial\theta}{\partial y} \tag{25}$$

This simplification comes from a feature of the derivative and integral of the $Sine$ and $Cosine$ functions used in the solution. The coefficients $\mathrm{k}_1,\ \mathrm{k}_2,\ A^{'},\ B^{'},\ \lambda,\ \mu$ are defined in equation (26).

$$A' = -\frac{1}{\lambda^2}\,, B' = -\frac{1}{\mu^2}\,, \qquad k_1 = \lambda^2\,, k_2 = \mu^2, \qquad \lambda = \frac{m\,\pi}{a}\,, \mu = \frac{\mathrm{n}\,\pi}{b} \tag{26}$$

3.5.2.2 Stress Tensor

The stress tensor is derived from the strain tensor in equation (27).

$$\sigma = \begin{Bmatrix} \sigma_x \\ \sigma_y \\ \tau_{xy} \\ \tau_{yz} \\ \tau_{xz} \end{Bmatrix} = \begin{bmatrix} C_{11} & C_{12} & 0 & 0 & 0 \\ C_{12} & C_{22} & 0 & 0 & 0 \\ 0 & 0 & C_{44} & 0 & 0 \\ 0 & 0 & 0 & C_{55} & 0 \\ 0 & 0 & 0 & 0 & C_{66} \end{bmatrix} . \begin{Bmatrix} \varepsilon_x - \alpha\Delta T - \beta\Delta C \\ \varepsilon_y - \alpha\Delta T - \beta\Delta C \\ \gamma_{xy} \\ \gamma_{yz} \\ \gamma_{xz} \end{Bmatrix} \tag{27}$$

The parameters C_{ij} are expressed as follows:

$$C_{11} = C_{22} = \frac{E}{1-v^2}\,,\ C_{12} = \frac{v\,E}{1-v^2}\,, C_{44} = C_{55} = C_{66} =\ C_{12} = \frac{v\,E}{2(1-v^2)}$$

α and β are the temperature and humidity coefficients, respectively, $\Delta T\ and\ \Delta C$ are the temperature and humidity gradients through the thickness and are described in equation (28).

$$\Delta T(x,y,z,t) = T_1(x,y,t) + \frac{z}{h}T_2(x,y,t) + \frac{f(z)}{h}T_3(x,y,t)$$
$$\Delta C(x,y,z,t) = C_1(x,y,t) + \frac{z}{h}C_2(x,y,t) + \frac{f(z)}{h}C_3(x,y,t) \tag{28}$$

where T_1, T_2, T_3 are the temperature loads and C_1, C_2, C_3 are the humid environment loads.

3.6 Governing Equations

After setting the strain and the stress tensors, we use the principle of virtual work to generate the governing differential equations. The principle applies the integral for the product of the stress and the variation of the strain in the xy domain first and then integrates along the plate thickness as shown in equation (29).

$$\int_{\frac{-h}{2}}^{\frac{h}{2}} \int_{\Omega} \left[\sigma_x \delta\varepsilon_x + \sigma_y \delta\varepsilon_y + \tau_{xy}\delta\gamma_{xy} + \tau_{xz}\delta\gamma_{xz} + \tau_{yz}\delta\gamma_{yz}\right] d\Omega\, dz$$
$$- \int_{\Omega} (q - f_e)\, \delta w\, d\Omega = 0 \tag{29}$$

where q is the mechanical load applied along the transverse direction (z) of the plate and f_e is the force coming from the foundation. The force is described according to the viscoelastic Winkler-Pasternack model [16] as shown in equation (30).

$$f_e = k_w\, w(x,y,t) - k_{p1} \frac{\partial^2 w(x,y,t)}{\partial x^2} - k_{p2} \frac{\partial^2 w(x,y,t)}{\partial y^2} + C_t \frac{\partial w(x,y,t)}{\partial t} \tag{30}$$

where $k_{\mathrm{p1}}\ and\ k_{\mathrm{p2}}$ are the shear parameters, k_w is the Winkler parameter, C_t is the damping coefficient.

By applying the principle of the first variation and substituting the expressions of stress and strain from equation (23), and integrating through the thickness, we get the following relation:

$$\int_{\Omega} \left[N_x \delta\varepsilon_x^0 + N_y \delta\varepsilon_y^0 + N_{xy}\delta\varepsilon_{xy}^0 + M_x^b \delta k_x^b + M_y^b \delta k_y^b + M_{xy}^b \delta k_{xy}^b\right.$$
$$\left. + M_x^s \delta k_x^s + M_y^s \delta k_y^s + M_{xy}^s \delta k_{xy}^s + S_{yz}^s \gamma_{yz}^s + S_{xz}^s \gamma_{xz}^s\right] d\Omega - \int_{\Omega} (q - f_e)\delta w d\Omega = 0 \tag{31}$$

The governing differential equations are expressed by setting the coefficient of the four-displacement variables $\delta u_0, \delta v_0, \delta w_0, \delta\theta$ to zero after using integration by parts to integrate the displacement gradients.

$$\delta u_0 : \quad \frac{\partial N_x}{\partial x} + \frac{\partial N_{xy}}{\partial y} = 0$$

$$\delta v_0 : \quad \frac{\partial N_y}{\partial y} + \frac{\partial N_{xy}}{\partial x} = 0$$

$$\delta w_0 : \quad \frac{\partial^2 M_X^b}{\partial x^2} + 2\frac{\partial^2 M_{xy}^b}{\partial x \partial y} + \frac{\partial^2 M_y^b}{\partial y^2} + q - f_e = 0 \tag{32}$$

$$\delta\theta : \quad -A'k_1 \frac{\partial^2 M_{xy}^s}{\partial x \partial y} - B'k_2 \frac{\partial^2 M_{xy}^s}{\partial x \partial y} - k_1 M_x^s - k_2 M_y^s + A'k_1 \frac{\partial S_{xz}}{\partial x} + B'k_2 \frac{\partial S_{yz}}{\partial y} = 0$$

The resultant forces N, M, S are expressed as:

$$\begin{bmatrix} N_x & N_y & N_{xy} \\ M_x^b & M_y^b & M_{xy}^b \\ M_x^s & M_y^s & M_{xy}^s \end{bmatrix} = \int_{-\frac{h}{2}}^{\frac{h}{2}} \begin{Bmatrix} 1 \\ z \\ f(z) \end{Bmatrix} . \left(\sigma_x, \sigma_y, \tau_{xy}\right) dz,$$

$$\begin{Bmatrix} S_{xz} \\ S_{yz} \end{Bmatrix} = \int_{-\frac{h}{2}}^{\frac{h}{2}} \begin{Bmatrix} \tau_{xz} \\ \tau_{yz} \end{Bmatrix} dz\, g(z) \tag{33}$$

3.7 Analytical solution

The analytical solution is obtained using the Navier method. The middle plane displacements are expressed by unknown constants $(U_0, V_0, W_0, \theta_0)$. They are multiplied by the $Sine, Cosine$ functions to satisfy the simply supported plate boundary conditions.

$$\begin{Bmatrix} u_0 \\ v_0 \\ w_0 \\ \theta \end{Bmatrix} = \sum_{m=1}^{\infty} \sum_{n=1}^{\infty} \begin{Bmatrix} U_0\, cos(\lambda\, x)\, sin(\mu\, y) \\ V_0\, sin(\lambda\, x)\, cos(\mu\, y) \\ W_0\, sin(\lambda\, x)\, sin(\mu\, y) \\ \theta_0\, sin(\lambda\, x)\, sin(\mu\, y) \end{Bmatrix} \cdot e^{(i\omega t)} \tag{34}$$

where ω is the circular frequency, i is the imaginary unit, and λ, μ are defined in equation (26), while m, n are the half wave numbers. The loads on the plate are also expressed in the Fourier form as follows:

$$\begin{Bmatrix} q \\ T_1 \\ T_2 \\ T_3 \\ C_1 \\ C_2 \\ C_3 \end{Bmatrix} = \sum_{m=1}^{\infty} \sum_{n=1}^{\infty} \begin{Bmatrix} q_0 \sin(\lambda\, x) \sin(\mu\, y) \\ t_1 \sin(\lambda\, x) \sin(\mu\, y) \\ t_2 \sin(\lambda\, x) \sin(\mu\, y) \\ t_3 \sin(\lambda\, x) \sin(\mu\, y) \\ c_1 \sin(\lambda\, x) \sin(\mu\, y) \\ c_2 \sin(\lambda\, x) \sin(\mu\, y) \\ c_3 \sin(\lambda\, x) \sin(\mu\, y) \end{Bmatrix} \cdot e^{(i\omega t)} \tag{35}$$

where q represents the uniform mechanical load, T_1, T_2, T_3 are the temperature loads, and C_1, C_2, C_3 are the moisture loads or the humid environment loads. The coefficients $q_0, t_1, t_2, t_3, c_1, c_2, c_3$ are the hygro-thermo-mechanical loads' coefficients.

Now, the supposed forms of the loads and the middle plane displacements are substituted in the governing differential equations to produce the following system of equations:

$$[A]\{\Delta\} = \{P\} \tag{36}$$

The vector $\{\Delta\}$ represents the displacement coefficients U_0, V_0, W_0, θ_0 and the $[A]$ matrix is expressed as:

$$[A] = \begin{bmatrix} a_{11} & a_{12} & a_{13} & a_{14} \\ a_{12} & a_{22} & a_{23} & a_{24} \\ a_{13} & a_{23} & a_{33} & a_{34} \\ a_{14} & a_{24} & a_{34} & a_{44} \end{bmatrix} \tag{37}$$

Matrix $[A]$ is symmetric, and its elements are shown in equation (38). The circular frequency of the viscous foundation is incorporated in the element a_{33} and given the value of 0.5 which is multiplied by the damping coefficient.

$$
\begin{aligned}
a_{11} &= -A_{66}\mu^2 - A_{11}\lambda^2 \\
a_{12} &= A_{12}(-\lambda)\mu + A_{66}(-\lambda)\mu \\
a_{13} &= B_{11}\lambda^3 + B_{12}\lambda\mu^2 + 2B_{66}\lambda\mu^2 \\
a_{14} &= A'd_{11}\lambda^3(-K_1) - A'D_{66}\lambda K_1\mu^2 + B'D_{12}\lambda(-K_2)\mu^2 - B'D_{66}\lambda \mathrm{K}_2\mu^2 \\
a_{22} &= A_{22}(-\mu^2) + A_{66}(-\lambda^2) \\
a_{23} &= B_{12}\lambda^2\mu + B_{22}\mu^3 + 2B_{66}\lambda^2\mu \\
a_{24} &= -A'D_{12}\lambda^2K_1\mu - A'D_{66}\lambda^2K_1\mu + B'D_{22}(-K_2)\mu^3 - B'D_{66}\lambda^2K_2\mu \\
a_{33} &= -\mathrm{i}\ 0.5\ \mathrm{c_t} - E_{11}\lambda^4 - 2E_{12}\lambda^2\mu^2 - E_{22}\mu^4 - 4E_{66}\lambda^2\mu^2 - \lambda^2K_{\mathrm{sl}} - K_{\mathrm{s2}}\mu^2 \\
&\qquad - K_{\mathrm{W}} \\
a_{34} &= A'F_{11}\lambda^4K_1 + A'F_{12}\lambda^2K_1\mu^2 + 2A'F_{66}\lambda^2K_1\mu^2 + B'F_{12}\lambda^2K_2\mu^2 \\
&\qquad + B'F_{22}K_2\mu^4 + 2B'F_{66}\lambda^2K_2\mu^2 \\
a_{44} &= -A_{s44}{B'}^2K_2^2\mu^2 + A_{s55}A^2\lambda^2(-K_1^2) \\
&\qquad + A'(-K_1)(A'G_{11}\lambda^4K_1 + B'G_{12}\lambda^2K_2\mu^2) \\
&\qquad - B'K_2(A'G_{12}\lambda^2K_1\mu^2 + B'G_{22}K_2\mu^4) \\
&\qquad - (A'K_l + B'K_2)(A'G_{66}\lambda^2K_l\mu^2 + B'G_{66}\lambda^2K_2\mu^2)
\end{aligned}
\tag{38}
$$

where:

$$
\begin{gathered}
\left(A_{ij}, B_{ij}, D_{ij}, E_{ij}, F_{ij}, G_{ij}\right) = \int_{-h/2}^{h/2} C_{ij}(1, z, f(z), z^2, zf(z), f(z)^2)dz \\
(i,j) = (1,2,6) \\
A_{ij}^s = \int_{-h/2}^{h/2} C_{ij}g(z)^2dz, (i,j) = (4,5)
\end{gathered}
\tag{39}
$$

The generalized force vector $\{P\}$ components are expressed as follows:

$$
\begin{aligned}
P_1 &= -\lambda\left(\left(L_1^T t_1 + \frac{M_1^T}{h} t_2 + \frac{M_1^{Ts}}{h} t_3\right) + \left(L_1^c c_1 + \frac{M_1^c}{h} c_2 + \frac{M_1^{cs}}{h} c_3\right)\right) \\
P_2 &= -\mu\left(\left(L_2^T t_1 + \frac{M_2^T}{h} t_2 + \frac{M_2^{Ts}}{h} t_3\right) + \left(L_2^c c_1 + \frac{M_2^c}{h} c_2 + \frac{M_2^{cs}}{h} c_3\right)\right) \\
P_3 &= -\left(\begin{array}{c} \left(M_1^T(\lambda^2+\mu^2)\right) t_1 + \dfrac{\left(N_1^T(\lambda^2+\mu^2)\right)}{h} t_2 + \dfrac{\left(N_1^{Ts}(\lambda^2+\mu^2)\right)}{h} t_3 \\ +\left(M_1^c(\lambda^2+\mu^2)\right) c_1 + \dfrac{\left(N_1^c(\lambda^2+\mu^2)\right)}{h} c_2 + \dfrac{\left(N_1^{cs}(\lambda^2+\mu^2)\right)}{h} c_3\Big) + q_0 \end{array}\right) \\
P_4 &= -\left(\begin{array}{c} M_1^{Ts}(A'k_1 + B'k_2) t_1 + \dfrac{\left((A'k_1 + B'k_2) N_1^{Ts}\right)}{h} \quad t_2 + \dfrac{\left((A'k_1 + B'k_2) H_1^{T_s}\right)}{h} t_3 \\ +\left((A'k_1 + B'k_2) M_1^{cs}\right) c_1 + \dfrac{\left((A'k_1 + Mk_2) N_1^{cs}\right)}{h} \quad c_2 + \dfrac{\left((A'k_1 + Mk_2) H_1^{cs}\right)}{h} \end{array}\right)
\end{aligned} \tag{40}
$$

where:

$$
\begin{aligned}
\left(L_i^T, M_i^T, N_i^T, M_i^{Ts}, N_i^{Ts}, H_i^{Ts}\right) &= \int_{-h/2}^{h/2} \alpha(z) C_{ij}\left(1, z, z^2, f(z), zf(z), f(z)^2\right) \mathrm{dz} \\
\left(L_i^C, M_i^C, N_i^C, M_i^{Cs}, N_i^{Cs}, H_i^{Cs}\right) &= \int_{-h/2}^{h/2} \beta(z) C_{ij}\left(1, z, z^2, f(z), zf(z), f(z)^2\right) \mathrm{dz}
\end{aligned} \tag{41}
$$

$$, (i,j) = (1,2)$$

3.8 Numerical Results and Discussion

The effect of the loads and Pasternak viscoelastic foundation on the FGM plate is discussed in this section with various numerical examples. The deflection and stresses of the plate are studied in various combinations of hygro-thermal environments. The plate is constructed from metal, here Titanium, and ceramic. The following table shows the mechanical material properties used in the analysis.

Table 1 Mechanical material properties of Titanium & Ceramic

Material	E (GPa)	ν	$\alpha(10^{-6}/^{o}C)$	β
Metal (Titanium, Ti-6A1-4V)	66.2	0.33	10.3	0.33
Ceramic (Zirconia, ZrO_2)	117	0.33	7.11	0

Non-dimensional stresses, deflection, and foundation parameters are used in finding the results as follows:

The central deflection: $\bar{w} = \frac{100D}{q_0 a^4} w\left(\frac{a}{2}, \frac{b}{2}, 0\right)$

Axial stress: $\bar{\sigma}_x = \frac{1}{100 q_0} \sigma_x \left(\frac{a}{2}, \frac{b}{2}, \frac{h}{2}\right)$

Longitudinal shear stress: $\bar{\tau}_{xy} = \frac{1}{10 q_0} \tau_{xy} \left(0,0,-\frac{h}{3}\right)$

Transverse shear stress: $\bar{\tau}_{xz} = \frac{1}{10 q_0} \tau_{xz} \left(0, \frac{b}{2}, z\right)$

Winkler foundation parameter: $k_w = \frac{a^4 k_w}{D}$

Pasternak foundation parameters: $k_{p1} = \frac{a^2 k_{p1}}{D}, k_{p2} = \frac{b^2 k_{p2}}{D}, C_t = \frac{c_t D \times 10^3}{a^4}$

where $D = \frac{E h^3}{12(1-\nu^2)}$.

Table 2 shows the sinusoidal loads' effect on the central non-dimensional deflection of a square FGM plate resting on a viscoelastic foundation with different material gradient index (p) values. The result shows that the Winkler viscoelastic foundation gives higher deflection values than the Pasternak viscoelastic foundation. Higher deflection is noticed when the plate is exposed to hygro-thermal loads than when subjected to a purely mechanical load. It is noticed that plate deflection tends to decrease when increasing the damping effect of the viscoelastic foundation (C_t). Furthermore, a noticeable reduction in the deflection is noticed when increasing the viscoelastic damping coefficient for any kind of loading. Moreover, reducing the plate rigidity by increasing the gradient index causes a noticeable increase in the plate's central deflection. This means that deflection is maximum for $p = \infty$ and minimum for $p = 0$.

Under the same loading conditions, deflection tends to decline by increasing the FGM plate's geometrical ratio (a/h). Also, the effect of the viscoelastic foundation parameters on the non-dimensional vertical displacement is greater for thick plates.

Table 2 Influence of gradient index (p) on the non-dimensional deflections of FGM square (b=a) plates resting on a viscoelastic foundation and under hygro-thermo-mechanical loading $(q_0 = 100)$

P	k_w	k_{p1}	k_{p2}	t_1	t_2	t_3	c_1	c_2	c_3	a/h=5					a/h=10					a/h=20				
										Ref[a]	Present				Ref[a]	Present				Ref[a]	Present			
										$\bar{c}_t = 0$	$\bar{c}_t = 0$	$\bar{c}_t = 0.05$	$\bar{c}_t = 0.1$	$\bar{c}_t = 1$	$\bar{c}_t = 0$	$\bar{c}_t = 0$	$\bar{c}_t = 0.05$	$\bar{c}_t = 0.1$	$\bar{c}_t = 1$	$\bar{c}_t = 0$	$\bar{c}_t = 0$	$\bar{c}_t = 0.05$	$\bar{c}_t = 0.1$	$\bar{c}_t = 1$
	100	0	0	0	0	0	0	0	0	0.2350	**0.2405**	**0.2268**	**0.2146**	**0.1092**	0.2122	**0.2136**	**0.2028**	**0.1930**	**0.1033**	0.2062	**0.2066**	**0.1965**	**0.1873**	**0.1016**
				0	10	0	0	100	0	1.8390	**1.8330**	**1.7290**	**1.6362**	**0.8323**	0.6251	**0.6258**	**0.5941**	**0.5654**	**0.3026**	0.3107	**0.3106**	**0.2953**	**0.2815**	**0.1528**
				0	10	10	0	100	100	3.4058	**3.0253**	**2.8537**	**2.7006**	**1.3737**	0.9574	**0.9354**	**0.8879**	**0.8451**	**0.4523**	0.3894	**0.3887**	**0.3696**	**0.3523**	**0.1912**
	0	100	100	0	0	0	0	0	0	0.0434	**0.0437**	**0.0432**	**0.0427**	**0.0358**	0.0426	**0.0427**	**0.0422**	**0.0418**	**0.0352**	0.0424	**0.0424**	**0.0420**	**0.0415**	**0.0350**
0				0	10	0	0	100	0	0.3404	**0.3329**	**0.3293**	**0.3258**	**0.2732**	0.1256	**0.1251**	**0.1238**	**0.1225**	**0.1031**	0.0638	**0.0638**	**0.0631**	**0.0624**	**0.0526**
				0	10	10	0	100	100	0.6305	**0.5494**	**0.5435**	**0.5377**	**0.4510**	0.1924	**0.1869**	**0.1850**	**0.1830**	**0.1541**	0.0800	**0.0798**	**0.0790**	**0.0781**	**0.0658**
	100	100	100	0	0	0	0	0	0	0.0416	**0.0418**	**0.0414**	**0.0410**	**0.0346**	0.0409	**0.0409**	**0.0405**	**0.0401**	**0.0340**	0.0407	**0.0407**	**0.0403**	**0.0399**	**0.0338**
				0	10	0	0	100	0	0.3262	**0.3190**	**0.3157**	**0.3124**	**0.2638**	0.1208	**0.1200**	**0.1187**	**0.1176**	**0.0996**	0.0612	**0.0612**	**0.0605**	**0.0599**	**0.0508**
				0	10	10	0	100	100	0.6042	**0.5265**	**0.5210**	**0.5157**	**0.4354**	0.1845	**0.1793**	**0.1775**	**0.1757**	**0.1488**	0.0768	**0.0765**	**0.0758**	**0.0750**	**0.0636**
	100	0	0	0	0	0	0	0	0	0.2862	**0.2923**	**0.2724**	**0.2550**	**0.1187**	0.2607	**0.2623**	**0.2462**	**0.2319**	**0.1135**	0.2540	**0.2544**	**0.2392**	**0.2257**	**0.1120**
				0	10	0	0	100	0	2.4129	**2.0862**	**1.9441**	**1.8202**	**0.8476**	0.8115	**0.7299**	**0.6850**	**0.6453**	**0.3158**	0.3936	**0.3726**	**0.3503**	**0.3305**	**0.1640**
				0	10	10	0	100	100	4.2935	**3.4318**	**3.1981**	**2.9942**	**1.3942**	1.2118	**1.0817**	**1.0152**	**0.9563**	**0.4679**	0.4991	**0.4616**	**0.4340**	**0.4095**	**0.2031**
	0	100	100	0	0	0	0	0	0	0.0450	**0.0451**	**0.0446**	**0.0441**	**0.0368**	0.0443	**0.0443**	**0.0439**	**0.0434**	**0.0363**	0.0441	**0.0441**	**0.0436**	**0.0432**	**0.0361**
1				0	10	0	0	100	0	0.3806	**0.3221**	**0.3185**	**0.3150**	**0.2628**	0.1383	**0.1234**	**0.1220**	**0.1207**	**0.1010**	0.0683	**0.0646**	**0.0639**	**0.0632**	**0.0529**
				0	10	10	0	100	100	0.7053	**0.5298**	**0.5239**	**0.5181**	**0.4323**	0.2133	**0.1828**	**0.1808**	**0.1789**	**0.1497**	0.0866	**0.0800**	**0.0792**	**0.0783**	**0.0656**
	100	100	100	0	0	0	0	0	0	0.0430	**0.0432**	**0.0427**	**0.0423**	**0.0355**	0.0424	**0.0425**	**0.0420**	**0.0416**	**0.0350**	0.0422	**0.0422**	**0.0418**	**0.0414**	**0.0349**
				0	10	0	0	100	0	0.3630	**0.3082**	**0.3049**	**0.3017**	**0.2535**	0.1320	**0.1181**	**0.1169**	**0.1157**	**0.0975**	0.0654	**0.0619**	**0.0612**	**0.0606**	**0.0511**
				0	10	10	0	100	100	0.6749	**0.5070**	**0.5015**	**0.4962**	**0.4169**	0.2043	**0.1751**	**0.1732**	**0.1714**	**0.1444**	0.0830	**0.0766**	**0.0758**	**0.0751**	**0.0633**
	100	0	0	0	0	0	0	0	0	0.3007	**0.3075**	**0.2855**	**0.2665**	**0.1212**	0.2732	**0.2750**	**0.2573**	**0.2418**	**0.1158**	0.2659	**0.2664**	**0.2498**	**0.2351**	**0.1142**
				0	10	0	0	100	0	2.5118	**2.1253**	**1.9736**	**1.8421**	**0.8376**	0.8483	**0.7512**	**0.7029**	**0.6604**	**0.3163**	0.4118	**0.3869**	**0.3627**	**0.3414**	**0.1659**
				0	10	10	0	100	100	4.6982	**3.4853**	**3.2365**	**3.0209**	**1.3736**	1.3138	**1.1086**	**1.0373**	**0.9746**	**0.4667**	0.5222	**0.4774**	**0.4476**	**0.4213**	**0.2047**
	0	100	100	0	0	0	0	0	0	0.0453	**0.0455**	**0.0450**	**0.0445**	**0.0370**	0.0446	**0.0447**	**0.0442**	**0.0437**	**0.0365**	0.0444	**0.0445**	**0.0440**	**0.0435**	**0.0364**
2				0	10	0	0	100	0	0.3786	**0.3143**	**0.3108**	**0.3073**	**0.2561**	0.1386	**0.1221**	**0.1207**	**0.1194**	**0.0998**	0.0688	**0.0646**	**0.0639**	**0.0632**	**0.0528**
				0	10	10	0	100	100	0.7083	**0.5154**	**0.5096**	**0.5040**	**0.4199**	0.2147	**0.1801**	**0.1782**	**0.1762**	**0.1472**	0.0872	**0.0797**	**0.0788**	**0.0779**	**0.0652**
	100	100	100	0	0	0	0	0	0	0.0434	**0.0435**	**0.0430**	**0.0426**	**0.0357**	0.0427	**0.0428**	**0.0423**	**0.0419**	**0.0352**	0.0425	**0.0426**	**0.0421**	**0.0417**	**0.0351**
				0	10	0	0	100	0	0.3623	**0.3006**	**0.2974**	**0.2942**	**0.2469**	0.1327	**0.1168**	**0.1156**	**0.1144**	**0.0963**	0.0659	**0.0618**	**0.0612**	**0.0605**	**0.0510**
				0	10	10	0	100	100	0.6776	**0.4930**	**0.4877**	**0.4825**	**0.4049**	0.2055	**0.1724**	**0.1706**	**0.1688**	**0.1421**	0.0835	**0.0763**	**0.0755**	**0.0747**	**0.0629**
	100	0	0	0	0	0	0	0	0	0.3154	**0.3230**	**0.2989**	**0.2781**	**0.1235**	0.2854	**0.2875**	**0.2682**	**0.2514**	**0.1180**	0.2774	**0.2780**	**0.2600**	**0.2441**	**0.1163**
5				0	10	0	0	100	0	2.6252	**2.1712**	**2.0090**	**1.8693**	**0.8303**	0.8892	**0.7745**	**0.7225**	**0.6771**	**0.3177**	0.4308	**0.4014**	**0.3753**	**0.3524**	**0.1680**
				0	10	10	0	100	100	4.9469	**3.5501**	**3.2849**	**3.0565**	**1.3576**	1.3799	**1.1390**	**1.0626**	**0.9959**	**0.4673**	0.5469	**0.4939**	**0.4618**	**0.4336**	**0.2066**
	0	100	100	0	0	0	0	0	0	0.0456	**0.0458**	**0.0453**	**0.0448**	**0.0373**	0.0449	**0.0450**	**0.0445**	**0.0440**	**0.0367**	0.0447	**0.0448**	**0.0443**	**0.0438**	**0.0366**

				0	10	0	0	100	0	0.3800	**0.3079**	**0.3044**	**0.3010**	**0.2505**	0.1400	**0.1212**	**0.1199**	**0.1186**	**0.0990**	0.0695	**0.0646**	**0.0639**	**0.0632**	**0.0528**
				0	10	10	0	100	100	0.7161	**0.5034**	**0.4977**	**0.4921**	**0.4096**	0.2173	**0.1783**	**0.1763**	**0.1744**	**0.1456**	0.0882	**0.0795**	**0.0787**	**0.0778**	**0.0650**
	100	100	100	0	0	0	0	0	0	0.0436	**0.0438**	**0.0433**	**0.0429**	**0.0359**	0.0430	**0.0431**	**0.0426**	**0.0422**	**0.0354**	0.0428	**0.0429**	**0.0424**	**0.0420**	**0.0353**
				0	10	0	0	100	0	0.3634	**0.2944**	**0.2912**	**0.2881**	**0.2415**	0.1340	**0.1160**	**0.1148**	**0.1136**	**0.0955**	0.0665	**0.0619**	**0.0612**	**0.0606**	**0.0510**
				0	10	10	0	100	100	0.6849	**0.4813**	**0.4761**	**0.4710**	**0.3949**	0.2080	**0.1706**	**0.1688**	**0.1670**	**0.1404**	0.0844	**0.0761**	**0.0753**	**0.0745**	**0.0627**
	100	0	0	0	0	0	0	0	0	0.3519	**0.3588**	**0.3292**	**0.3042**	**0.1284**	0.3224	**0.3244**	**0.3001**	**0.2791**	**0.1237**	0.3146	**0.3152**	**0.2922**	**0.2723**	**0.1224**
				0	10	0	0	100	0	2.9516	**2.3127**	**2.1223**	**1.9609**	**0.8278**	1.0017	**0.8391**	**0.7761**	**0.7220**	**0.3200**	0.4872	**0.4456**	**0.4131**	**0.3849**	**0.1730**
				0	10	10	0	100	100	5.4908	**3.7755**	**3.4647**	**3.2012**	**1.3513**	1.5485	**1.2256**	**1.1336**	**1.0545**	**0.4674**	0.6173	**0.5436**	**0.5039**	**0.4696**	**0.2110**
	0	100	100	0	0	0	0	0	0	0.0463	**0.0465**	**0.0459**	**0.0454**	**0.0377**	0.0458	**0.0458**	**0.0453**	**0.0448**	**0.0373**	0.0456	**0.0456**	**0.0451**	**0.0446**	**0.0372**
∞				0	10	0	0	100	0	0.3888	**0.2994**	**0.2960**	**0.2926**	**0.2430**	0.1422	**0.1185**	**0.1172**	**0.1159**	**0.0964**	0.0706	**0.0645**	**0.0638**	**0.0631**	**0.0525**
				0	10	10	0	100	100	0.7233	**0.4889**	**0.4832**	**0.4778**	**0.3967**	0.2198	**0.1731**	**0.1712**	**0.1692**	**0.1409**	0.0895	**0.0787**	**0.0778**	**0.0770**	**0.0641**
	100	100	100	0	0	0	0	0	0	0.0443	**0.0444**	**0.0439**	**0.0434**	**0.0363**	0.0437	**0.0438**	**0.0433**	**0.0429**	**0.0359**	0.0436	**0.0436**	**0.0432**	**0.0427**	**0.0358**
				0	10	0	0	100	0	0.3716	**0.2862**	**0.2830**	**0.2799**	**0.2342**	0.1360	**0.1133**	**0.1121**	**0.1109**	**0.0930**	0.0675	**0.0617**	**0.0610**	**0.0604**	**0.0507**
				0	10	10	0	100	100	0.6913	**0.4672**	**0.4620**	**0.4570**	**0.3823**	0.2102	**0.1655**	**0.1637**	**0.1620**	**0.1358**	0.0856	**0.0753**	**0.0745**	**0.0737**	**0.0618**

Ref[a] *Taken from Sayyad and Ghugal* [61]

Table 3 Influence of gradient index on non-dimensional deflections and stresses of FGM rectangular plates $(b/a = 3)$ subjected to pure mechanical load and resting on a viscoelastic foundation.

p	k_w	k_{p1}	k_{p2}	*Theory*	$\bar{c}_t$	$\bar{w}$	$\bar{\sigma}_x$	$\bar{\sigma}_{xy}$	$\bar{\sigma}_{xz}$
0	100	100	100	CPT	$\bar{c}_t = 0$	0.08201	0.05035	0.07193	-
				Mindlin [3]	$\bar{c}_t = 0$	0.08228	0.04890	0.06986	0.03293
				Touratier [9]	$\bar{c}_t = 0$	0.08227	0.04919	0.06972	0.04246
				Reddy [62]	$\bar{c}_t = 0$	0.08228	0.04919	0.06972	0.04116
				Zidi et al. [63]	$\bar{c}_t = 0$	0.08228	0.04919	0.06972	0.04116
				Ref[(a)]	$\bar{c}_t = 0$	0.08227	0.04927	0.07068	0.03700
				Present	$\bar{c}_t = 0$	**0.08226**	**0.04920**	**0.07009**	**0.04356**
					$\bar{c}_t = 0.05$	**0.08061**	**0.04821**	**0.06867**	**0.04268**
					$\bar{c}_t = 0.1$	**0.07901**	**0.04726**	**0.06732**	**0.04184**
					$\bar{c}_t = 1$	**0.05829**	**0.03486**	**0.04966**	**0.03087**
1	100	100	100	CPT	$\bar{c}_t = 0$	0.08399	0.04683	0.05353	-
				Mindlin [3]	$\bar{c}_t = 0$	0.08418	0.04546	0.05198	0.02572
				Touratier [9]	$\bar{c}_t = 0$	0.08418	0.04574	0.05191	0.03318
				Reddy [62]	$\bar{c}_t = 0$	0.08417	0.04574	0.05190	0.03214
				Zidi et al. [63]	$\bar{c}_t = 0$	0.08418	0.04574	0.05190	0.03214
				Ref[(a)]	$\bar{c}_t = 0$	0.08416	0.04580	0.05181	0.02924
				Present	$\bar{c}_t = 0$	**0.08417**	**0.04575**	**0.05217**	**0.03403**
					$\bar{c}_t = 0.05$	**0.08244**	**0.04480**	**0.05109**	**0.03333**
					$\bar{c}_t = 0.1$	**0.08077**	**0.04390**	**0.05006**	**0.03265**
					$\bar{c}_t = 1$	**0.05924**	**0.03220**	**0.03672**	**0.02395**
2	100	100	100	CPT	$\bar{c}_t = 0$	0.08437	0.04655	0.04931	-
				Mindlin [3]	$\bar{c}_t = 0$	0.08457	0.04515	0.04781	0.02303
				Touratier [9]	$\bar{c}_t = 0$	0.08457	0.04540	0.04770	0.03050
				Reddy [62]	$\bar{c}_t = 0$	0.08457	0.04539	0.04770	0.02951
				Zidi et al. [63]	$\bar{c}_t = 0$	0.08457	0.04539	0.04770	0.02951
				Ref[(a)]	$\bar{c}_t = 0$	0.08453	0.04549	0.04776	0.02633
				Present	$\bar{c}_t = 0$	**0.08456**	**0.04541**	**0.04794**	**0.03131**
					$\bar{c}_t = 0.05$	**0.08281**	**0.04447**	**0.04695**	**0.03066**
					$\bar{c}_t = 0.1$	**0.08113**	**0.04357**	**0.04600**	**0.03004**
					$\bar{c}_t = 1$	**0.05943**	**0.03192**	**0.03370**	**0.02201**
5	100	100	100	CPT	$\bar{c}_t = 0$	0.08471	0.04780	0.04714	-
				Mindlin [3]	$\bar{c}_t = 0$	0.08491	0.04630	0.04568	0.02085
				Touratier [9]	$\bar{c}_t = 0$	0.08492	0.04656	0.04549	0.02832
				Reddy [62]	$\bar{c}_t = 0$	0.08491	0.04652	0.04549	0.02735
				Zidi et al. [63]	$\bar{c}_t = 0$	0.08491	0.04652	0.04549	0.02735
				Ref[(a)]	$\bar{c}_t = 0$	0.08487	0.04665	0.04616	0.02450
				Present	$\bar{c}_t = 0$	**0.08491**	**0.04655**	**0.04574**	**0.02910**
					$\bar{c}_t = 0.05$	**0.08314**	**0.04558**	**0.04479**	**0.02849**
					$\bar{c}_t = 0.1$	**0.08145**	**0.04465**	**0.04388**	**0.02791**
					$\bar{c}_t = 1$	**0.05960**	**0.03268**	**0.03211**	**0.02043**
∞	100	100	100	CPT	$\bar{c}_t = 0$	0.08569	0.02978	0.04250	-
				Mindlin [3]	$\bar{c}_t = 0$	0.08584	0.02888	0.04126	0.01943
				Touratier [9]	$\bar{c}_t = 0$	0.08584	0.02906	0.04116	0.02507
				Reddy [62]	$\bar{c}_t = 0$	0.08584	0.02905	0.04115	0.02428
				Zidi et al. [63]	$\bar{c}_t = 0$	0.08584	0.02905	0.04115	0.02428
				Ref[(a)]	$\bar{c}_t = 0$	0.08582	0.02909	0.04174	0.02184
				Present	$\bar{c}_t = 0$	**0.08583**	**0.02905**	**0.04137**	**0.02572**
					$\bar{c}_t = 0.05$	**0.08403**	**0.02844**	**0.04050**	**0.02518**
					$\bar{c}_t = 0.1$	**0.08230**	**0.02785**	**0.03967**	**0.02466**
					$\bar{c}_t = 1$	**0.06006**	**0.02033**	**0.02895**	**0.01799**

Ref[(a)] *Taken from Sayyad and Ghugal* [61]

Table 3 presents the influence of elevating the gradient index (p) on the deflection and stresses of the FGM plate subjected to pure bending while keeping the Winkler and Pasternak coefficients constants. When setting the viscoelastic foundation's damping effect to $zero$, the deflection is of good agreement with both, the classical plate theory and the results taken from the literature as shown in the same table. It is important to observe that elevating the value of the gradient index causes an increase in the central deflection and a decrease in the longitudinal and shear stresses of the FGM plate. Furthermore, when increasing the viscoelastic foundation damping value (C_t), the deflection and stresses of the FGM plate declined noticeably. This fact shows that plate design capacity is greatly influenced by considering the viscoelastic foundation effect.

Table 4 illustrates the impact of including the linear hygro-thermal load, along with the mechanical loading on a rectangular FGM plate supported by a viscoelastic foundation. The deflection and stresses are higher than the case for pure bending noticed in Table 3. This tells us that environment influences the durability of the material and the induced stresses and deflection. It is also observed that with increasing the material index p from $zero$ to $infinity$, deflection tends to increase and stresses to decrease. Additionally, elevating the viscoelastic foundation damping coefficient C_t, reduces both deflection and stresses, as illustrated in Figure 2.

When considering the case of the combined mechanical and nonlinear hygro-thermal loads presented in Table 5, it is noticed that stresses and deflection are sharper than the two cases of linear hygro-thermo-mechanical loads presented in Table 3, and the pure mechanical load shown in Table 4. This noticeable rise is attributed to the expansion of the plate under elevated temperatures.

Table 4 Influence of gradient index on non-dimensional deflections and stresses of AFG rectangular plates resting on a viscoelastic foundation and under linear hygro-thermo-mechanical load $(a/h = 10, q_0 = 100, t_1 = t_3 = 0, t_2 = 10, c_1 = c_3 = 0, c_2 = 100)$

p	k_w	k_{p1}	k_{p2}	*Theory*	$\bar{c}_t$	$\bar{w}$	$\bar{\sigma}_x$	$\bar{\sigma}_{xy}$	$\bar{\sigma}_{xz}$
0	100	100	100	Zidi et al.[63]	$\bar{c}_t = 0$	0.17309	-0.50498	0.17490	0.38766
				Present	$\bar{c}_t = 0$	**0.17266**	**-0.50297**	**0.17581**	**-0.40819**
					$\bar{c}_t = 0.05$	**0.16918**	**-0.50505**	**0.17285**	**-0.41004**
					$\bar{c}_t = 0.1$	**0.16584**	**-0.50705**	**0.17000**	**-0.41181**
					$\bar{c}_t = 1$	**0.12234**	**-0.53307**	**0.13294**	**-0.43484**
1	100	100	100	Zidi et al.[63]	$\bar{c}_t = 0$	0.18504	-0.51450	0.15631	0.44545
				Present	$\bar{c}_t = 0$	**0.18457**	**-0.51268**	**0.15698**	**-0.46946**
					$\bar{c}_t = 0.05$	**0.18076**	**-0.51475**	**0.15462**	**-0.47099**
					$\bar{c}_t = 0.1$	**0.17711**	**-0.51673**	**0.15236**	**-0.47247**
					$\bar{c}_t = 1$	**0.12990**	**-0.54239**	**0.12310**	**-0.49156**
2	100	100	100	Zidi et al.[63]	$\bar{c}_t = 0$	0.18560	-0.50336	0.13451	0.43831
				Present	$\bar{c}_t = 0$	**0.18511**	**-0.50165**	**0.13522**	**-0.46362**
					$\bar{c}_t = 0.05$	**0.18128**	**-0.50371**	**0.13305**	**-0.46504**
					$\bar{c}_t = 0.1$	**0.17760**	**-0.50569**	**0.13096**	**-0.46640**
					$\bar{c}_t = 1$	**0.13010**	**-0.53120**	**0.10403**	**-0.48399**
5	100	100	100	Zidi et al.[63]	$\bar{c}_t = 0$	0.18696	-0.48940	0.12417	0.43754
				Present	$\bar{c}_t = 0$	**0.18646**	**-0.48782**	**0.12494**	**-0.46400**
					$\bar{c}_t = 0.05$	**0.18259**	**-0.48994**	**0.12285**	**-0.46533**
					$\bar{c}_t = 0.1$	**0.17887**	**-0.49198**	**0.12085**	**-0.46661**
					$\bar{c}_t = 1$	**0.13089**	**-0.51829**	**0.09501**	**-0.48305**
∞	100	100	100	Zidi et al.[63]	$\bar{c}_t = 0$	0.18840	-0.43095	0.12087	0.45993
				Present	$\bar{c}_t = 0$	**0.18791**	**-0.59246**	**0.12150**	**-0.48443**
					$\bar{c}_t = 0.05$	**0.18397**	**-0.59379**	**0.11960**	**-0.48562**
					$\bar{c}_t = 0.1$	**0.18018**	**-0.59508**	**0.11777**	**-0.48675**
					$\bar{c}_t = 1$	**0.13149**	**-0.61156**	**0.09430**	**-0.50134**

An important observation from Tables 4 and 5 is the effect of increasing the viscoelastic foundation damping coefficient. It is noticed that FGM plates with nonlinear hygrothermal loads and a high viscoelastic damping coefficient have similar deflection to FGM plates with linear hygro-thermal loads with a small viscoelastic damping effect.

to Figure 13 show that, for all kinds of loadings, deflection decreases by increasing the damping coefficient C_t.

Figure 14 shows that the normal stress values change from negative to positive when moving from the bottom to the top surface of the plate. When including the non-linear environmental loading, deflection reverses its behavior across the plate thickness.

Table 5 Influence of power-law exponent (p) on the non-dimensional deflection and stresses of FGM rectangular $(b/a = 3)$ plates resting on a viscoelastic foundation subjected to nonlinear hygro-thermo-mechanical loads.

$$(a/h = 10, q_0 = 100, t_1 = 0, t_2 = t_3 = 10, c_1 = 0, c_2 = c_3 = 100)$$

P	$\bar{K}_w$	$\bar{K}_{p1}$	$\bar{K}_{p2}$	*Theory*	$\bar{c}_t$	$\bar{w}$	$\bar{\sigma}_x$	$\bar{\sigma}_{xy}$	$\bar{\sigma}_{xz}$
0	100	100	100	Zidi et al.[63]	$\bar{c}_t = 0$	0.24336	-0.84804	0.25658	0.72442
				Present	$\bar{c}_t = 0$	**0.24058**	**-0.83031**	**0.25516**	**-0.75437**
					$\bar{c}_t = 0.05$	**0.23573**	**-0.83321**	**0.25103**	**-0.75694**
					$\bar{c}_t = 0.1$	**0.23107**	**-0.83600**	**0.24706**	**-0.75940**
					$\bar{c}_t = 1$	**0.17046**	**-0.87225**	**0.19543**	**-0.79150**
1	100	100	100	Zidi et al.[63]	$\bar{c}_t = 0$	0.26330	-0.86205	0.23762	0.82148
				Present	$\bar{c}_t = 0$	**0.26023**	**-0.84446**	**0.23597**	**-0.85629**
					$\bar{c}_t = 0.05$	**0.25486**	**-0.84738**	**0.23264**	**-0.85846**
					$\bar{c}_t = 0.1$	**0.24972**	**-0.85018**	**0.22945**	**-0.86054**
					$\bar{c}_t = 1$	**0.18315**	**-0.88636**	**0.18820**	**-0.88745**
2	100	100	100	Zidi et al.[63]	$\bar{c}_t = 0$	0.26396	-0.84138	0.20133	0.80652
				Present	$\bar{c}_t = 0$	**0.26086**	**-0.82417**	**0.20015**	**-0.84372**
					$\bar{c}_t = 0.05$	**0.25546**	**-0.82707**	**0.19709**	**-0.84572**
					$\bar{c}_t = 0.1$	**0.25028**	**-0.82985**	**0.19415**	**-0.84763**
					$\bar{c}_t = 1$	**0.18334**	**-0.86581**	**0.15620**	**-0.87242**
5	100	100	100	Zidi et al.[63]	$\bar{c}_t = 0$	0.26601	-0.81745	0.18459	0.80297
				Present	$\bar{c}_t = 0$	**0.26287**	**-0.80073**	**0.18369**	**-0.84213**
					$\bar{c}_t = 0.05$	**0.25740**	**-0.80373**	**0.18075**	**-0.84400**
					$\bar{c}_t = 0.1$	**0.25216**	**-0.80660**	**0.17793**	**-0.84580**
					$\bar{c}_t = 1$	**0.18453**	**-0.84369**	**0.14150**	**-0.86898**
∞	100	100	100	Zidi et al.[63]	$\bar{c}_t = 0$	0.26774	-0.71656	0.18286	0.84003
				Present	$\bar{c}_t = 0$	**0.26461**	**-0.96475**	**0.18172**	**-0.87504**
					$\bar{c}_t = 0.05$	**0.25905**	**-0.96663**	**0.17905**	**-0.87670**
					$\bar{c}_t = 0.1$	**0.25372**	**-0.96843**	**0.17648**	**-0.87830**
					$\bar{c}_t = 1$	**0.18515**	**-0.99164**	**0.14342**	**-0.89885**

Figure 15 Non-dimensional variation of in-plane stress $\bar{\boldsymbol{\tau}}_{xy}$ across the thickness of AFG plate resting on a viscoelastic foundation. Figure 16 Non-dimensional variation of transverse shear stress $\bar{\boldsymbol{\tau}}_{xz}$ across the thickness of AFG rectangular plate resting on a viscoelastic foundation. shows the effect of the viscoelastic foundation damping coefficient on the variation of the non-dimensional in-plane shear stress $\bar{\tau}_{xy}$ across the FG plate thickness. The in-plane shear stress $\bar{\tau}_{xy}$ is maximum at the top and bottom of the plate. Figure 16 shows the transverse shear stress $\bar{\tau}_{xz}$. It is maximum at the middle of the plate and $zero$ at the top and bottom surfaces, without the need for a shear correction factor, which is the advantage of the higher-order shear deformation theories. It is observed that increasing the damping coefficient (C_t) causes a reduction in the transverse shear stress of the plate.

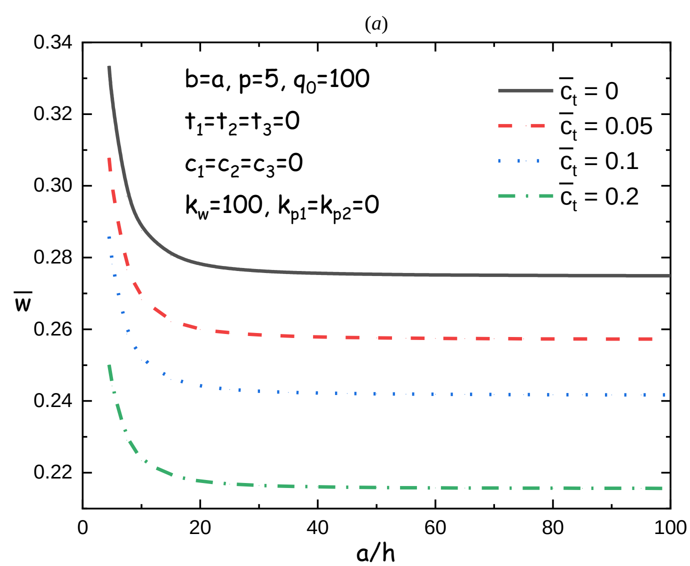

(b)

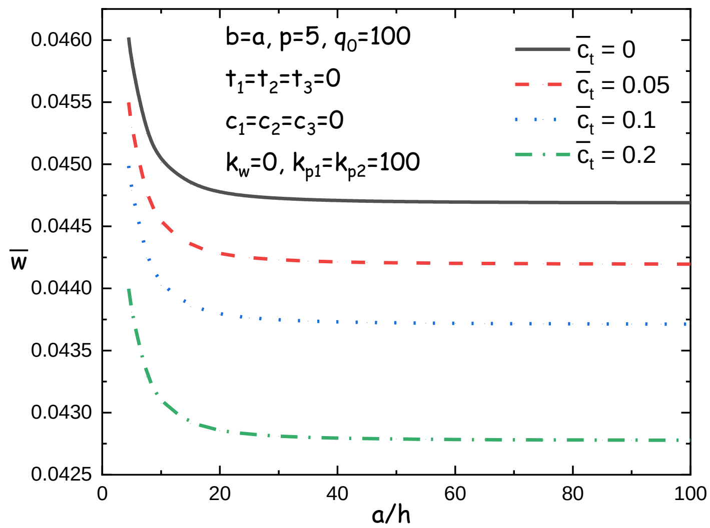

(c)

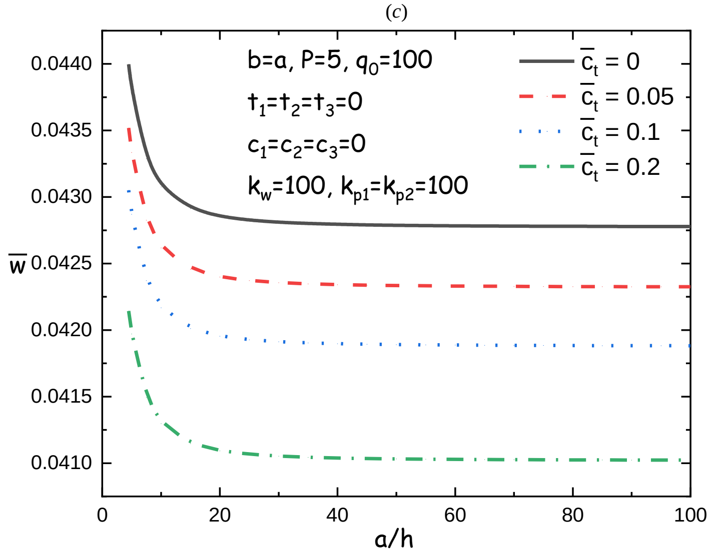

Figure 11 Aspect ratio (a/h) influence on the non-dimensional deflection ($\overline{w}$) of AFG square plate pure mechanical load and resting on a viscoelastic foundation.

(*a*)

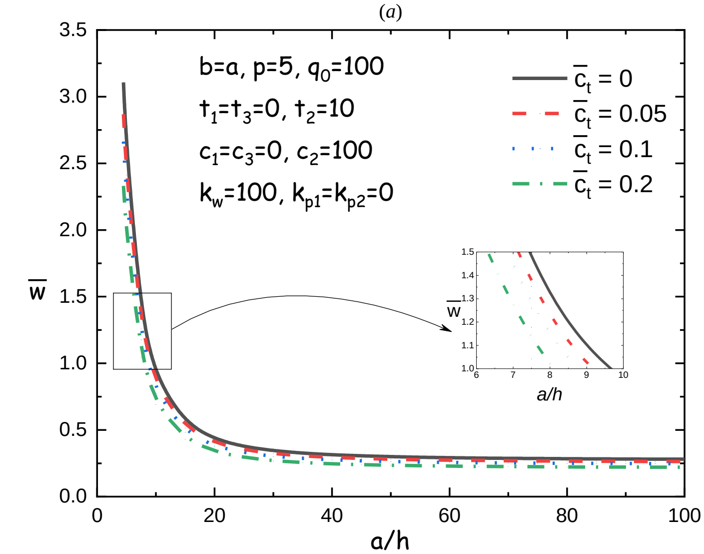
b=a, p=5, q0=100
t1=t3=0, t2=10
c1=c3=0, c2=100
kw=100, kp1=kp2=0
ct = 0
ct = 0.05
ct = 0.1
ct = 0.2
w
a/h

(*b*)

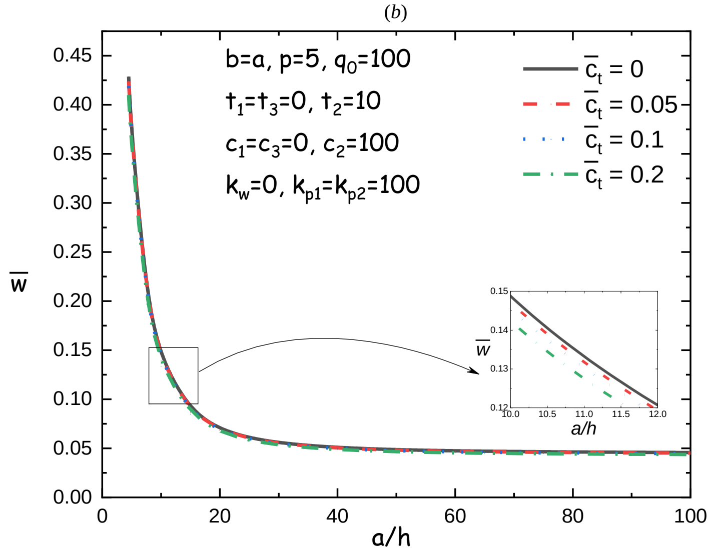
b=a, p=5, q0=100
t1=t3=0, t2=10
c1=c3=0, c2=100
kw=0, kp1=kp2=100
ct = 0
ct = 0.05
ct = 0.1
ct = 0.2
w
a/h

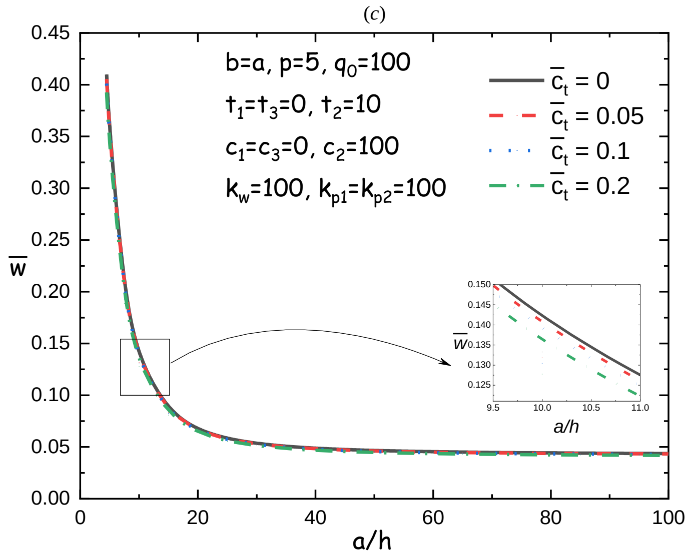

Figure 12 Aspect ratio (a/h) influence on the non-dimensional deflection ($\bar{w}$) of AFG square plate under linear hygro-thermo-mechanical load and resting on a viscoelastic foundation.

(*a*)

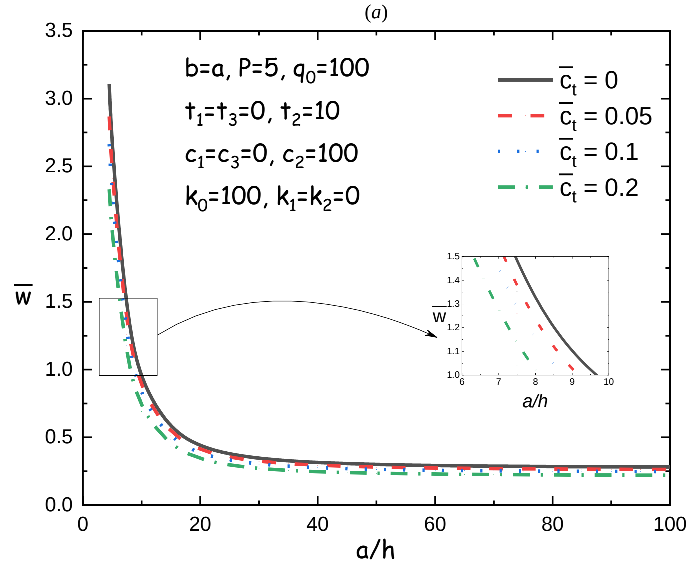
b=a, P=5, q_0=100
t_1=t_3=0, t_2=10
c_1=c_3=0, c_2=100
k_0=100, k_1=k_2=0
$\bar{c}_t$ = 0
$\bar{c}_t$ = 0.05
$\bar{c}_t$ = 0.1
$\bar{c}_t$ = 0.2
$\bar{w}$
a/h

(*b*)

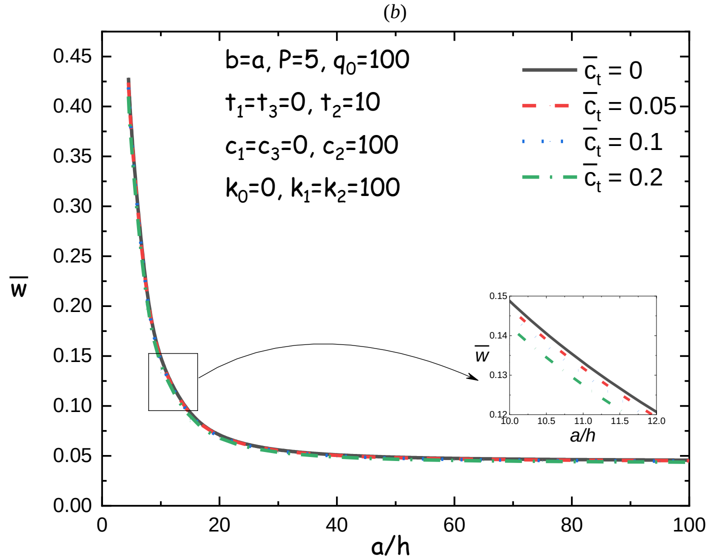
b=a, P=5, q_0=100
t_1=t_3=0, t_2=10
c_1=c_3=0, c_2=100
k_0=0, k_1=k_2=100
$\bar{c}_t$ = 0
$\bar{c}_t$ = 0.05
$\bar{c}_t$ = 0.1
$\bar{c}_t$ = 0.2
$\bar{w}$
a/h

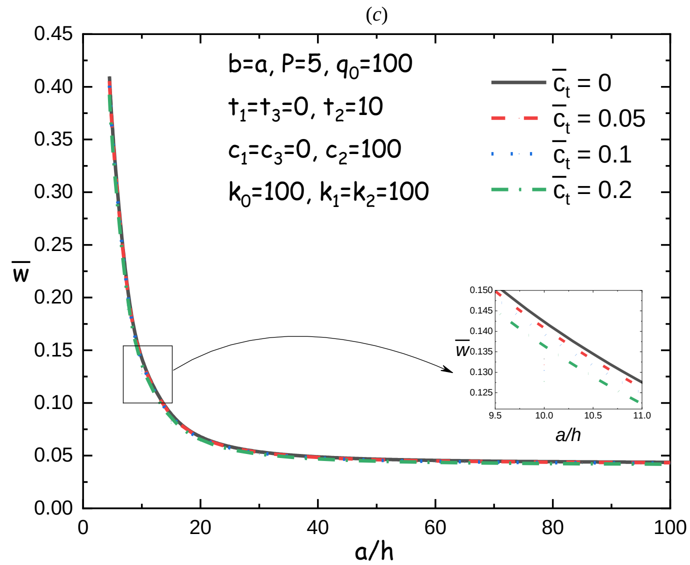

Figure 13 Aspect ratio (a/h) influence on the non-dimensional deflection ($\bar{\boldsymbol{w}}$) of AFG square plate under non-linear hygro-thermo-mechanical load and resting on a viscoelastic foundation.

(a)

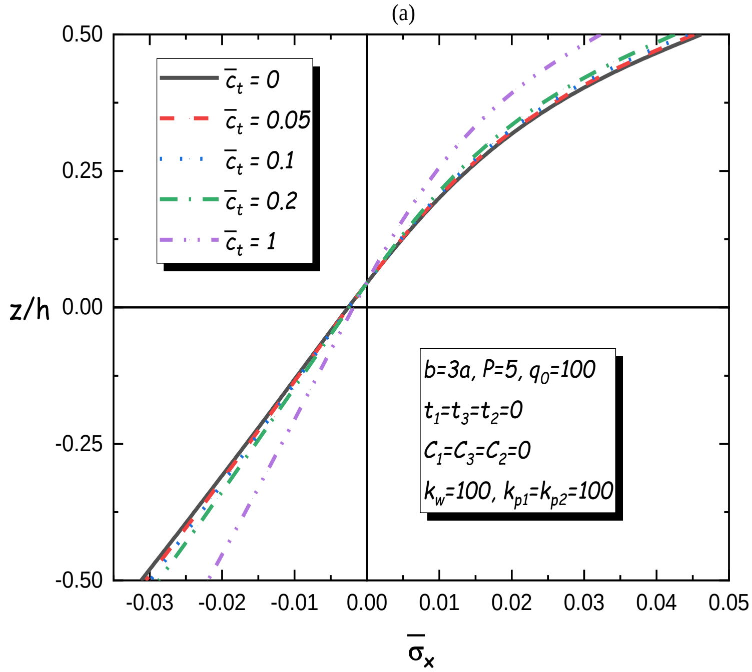
$\bar{c}_t$ = 0
$\bar{c}_t$ = 0.05
$\bar{c}_t$ = 0.1
$\bar{c}_t$ = 0.2
$\bar{c}_t$ = 1
b=3a, P=5, q_0=100
t_1=t_3=t_2=0
C_1=C_3=C_2=0
k_w=100, k_{p1}=k_{p2}=100
z/h
0.50
0.25
0.00
-0.25
-0.50
-0.03
-0.02
-0.01
0.00
0.01
0.02
0.03
0.04
0.05
$\bar{\sigma}_x$

(b)

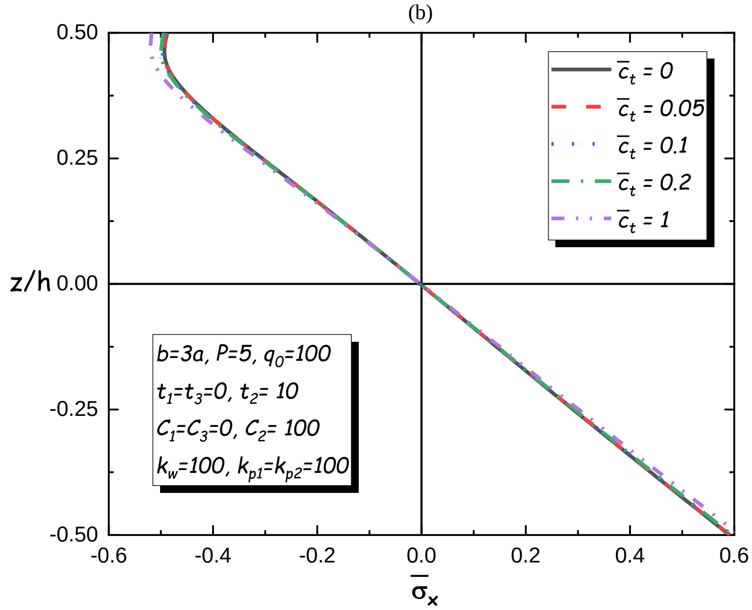
$\bar{c}_t$ = 0
$\bar{c}_t$ = 0.05
$\bar{c}_t$ = 0.1
$\bar{c}_t$ = 0.2
$\bar{c}_t$ = 1
b=3a, P=5, q_0=100
t_1=t_3=0, t_2= 10
C_1=C_3=0, C_2= 100
k_w=100, k_{p1}=k_{p2}=100
z/h
0.50
0.25
0.00
-0.25
-0.50
-0.6
-0.4
-0.2
0.0
0.2
0.4
0.6
$\bar{\sigma}_x$

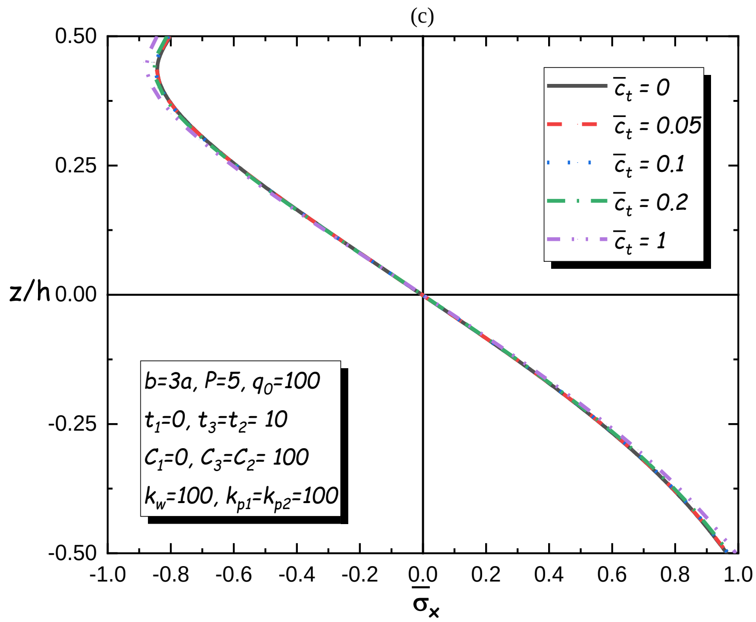

Figure 14 Non-dimensional variation of in-plane stress $\overline{\boldsymbol{\sigma}}_{\boldsymbol{x}}$ across the thickness of AFG rectangular plate resting on a viscoelastic foundation.

(a)

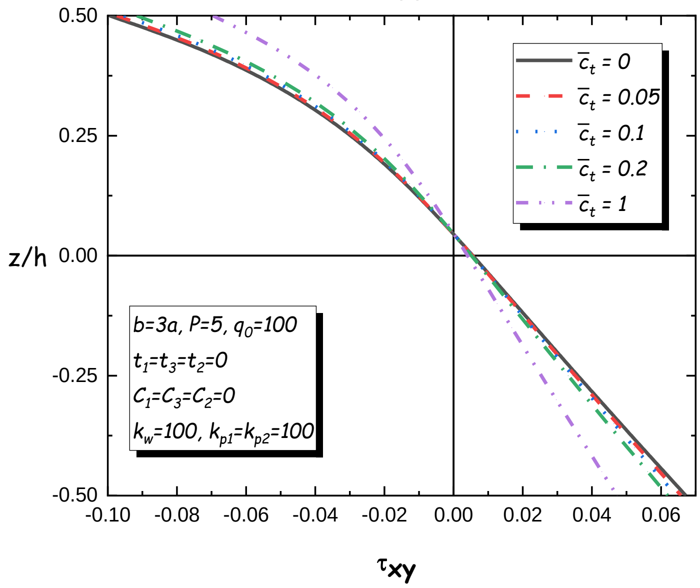

z/h
τxy
$\bar{c}_t$ = 0
$\bar{c}_t$ = 0.05
$\bar{c}_t$ = 0.1
$\bar{c}_t$ = 0.2
$\bar{c}_t$ = 1
b=3a, P=5, q_0=100
t_1=t_3=t_2=0
C_1=C_3=C_2=0
k_w=100, k_{p1}=k_{p2}=100

(b)

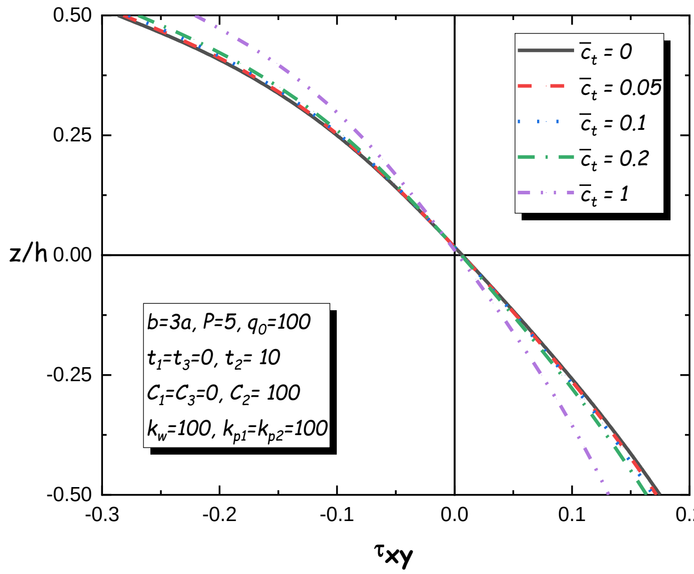

z/h
τxy
$\bar{c}_t$ = 0
$\bar{c}_t$ = 0.05
$\bar{c}_t$ = 0.1
$\bar{c}_t$ = 0.2
$\bar{c}_t$ = 1
b=3a, P=5, q_0=100
t_1=t_3=0, t_2= 10
C_1=C_3=0, C_2= 100
k_w=100, k_{p1}=k_{p2}=100

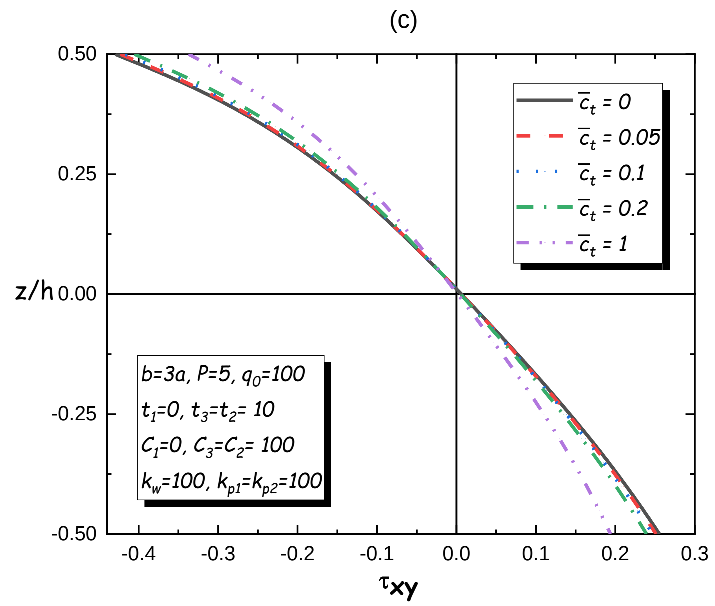

Figure 15 Non-dimensional variation of in-plane stress $\bar{\tau}_{xy}$ across the thickness of AFG plate resting on a viscoelastic foundation.

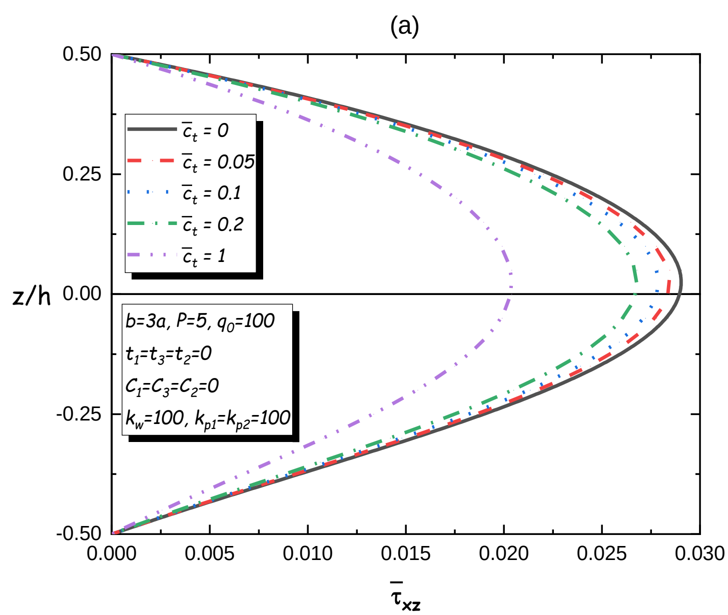

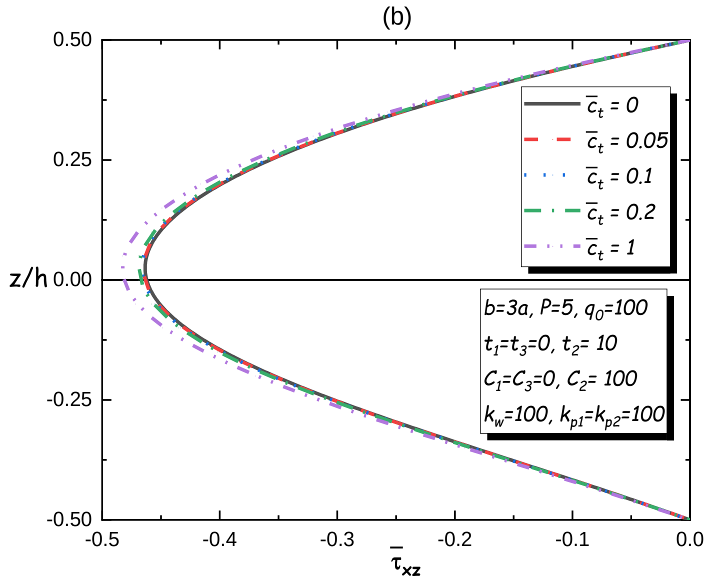

Figure 16 Non-dimensional variation of transverse shear stress $\bar{\tau}_{xz}$ across the thickness of AFG rectangular plate resting on a viscoelastic foundation.

3.9 Acknowledgments

This work is supported through Project No. DF181032 funded by the Deanship of Scientific Research (DSR) at King Fahd University of Petroleum and Minerals (KFUPM), Saudi Arabia. The authors also acknowledge the support of the Civil and Environmental Engineering department.

CHAPTER 4

Journal Article 2

Hygro-Thermo-Mechanical Bending Behavior of Functionally Graded Plates Resting on a Viscoelastic Foundations Using an Integral Quasi-3D Shear Deformation Theory

Ismail M. Mudhaffar[1], Abdelouahed Tounsi∗[1,2,3], Abdelbaki Chikh[3,4], Mohammed A. Al-Osta[1], Mesfer M. Al-Zahrani[1] and Salah U. Al-Dulaijan[1]

1Department of Civil and Environmental Engineering, King Fahd University of Petroleum & Minerals, 31261 Dhahran, Eastern Province, Saudi Arabia
2YFL (Yonsei Frontier Lab), Yonsei University, Seoul, Korea
3Material and Hydrology Laboratory, University of Sidi Bel Abbes, Faculty of Technology, Civil Engineering Department, Algeria
4Université Ibn Khaldoun, BP 78 Zaaroura, 14000 Tiaret, Algérie

4.1 Abstract

This work applies a four-unknown quasi-3D shear deformation theory to investigate the bending behavior of a functionally graded plate resting on a viscoelastic foundation and subjected to hygro-thermo-mechanical loading. The theory utilizes a trigonometric shape function to predict the transverse shear stress, and the transverse stretching effect of the plate is considered. The viscoelastic foundation model is included using a viscosity time-dependent parameter in addition to the Winkler's, and Pasternak parameters. The principle of virtual displacement is applied to obtain the governing differential equations, and the Navier method that comprises an exponential term is used to obtain the solution. Numerical examples are presented to validate the theory, and a parametric study is conducted to study the effect of the damping coefficient, the linear and non-linear loadings, power-law index, and the plate width to thickness ratio on the plate bending response.

Keywords*:* Quasi-3D theory, Viscoelastic foundation, Static bending response, Hygrothermal environment.

4.2 Introduction

Lightweight composite structures exhibit high strength/weight ratios; hence they are widely employed in industries and engineering applications. However, their properties do not sustain aggressive thermal environments in which the stress concentration at the plies' interfaces causes cracks, delamination of the layers, and other failure mechanisms. Functionally graded materials (FGMs) are novel types of composites that exhibit unique properties in terms of strength and high-temperature resistance [18]. In FGMs the material particles are gradually distributed through the thickness according to the intended usage, hence called functionally graded. The first application of FGMs was in 1984 in Japan by material scientists to prepare thermal insulation materials [24]. Nowadays, Many engineering fields utilize FGMs for example, in civil engineering, they are utilized to manufacture fiber-reinforced polymers (FRP) used for reinforcing bridge concrete materials which enhance resistance to corrosion [18], while the aerospace and automotive industries use them in the production of external and internal parts of aircraft, rockets, and engines [19]. Some types of FGMs include compositional gradients which are applied in defense, porosity gradients used in filters and dental, while other types of FGMs include microstructural gradients used in armory [20]. For this importance, researchers extensively studied the static and dynamic responses of these materials under various loading conditions.

Functionally graded (FG) plates are studied based on various theories. The basic is the classical plate theory by Leissa [2] which neglects the transverse shear effect leading to inaccurate results for thick plates. The first-order shear deformation theory by Mindlin [3] included the transverse shear effect. However, it requires a shear correction factor to ensure zero shear stress at the plate surfaces. Higher-order shear deformation theories (HOSDT) likes the third-order theory by Reddy [4] predict the plate behavior without the need to shear correction factors. The mentioned theories are called two-dimensional theories since they neglect the thickness stretching effect. Tahir et al. [64] used an integral four-unknowns theory to study the wave propagation of FGM plates resting on viscoelastic foundations. A new type of theories called quasi-3D theories considers the vertical stretching effect of the plate thickness to provide even better results. Zhang et al. [65] investigated the vibration response of a non-FGM plate under hygro-thermal loads using a HOSDT. The thickness stretching effect was considered and a trigonometric shape function was selected to depict the shear stress effect across the plate's thickness. Sayyad and Ghumare [66] used a polynomial-type quasi-3D theory to investigate the bending behavior of a FG sandwich plate under thermomechanical loadings. Sayyad and Ghumare [67] used a five-unknowns quasi-3D shear deformation theory to investigate the static response of the FGM plate resting on elastic foundation. Zenkour et al. [68] studied the vibration of an FGM porous plate using a five-unknows quasi-3D theory.

There are several models to predict the plates' foundations' behavior. Winkler's model [14] assumes the foundation to be closely-spaced springs that are in contact with the plate bottom surface. However, this model does not imitate the reality where the effect also occurs in the neighboring springs. Pasternak's model [33] overcomes this issue by adding a sheer layer above the spaced springs that distribute the loads according to the location of the springs from the plate. Generally, Winkler's and Pasternak's models are the famous models used in research. However, these two models lack the creep time effect. When loading the plate, an immediate settlement occurs in the foundation, but with time there is a substantial increase in the settlement which is affecting the plate's behavior. The viscoelastic foundation considers the viscosity effect by including a viscosity damping parameter to the elastic Winkler's-Pasternak's model [16].

Plates' behavior has been investigated heavily in literature. Reddy [69] investigated the response of FGM plates using a third-order shear deformation theory. Akavci and Tanrikulu [70] studied the static and dynamic responses of a one-layer FG plate using a 2D and quasi-3D theory using a hyperbolic shape function. They concluded that the transverse normal strain and transverse normal shear strain have equal importance on the plate bending and vibrational responses. Hasheminejad and Gheshlaghi [71] used a three-dimensional analysis to study the transient vibrational response of a thick FG plate resting on a stiff and soft viscoelastic foundation under uniform blast loads and moving transverse forces. They observed that the effect of the vertical material distribution is more influential on the plate-induced stress concentrations than on its displacement response.

The literature is rich with the static and dynamic investigation of FGM plates. Naghavi [72] performed a static analysis of a FG plate under sinusoidal mechanical loading using a finite strip method that is based on a refined plate theory. Hassan et al. [73] used a multi-term Kantorovich approach to investigate the bending of a skew FGM plate on elastic foundations subjected to uniform loading. The classical plate theory was used to formulate the models and the results were validated by comparison with a finite element model. Mechab et al. [74] studied the FGM plate's bending response using a two-variable theory of four unknowns. Sahraee [75] used Levinson's plate theory that is based on the classical and first-order shear deformation theories to study the bending behavior of FGM plates. Ahmed Houari et al. [76] used two variables HOSDT to investigate the thermoelastic bending response of FGM sandwich plates. Joshi et al. [77] used an analytical approach to study the effect of thermal environments on the vibration response of a cracked plate using the classical plate theory. Matsunaga [78] presented a two-dimensional HOSDT for evaluating the plate displacement and stress responses. Hadj et al. [79] studied the effect of porosity distribution on the static and dynamic response of an FGM plate and concluded that the type of porosity distribution significantly affects the vibration response of the rectangular FG plate. Tahir et al. [80] investigated the wave propagation of FGM sandwich plates on viscoelastic foundation subjected to the hygrothermal environment by considering six porosity models.

It is noticed that no one has applied a quasi-3D integral theory to study the bending of FGM plates resting on viscoelastic foundations and subjected to mechanical loading in a hygrothermal environment. Therefore, this work investigated the bending response of an advanced FGM plate resting on a viscoelastic foundation. The plate is subjected to mechanical loading in addition to loads of humidity and temperature.

4.3 Functionally Graded Plate Geometry

The rectangular plate in fig.1 has a length, width, and thickness of a, b, and h, respectively. The cartesian coordinate system x, y, z has an origin at the middle plane with $z = 0$. The plate is resting on a viscoelastic foundation modeled by separated springs in parallel with viscous dampers while both are covered by a shear layer that ensures distributing the load to the neighboring springs, not in contact with the plate.

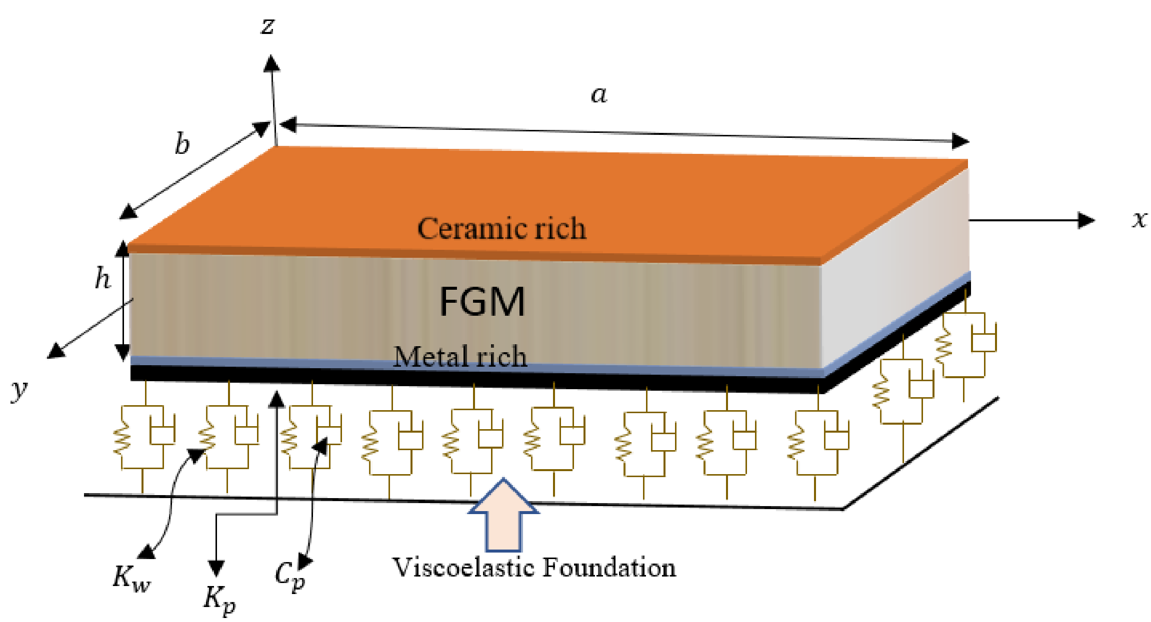

Figure 17 FGM plate on Elastic Foundation

The material properties are varied across the thickness according to the power-law function shown in equation (43) so that the bottom surface is metal-rich, and the top surface is ceramic reach while the middle portion of the plate is a mixture of both. The volume fraction of the constituents $v(z)$ is expressed as:

$$V(z) = \left(\frac{z}{h} + \frac{1}{2}\right)^p, -\frac{h}{2} \leq z \leq \frac{h}{2} \tag{42}$$

where p is the power index or sometimes referred to as the material index. The value of p defines the profile distribution of the materials across the thickness. The power-law function depends on the volume fraction and is expressed as:

$$P(z) = P_t V_t(z) + P_b\, V_b(z) \tag{43}$$

where $P(z)$ is the effective material property across the plate's thickness, whereas P_t, V_t, P_b, V_b are the properties and volume fractions of the materials at the top and bottom of the plate, respectively. The effective young's modulus and shear modulus are shown in equation (1).

$$\begin{aligned} E(z) &= V(z)\, E_t + [1 - V(z)]\, E_b \\ G(z) &= V(z)\, G_t + [1 - V(z)]\, G_b \end{aligned} \tag{44}$$

where $E(z), \alpha(z)$ are the effective Young's and shear moduli, and E_t, E_b, G_t, G_b are the martial moduli at the top and bottom surfaces, here we use ceramic at the top and metal at the bottom of the plate.

4.4 Constitutive Relations

4.4.1 Displacement Field

The displacement field is expressed as in (Chikh et al., 2017) [81] as shown in equation (45). The displacement field incorporates the stretching effect while using only four unknowns by utilizing an integral term. This greatly reduces the computational cost compared to other qausi-3D theories of more than five unknowns.

$$
\begin{aligned}
U(x,y,z,t) &= u_0(x,y,t) - z\frac{\partial\, w_0(x,y,t)}{\partial x} + k_1\, f(z)\int \theta(x,y,t)\,\mathrm{d}x \\
V(x,y,z,t) &= v_0(x,y,t) - z\frac{\partial\, w_0(x,y,t)}{\partial y} + k_2\, f(z)\int \theta(x,y,t)\,\mathrm{d}y \\
W(x,y,z,t) &= w_0(x,y,t) + g(z)\ \theta(x,y,t)
\end{aligned}
\tag{45}
$$

where U,V,W are the x,y,z displacements of any point in the plate, u_0, v_0 are the displacements of the middle plane in the $x, and\ y\ directions$, while w_0, θ are the vertical displacements due to bending and shear, respectively. k_1, k_2 are the plate's geometry parameters defined in equation (52). $f(z\ ), g(z)$ are defined in equation (46).

$$
\begin{aligned}
f(z) &= \frac{h}{\pi} sin\left(\frac{\pi z}{h}\right) \\
g(z) &= \frac{df(z)}{dz}
\end{aligned}
\tag{46}
$$

4.4.2 Strain Tensor

The strain tensor is derived from the well-known strain-displacement relation shown in equation (47).

$$\varepsilon_{ij} = \frac{1}{2}\left(\frac{\partial u_i}{\partial x_j} + \frac{\partial u_j}{\partial x_i}\right) \tag{47}$$

where $i, j = 1 \dots 3$. Assuming small strains and applying the previous formula, the strain is expressed as follows:

$$\begin{gathered}
\begin{Bmatrix} \varepsilon_x \\ \varepsilon_y \\ \gamma_{xy} \end{Bmatrix} = \begin{Bmatrix} \varepsilon_x^0 \\ \varepsilon_y^0 \\ \gamma_{xy}^0 \end{Bmatrix} - z \begin{Bmatrix} \varepsilon_x^b \\ \varepsilon_y^b \\ \gamma_{xy}^b \end{Bmatrix} + f(z) \begin{Bmatrix} \varepsilon_x^s \\ \varepsilon_y^s \\ \gamma_{xy}^s \end{Bmatrix}, \\
\begin{Bmatrix} \gamma_{xz} \\ \gamma_{yz} \end{Bmatrix} = f'(z) \begin{Bmatrix} \gamma_{xz}^0 \\ \gamma_{yz}^0 \end{Bmatrix} + g(z) \begin{Bmatrix} \gamma_{xz}^1 \\ \gamma_{yz}^1 \end{Bmatrix}, \qquad \varepsilon_z = g'(z)\, \varepsilon_z^0
\end{gathered} \tag{48}$$

where:

$$\begin{gathered}
\begin{Bmatrix} \varepsilon_x^0 \\ \varepsilon_y^0 \\ \gamma_{xy}^0 \end{Bmatrix} = \begin{Bmatrix} \dfrac{\partial u_0}{\partial x} \\ \dfrac{\partial v_0}{\partial y} \\ \dfrac{\partial u_0}{\partial y} + \dfrac{\partial v_0}{\partial x} \end{Bmatrix}, \qquad \begin{Bmatrix} \varepsilon_x^b \\ \varepsilon_y^b \\ \gamma_{xy}^b \end{Bmatrix} = \begin{Bmatrix} \dfrac{\partial^2 w_0}{\partial x^2} \\ \dfrac{\partial^2 w_0}{\partial y^2} \\ 2\dfrac{\partial^2 w_0}{\partial x \partial y} \end{Bmatrix}, \\
\begin{Bmatrix} \varepsilon_x^s \\ \varepsilon_y^s \\ \gamma_{xy}^s \end{Bmatrix} = \begin{Bmatrix} k_1\, \theta \\ k_2\, \theta \\ k_1 \dfrac{\partial}{\partial y}\displaystyle\int \theta \, \mathrm{d}x + k_2 \dfrac{\partial}{\partial x}\displaystyle\int \theta \, \mathrm{d}y \end{Bmatrix}
\end{gathered} \tag{49}$$

$$\begin{Bmatrix} \gamma_{xz}^{0} \\ \gamma_{yz}^{0} \end{Bmatrix} = \begin{Bmatrix} \mathrm{k}_1 \int \theta\, \mathrm{dx} \\ \mathrm{k}_2 \int \theta\, \mathrm{dy} \end{Bmatrix}, \begin{Bmatrix} \gamma_{xz}^{1} \\ \gamma_{yz}^{1} \end{Bmatrix} = \begin{Bmatrix} \frac{\partial \theta}{\partial x} \\ \frac{\partial \theta}{\partial y} \end{Bmatrix}, \varepsilon_z^0 = \theta,\ g'(z) = \frac{dg(z)}{dz} \tag{50}$$

The integral term in the above equations is resolved with the idea that the shear displacement integral and derivative are proportional to each other as shown in equation (51), and the Navier solution is indeed expressed here in terms of the $Sine$ and $Cosine$ functions where the assumed solution appears again after taking the derivative or the integral.

$$\begin{gathered} \frac{\partial}{\partial y}\int \theta\, dx = A' \frac{\partial^2 \theta}{\partial x \partial y}, \qquad \frac{\partial}{\partial x}\int \theta\, dy = B' \frac{\partial^2 \theta}{\partial x \partial y}, \\ \int \theta\, dx = A' \frac{\partial \theta}{\partial x}, \int \theta\, dy = B' \frac{\partial \theta}{\partial y} \end{gathered} \tag{51}$$

The coefficients $A^{'}, B^{'}$ are defined in the following equation:

$$\begin{gathered} A' = -\frac{1}{\lambda^2}, B' = -\frac{1}{\mu^2}, \\ k_1 = \lambda^2, k_2 = \mu^2, \qquad \lambda = \frac{m\,\pi}{a}, \mu = \frac{\mathrm{n}\,\pi}{b} \end{gathered} \tag{52}$$

4.4.3 Stress Tensor

The stress-strain relation is shown in equation (53).

$$\begin{Bmatrix} \sigma_x \\ \sigma_y \\ \sigma_z \\ \tau_{xy} \\ \tau_{yz} \\ \tau_{xz} \end{Bmatrix} = \begin{bmatrix} Q_{11} & Q_{12} & Q_{13} & 0 & 0 & 0 \\ Q_{12} & Q_{22} & Q_{23} & 0 & 0 & 0 \\ Q_{13} & Q_{23} & Q_{33} & 0 & 0 & 0 \\ 0 & 0 & 0 & Q_{66} & 0 & 0 \\ 0 & 0 & 0 & 0 & Q_{55} & 0 \\ 0 & 0 & 0 & 0 & 0 & Q_{44} \end{bmatrix} \cdot \begin{Bmatrix} \varepsilon_x - \alpha\Delta T - \beta\Delta C \\ \varepsilon_y - \alpha\Delta T - \beta\Delta C \\ \varepsilon_z - \alpha\Delta T - \beta\Delta C \\ \gamma_{xy} \\ \gamma_{yz} \\ \gamma_{xz} \end{Bmatrix} \tag{53}$$

where (σ_x, σ_y, σ_z, τ_{xy}, τ_{yz}, τ_{xz}) and $\left(\varepsilon_x,\ \varepsilon_y,\ \varepsilon_z,\ \gamma_{xy},\ \gamma_{xy},\ \gamma_{yz},\ \gamma_{xz}\right)$ are the stresses and strains components of the FGM plate, respectively. The stiffness coefficients Q_{ij} are shown in equation (54). α and β are the temperature and humidity coefficients of the FGM plate, respectively. $\Delta T, \Delta C$ are the through thickness gradients of the temperature and humidity, respectively and they are described in equation (14).

$$\begin{gathered} Q_{11} = Q_{22} = Q_{33} = \frac{(1-v)E(z)}{(1-2v)(1+v)} \\ Q_{12} = Q_{13} = Q_{23} = \frac{vE(z)}{(1-2v)(1+v)} \\ Q_{44} = Q_{55} = Q_{66} = \frac{E(z)}{2(1+v)} \end{gathered} \tag{54}$$

$$\begin{gathered} \Delta T(x,y,z,t) = T_1(x,y,t) + \frac{z}{h} T_2(x,y,t) + \frac{f(z)}{h} T_3(x,y,t) \\ \\ \Delta C(x,y,z,t) = C_1(x,y,t) + \frac{z}{h} C_2(x,y,t) + \frac{f(z)}{h} C_3(x,y,t) \end{gathered} \tag{55}$$

WhereT_1, T_2, T_3 are the thermal loads, while C_1, C_2, C_3 are loads of the humid environment.

4.5 Governing Equations

The principle of virtual work is used to obtain the governing equations. The product of the stresses with the first variation of the strains gives the internal energy of the plate which is integrated in the $x\,y$ domain first, then through the plate’s thickness. The external energy on the current plate is obtained by the product of the sum of the vertical external forces with the plate transverse displacement. The addition of the internal energy and external energy of the plate gives the principle of virtual work shown in (56).

$$\int_{\frac{-h}{2}}^{\frac{h}{2}}\int_{\Omega}\left[\sigma_x\delta\varepsilon_x+\sigma_y\delta\varepsilon_y+\sigma_z\delta\varepsilon_z+\tau_{xy}\delta\gamma_{xy}+\tau_{xz}\delta\gamma_{xz}+\tau_{yz}\delta\gamma_{yz}\right]d\Omega\,dz \\ -\int_{\Omega}(q-f_e)\,\delta w\,d\Omega=0 \tag{56}$$

where Ω is the top surface of the plate, q is the transverse mechanical load on the plate, f_e is the reaction force from the viscoelastic foundation on the FGM plate [16], and it is described in equation (57).

$$f_e=k_w\,w(x,y,t)-k_{p1}\frac{\partial^2 w(x,y,t)}{\partial x^2}-k_{p2}\frac{\partial^2 w(x,y,t)}{\partial y^2}+C_t\frac{\partial w(x,y,t)}{\partial t} \tag{57}$$

where k_w is the Winkler's Parameter, k_{p1} and k_{p2} are the Pasternak parameters, while C_t is the viscous damping coefficient.

Substituting the strain and stresses from equations (48) and (53) into the principle of virtual displacement in equation (15) and then integrating through the thickness, we would obtain the following equation:

$$\int_{\Omega}(N_x\delta\varepsilon_x^0+N_y\delta\varepsilon_y^0+N_z\delta\varepsilon_z^0+N_{xy}\delta\gamma_{xy}^0+M_x^b\delta k_x^b+M_y^b\delta k_y^b \\ +M_{xy}^b\delta k_{xy}^b+M_x^s\delta k_x^s+M_y^s\delta k_y^s+M_{xy}^s\delta k_{xy}^s+Q_{yz}^s\delta\gamma_{yz}^0 \\ +S_{yz}^s\delta\gamma_{yz}^1+Q_{xz}^s\delta\gamma_{xz}^0+S_{xz}^s\delta\gamma_{xz}^1)dA \tag{58}$$

Now, we integrate the displacement gradients in equations (58) by parts and set the coefficients of $\delta u_0, \delta v_0, \delta w_0, \delta\theta_0$ to zero to get the four governing differential equations shown in equation (59).

$$u_0: \quad \frac{\partial N_x}{\partial x} + \frac{\partial N_{xy}}{\partial y} = 0$$

$$\delta v_0: \quad \frac{\partial N_y}{\partial y} + \frac{\partial N_{xy}}{\partial x} = 0$$

$$\delta w_0: \quad \frac{\partial^2 M_X^b}{\partial x^2} + 2\frac{\partial^2 M_{xy}^b}{\partial x \partial y} + \frac{\partial^2 M_y^b}{\partial y^2} + q - f_e = 0 \tag{59}$$

$$\delta\theta: \quad -k_1 A' \frac{\partial^2 M_x^s}{\partial x^2} - k_2 B' \frac{\partial^2 M_y^s}{\partial y^2} - (k_1 A' + k_2 B') \frac{\partial^2 M_{xy}^s}{\partial x\, \partial y} + k_1 A' \frac{\partial Q_{xz}}{\partial x}$$
$$+ k_2 B' \frac{\partial Q_{yz}}{\partial y} + \frac{\partial S_{xz}^s}{\partial x} + \frac{\partial S_{yz}^s}{\partial y} - N_z = 0$$

The stress resultant forces are defined in equation (60).

$$\begin{aligned}
\left(N_i, M_i^b, M_i^s\right) &= \int_{-\frac{h}{2}}^{\frac{h}{2}} (1, z, f)\sigma_i \, dz, (i = x, y, xy) \\
N_z &= \int_{-h/2}^{h/2} g'(z)\sigma_z dz \\
\left(S_{xz}^s, S_{yz}^s\right) &= \int_{-h/2}^{h/2} g(z)\left(\tau_{xz}, \tau_{yz}\right) dz \\
\left(Q_{xz}^s, Q_{yz}^s\right) &= \int_{-h/2}^{h/2} f'(z)\left(\tau_{xz}, \tau_{yz}\right) dz
\end{aligned} \tag{60}$$

4.6 Analytical Solution

Navier's method is used to obtain the solution for the rectangular FG plate. The simply support boundary conditions are satisfied by assuming the solution to be a multiplication of the unknown middle plane displacements $(U_0, V_0, W_0, \theta_0)$ with the trigonometric $Sine$ and $Cosine$ functions as shown in equation (61). This solution ensures zero bending moments and transversal displacements at the plate edges.

$$\begin{Bmatrix} u_0 \\ v_0 \\ w_0 \\ \theta \end{Bmatrix} = \sum_{m=1}^{\infty} \sum_{n=1}^{\infty} \begin{Bmatrix} U_0\, cos(\lambda\, x)\, sin(\mu\, y) \\ V_0\, sin(\lambda\, x)\, cos(\mu\, y) \\ W_0\, sin(\lambda\, x)\, sin(\mu\, y) \\ \theta_0\, sin(\lambda\, x)\, sin(\mu\, y) \end{Bmatrix} \cdot e^{(i\omega t)} \tag{61}$$

The geometry parameters λ, μ are defined in equation (52). i is the imaginary number, m, n are the half wave numvers, while ω is the plate's angular frequency. The loads assumed solution is shown in equation (62). The investigation is for the static response which is dealt with without the need for Hamilton's principle which contains the kinetic energy. The time variable is included only to consider the viscosity effect of the foundation. After substituting in the governing equations, the exponential terms shall cancel out.

$$\begin{Bmatrix} q \\ T_1 \\ T_2 \\ T_3 \\ C_1 \\ C_2 \\ C_3 \end{Bmatrix} = \sum_{m=1}^{\infty} \sum_{n=1}^{\infty} \begin{Bmatrix} q_0 \sin(\lambda\, x) \sin(\mu\, y) \\ t_1 \sin(\lambda\, x) \sin(\mu\, y) \\ t_2 \sin(\lambda\, x) \sin(\mu\, y) \\ t_3 \sin(\lambda\, x) \sin(\mu\, y) \\ c_1 \sin(\lambda\, x) \sin(\mu\, y) \\ c_2 \sin(\lambda\, x) \sin(\mu\, y) \\ c_3 \sin(\lambda\, x) \sin(\mu\, y) \end{Bmatrix} \cdot e^{(i\omega t)} \tag{62}$$

where q_0 is the uniform mechanical load coefficient, while $t_1, t_2, t_3, c_1, c_2, c_3$ are the hygrothermal load coefficients.

When substituting the assumed solutions of the loads and displacements into the governing equations, the exponential term will appear again after taking the first derivative, then it is taken as a common factor that cancels out to be left with the system shown in equation (63).

$$[A]\{\Delta\} = \{P\} \tag{63}$$

$\{\Delta\}$ is the vector representing the displacement coefficients U_0, V_0, W_0, θ_0, and the matrix $[A]$ is shown in equation (64).

$$[A] = \begin{bmatrix} a_{11} & a_{12} & a_{13} & a_{14} \\ a_{12} & a_{22} & a_{23} & a_{24} \\ a_{13} & a_{23} & a_{33} & a_{34} \\ a_{14} & a_{24} & a_{34} & a_{44} \end{bmatrix} \tag{64}$$

The circular frequency of the plate will be a common factor in equation (63) which will cancel out from both sides of the equation. For the foundation, the angular frequency ω will appear in the term a_{33} of equation (63) and is given the value of 0.5 which is multiplied by the damping coefficient C_t. The elements of the stiffness matrix $[A]$ are shown in equation (65).

$$\begin{aligned} a_{11} &= -A_{11}\lambda^2 - A_{66}\mu^2 \\ a_{12} &= -A_{12}\lambda\mu - A_{66}\lambda\mu \\ \mathrm{a}_{13} &= B_{11}\lambda^3 + B_{12}\lambda\mu^2 + 2B_{66}\lambda\mu^2 \\ \mathrm{a}_{14} &= -\mathrm{A}'k_1D_{66}\lambda\mu^2 - \mathrm{B}'k_2D_{66}\lambda\mu^2 + k_1D_{11}\lambda + k_2D_{12}\lambda + H_{13}\lambda \end{aligned} \tag{65}$$

$$a_{21} = -A_{12}\lambda\mu - A_{66}\lambda\mu$$

$$a_{22} = -A_{22}\mu^2 - A_{66}\lambda^2$$

$$a_{23} = B_{12}\lambda^2\mu + B_{22}\mu^3 + 2B_{66}\lambda^2\mu$$

$$a_{24} = -A'k_1D_{66}\lambda^2\mu - B'k_2D_{66}\lambda^2\mu + k_1D_{12}\mu + k_2D_{22}\mu + H_{23}\mu$$

$$a_{31} = B_{11}\lambda^3 + B_{12}\lambda\mu^2 + 2B_{66}\lambda\mu^2$$

$$a_{32} = B_{12}\lambda^2\mu + \mathrm{B22}\mu^3 + 2B_{66}\lambda^2\mu$$

$$a_{33} = -E_{11}\lambda^4 - 2E_{12}\lambda^2\mu^2 - E_{22}\mu^4 - 4E_{66}\lambda^2\mu^2 - k_{S1}\lambda^2 - k_{S2}\mu^2 + 0.5\,C_t - k_w$$

$$a_{34} = 2A'F_{66}k_1\lambda^2\mu^2 + 2B'F_{66}k_2\lambda^2\mu^2 - F_{11}k_1\lambda^2 - F_{12}k_1\mu^2 - F_{12}k_2\lambda^2 - F_{22}k_2\mu^2 - g(z)k_{S1}\lambda^2 - g(z)k_{S2}\mu^2 - I_{13}\lambda^2 - I_{23}\mu^2 + g(z)C_t0.5 - g(z)k_w$$

$$a_{41} = -A'k_1D_{66}\lambda\mu^2 - B'k_2D_{66}\lambda\mu^2 + k_1D_{11}\lambda + k_2D_{12}\lambda + H_{13}\lambda$$

$$a_{42} = -A'k_1D_{66}\lambda^2\mu - B'k_2D_{66}\lambda^2\mu + k_1D_{12}\mu + k_2D_{22}\mu + H_{23}\mu$$

$$a_{43} = 2A'F_{66}k_1\lambda^2\mu^2 + 2B'F_{66}k_2\lambda^2\mu^2 - F_{11}k_1\lambda^2 - F_{12}k_1\mu^2 - F_{12}k_2\lambda^2 - F_{22}k_2\mu^2 - I_{13}\lambda^2 - I_{23}\mu^2$$

$$a_{44} = -A'^2G_{66}{k_1}^2\lambda^2\mu^2 - 2A'B'G_{66}k_1k_2\lambda^2\mu^2 - B'^2G_{66}{k_2}^2\lambda^2\mu^2 - A'^2AS_{55}{k_1}^2\lambda^2 - AS_{44}B'^2{k_2}^2\mu^2 - 2A'AS_{55}k_1\lambda^2 - 2AS_{44}B'k_2\mu^2 - AS_{44}\mu^2 - AS_{55}\lambda^2 - G_{11}{k_1}^2 - 2G_{12}k_1k_2 - G_{22}{k_2}^2 - 2\,IS_{13}k_1 - 2IS_{23}k_2 - IC_{33}$$

where:

$$\left(A_{ij}, B_{ij}, D_{ij}, E_{ij}, F_{ij}, G_{ij}\right) = \int_{-\frac{h}{2}}^{\frac{h}{2}} Q_{ij}(1, z, f(z), z^2, zf(z), f(z)^2)dz, \quad (i,j) = (1,2,6) \tag{66}$$

$$A_{ij}^s = \int_{-\frac{h}{2}}^{\frac{h}{2}} Q_{ij}g(z)^2dz, (i,j) = (4,5)$$

$$\left(\mathrm{H}_{ij}, \mathrm{I}_{ij}, \mathrm{IS}_{ij}, \mathrm{IC}_{\mathrm{ij}}\right) = \int_{-\frac{h}{2}}^{\frac{h}{2}} Q_{ij} g'(z)\left(1, z, f(z), g'(z)\right) dz,$$

$$(i, j) = (1,2,3)$$

The components of the force vector $\{p\}$ are described in equation (67).

$$\begin{aligned}
\mathrm{P}_1 = \frac{\lambda}{h}(&hC_1(\mathrm{LC}_{11} + \mathrm{LC}_{12} + \mathrm{LC}_{13}) - h\mathrm{T}_0\mathrm{LT}_{11} - h\mathrm{T}_0\mathrm{LT}_{12} - h\mathrm{T}_0\mathrm{LT}_{13} \\
&+ C_2(\mathrm{MC}_{11} + \mathrm{MC}_{12} + \mathrm{MC}_{13}) + C_3\mathrm{MCS}_{11} + C_3\mathrm{MCS}_{12} \\
&+ C_3\mathrm{MCS}_{13} + h\,\mathrm{LT}_{11}T_1 + h\mathrm{LT}_{12}T_1 + h\mathrm{LT}_{13}T_1 + \mathrm{MT}_{11}T_2 \\
&+ \mathrm{MT}_{12}T_2 + \mathrm{MT}_{13}T_2 + \mathrm{MTS}_{11}T_3 + \mathrm{MTS}_{12}T_3 + \mathrm{MTS}_{13}T_3)
\end{aligned} \tag{67}$$

$$\begin{aligned}
P_2 = \frac{\lambda}{h}((&C_1 h(\mathrm{LC}_{12} + \mathrm{LC}_{22} + \mathrm{LC}_{23}) + C_2(\mathrm{MC}_{12} + \mathrm{MC}_{22} + \mathrm{MC}_{23}) \\
&+ C_3\mathrm{MCS}_{12} + C_3\mathrm{MCS}_{22} + C_3\mathrm{MCS}_{23} + h\,\mathrm{LT}_{12}T_1 \\
&+ h\,\mathrm{LT}_{22}T_1 + h\,\mathrm{LT}_{23}T_1 + \mathrm{MT}_{12}T_2 + \mathrm{MT}_{22}T_2 + \mathrm{MT}_{23}T_2 \\
&+ \mathrm{MTS}_{12}T_3 + \mathrm{MTS}_{22}T_3 + \mathrm{MTS}_{23}T_3))
\end{aligned}$$

$$
\begin{aligned}
\mathrm{P3} = -\frac{1}{h}\Big(& h(\mathrm{LT}_{12} + \mathrm{LT}_{22} + \mathrm{LT}_{23})\mathrm{T}_0\mu \\
& + C_1 h\big(\mathrm{MC}_{11}\lambda^2 + \mathrm{MC}_{13}\lambda^2 + \mathrm{MC}_{22}\mu^2 + \mathrm{MC}_{23}\mu^2 \\
& + \mathrm{MC}_{12}(\lambda^2 + \mu^2)\big) \\
& + h\,T_1\big(\mathrm{MT}_{11}\lambda^2 + \mathrm{MT}_{13}\lambda^2 + \mathrm{MT}_{22}\mu^2 + \mathrm{MT}_{23}\mu^2 \\
& + \mathrm{MT}_{12}(\lambda^2 + \mu^2)\big) \\
& + C_2\big(\mathrm{NC}_{11}\lambda^2 + \mathrm{NC}_{13}\lambda^2 + \mathrm{NC}_{22}\mu^2 + \mathrm{NC}_{23}\mu^2 \\
& + \mathrm{NC}_{12}(\lambda^2 + \mu^2)\big) \\
& + C_3\big(\mathrm{NCS}_{11}\lambda^2 + \mathrm{NCS}_{13}\lambda^2 + \mathrm{NCS}_{22}\mu^2 + \mathrm{NCS}_{23}\mu^2 \\
& + \mathrm{NCS}_{12}(\lambda^2 + \mu^2)\big) \\
& + T_2\big(\mathrm{NT}_{11}\lambda^2 + \mathrm{NT}_{13}\lambda^2 + \mathrm{NT}_{22}\mu^2 + \mathrm{NT}_{23}\mu^2 \\
& + \mathrm{NT}_{12}(\lambda^2 + \mu^2)\big) \\
& + T_3\big(\mathrm{NTS}_{11}\lambda^2 + \mathrm{NTS}_{13}\lambda^2 + \mathrm{NTS}_{22}\mu^2 + \mathrm{NTS}_{23}\mu^2 \\
& + \mathrm{NTS}_{12}(\lambda^2 + \mu^2)\big)\Big)
\end{aligned}
$$

$$\begin{aligned}
\mathrm{P4} = -\frac{1}{h}\big(&C_3(\mathrm{ICSS}_{13} + \mathrm{ICSS}_{23} + \mathrm{ICSS}_{33} + \mathrm{HCS}_{11}K_1 + \mathrm{HCS}_{12}K_1 \\
&+ \mathrm{HCS}_{13}K_1 + \mathrm{HCS}_{12}K_2 + \mathrm{HCS}_{22}K_2 + \mathrm{HCS}_{23}K_2) \\
&+ C_1 h(\mathrm{ICS}_{13} + \mathrm{ICS}_{23} + \mathrm{ICS}_{33} + K_1\mathrm{MCS}_{11} + K_1\mathrm{MCS}_{12} \\
&+ K_2\mathrm{MCS}_{12} + K_1\mathrm{MCS}_{13} + K_2\mathrm{MCS}_{22} + K_2\mathrm{MCS}_{23}) \\
&+ C_2(\mathrm{ICBS}_{13} + \mathrm{ICBS}_{23} + \mathrm{ICBS}_{33} + K_1\mathrm{NCS}_{11} + K_1\mathrm{NCS}_{12} \\
&+ K_2\mathrm{NCS}_{12} + K_1\mathrm{NCS}_{13} + K_2\mathrm{NCS}_{22} + K_2\mathrm{NCS}_{23}) \\
&- h(\mathrm{ITS}_{13} + \mathrm{ITS}_{23} + \mathrm{ITS}_{33} + K_1\mathrm{MTS}_{11} + K_1\mathrm{MTS}_{12} \\
&+ K_2\mathrm{MTS}_{12} + K_1\mathrm{MTS}_{13} + K_2\mathrm{MTS}_{22} + K_2\mathrm{MTS}_{23})\mathrm{T}_0 \\
&+ h(\mathrm{ITS}_{13} + \mathrm{ITS}_{23} + \mathrm{ITS}_{33} + K_1\mathrm{MTS}_{11} + K_1\mathrm{MTS}_{12} \\
&+ K_2\mathrm{MTS}_{12} + K_1\mathrm{MTS}_{13} + K_2\mathrm{MTS}_{22} + K_2\mathrm{MTS}_{23})T_1 \\
&+ (\mathrm{ITBS}_{13} + \mathrm{ITBS}_{23} + \mathrm{ITBS}_{33} + K_1\mathrm{NTS}_{11} + K_1\mathrm{NTS}_{12} \\
&+ K_2\mathrm{NTS}_{12} + K_1\mathrm{NTS}_{13} + K_2\mathrm{NTS}_{22} + K_2\mathrm{NTS}_{23})T_2 \\
&+ (\mathrm{ITSS}_{13} + \mathrm{ITSS}_{23} + \mathrm{ITSS}_{33} + \mathrm{HTS}_{11}K_1 + \mathrm{HTS}_{12}K_1 \\
&+ \mathrm{HTS}_{13}K_1 + \mathrm{HTS}_{12}K_2 + \mathrm{HTS}_{22}K_2 + \mathrm{HTS}_{23}K_2)T_3\big)
\end{aligned}$$

where:

$$\begin{aligned}
&(LT_{ij}, \mathrm{MT}_{\mathrm{ij}}, MTS_{ij}, NT_{ij}, NTS_{ij}, HTS_{ij}) = \\
&\qquad \int_{-h/2}^{h/2} \alpha(z) Q_{ij}\big(1, z, f(z), z^2, zf(z), f(z)^2, g'(z)\big)\mathrm{dz}, (i,j) = \\
&(1,2,3) \\
&(LC, \mathrm{MC}_{\mathrm{ij}}, MCS_{ij}, NC_{ij}, NCS_{ij}, HCS_{ij}) = \\
&\qquad \int_{-h/2}^{h/2} \beta(z) Q_{ij}\big(1, z, f(z), z^2, zf(z), f(z)^2, g'(z)\big)\mathrm{dz}, (i,j) = \\
&(1,2,3)
\end{aligned} \tag{68}$$

$$(\mathrm{I}TS_{ij}, \mathrm{I}TBS_{ij}, \mathrm{I}TSS_{ij}) = \int_{-h/2}^{h/2} \alpha(z)Q_{ij}\big(g'(z), \mathrm{z}\, g'(z), \mathrm{f(z)}g'(z)\big)\mathrm{dz},$$

$$(i, j) = (1,2,3)$$

4.7 Numerical Results

To validate the accuracy of the current approach in evaluating the FGM rectangular plate that is resting on viscoelastic foundation and subjected to hygro-thermo-mechanical loading, numerical results are presented in this section and compared with the literature.

The FGM plate is composed of ceramic and metal which have the properties shown in table.

Table 6 Mechanical material properties of Titanium and Ceramic

Material	$\boldsymbol{E}$ **(GPa)**	$\boldsymbol{\nu}$	$\boldsymbol{\alpha(10^{-6}/^{o}C)}$	$\boldsymbol{\beta}$
Titanium, Ti-6A1-4V	66.2	0.33	10.3	0.33
Zirconia, $\boldsymbol{ZrO_2}$	117	0.33	7.11	0

The non-dimensional quantities are shown in equation (69).

$$\overline{\mathrm{w}} = \frac{10^2\mathrm{D}}{\mathrm{q_0 a^4}}\mathrm{w}\left(\frac{\mathrm{a}}{2}, \frac{\mathrm{b}}{2}, 0\right), \bar{\sigma}_x = \frac{1}{10^2 q_0}\sigma_x\left(\frac{a}{2}, \frac{b}{2}, \frac{h}{2}\right), \bar{\sigma}_z = \frac{1}{10^2 q_0}\sigma_z\left(\frac{a}{2}, \frac{b}{2}, \frac{h}{2}\right),$$

$$\bar{\tau}_{xy} = \frac{1}{10 q_0}\tau_{xy}\left(0,0,-\frac{h}{3}\right), \bar{\tau}_{xz} = \frac{1}{10 q_0}\tau_{xz}\left(0, \frac{b}{2}, 0\right) \tag{69}$$

$$k_w = \frac{a^4 k_w}{D}, k_{p1} = \frac{a^2 k_{p1}}{D}, k_{p2} = \frac{b^2 k_{p2}}{D}, C_t = \frac{\mathrm{c_t}\, D \times 10^3}{a^4}$$

where $D = \frac{E\,h^3}{12(1-v^2)}$

Table 7 Effects of hygrothermal parameters on the deflection and stresses of FG square plates resting on Winkler–Pasternak foundation ($a = 10h;\ k_w = k_p = 10;\ C = 0, q = 100$).

p	t2	t3	$\bar{\sigma}_z$				$\bar{\tau}_{xz}$			
			a=b		a=3b		a=b		a=3b	
			Zenkour and Radwan-2019	present	Zenkour and Radwan-2019	present	Zenkour and Radwan-2019	present	Zenkour and Radwan-2019	present
1	0	50	1.01346	1.01346	1.81455	1.27393	3.19249	4.17452	1.46289	1.70460
	50	0	1.28029	1.28029	1.27392	1.63318	5.41912	5.41912	2.17549	2.17549
	50	50	2.20977	2.20977	2.88224	2.88224	9.76666	9.76666	3.92284	3.92284
3	0	50	0.70539	0.70540	1.38628	0.93973	2.75433	3.62871	1.32158	1.54792
	50	0	0.90245	0.90245	0.93973	1.22039	4.72572	4.72572	1.98281	1.98281
	50	50	1.53504	1.53504	2.13802	2.13802	8.50262	8.50262	3.56974	3.56974
5	0	50	0.54497	0.54497	1.07195	0.73190	2.66117	3.51826	1.29122	1.51659
	50	0	0.68188	0.68188	0.73189	0.93579	4.58793	4.58793	1.94566	1.94566
	50	50	1.16882	1.16882	1.64981	1.64981	8.24905	8.24905	3.50058	3.50058
10	0	50	0.37277	0.37143	0.70768	0.49711	2.69288	3.57417	1.31289	1.53275
	50	0	0.43925	0.43925	0.49869	0.61024	4.66649	4.66650	1.96915	1.96915
	50	50	0.77286	0.77151	1.09656	1.09497	8.39349	8.38474	3.55701	3.54092

Table 7 validates the current model. The transverse stress of the plate shows excellent agreement for the square FGM plate and a good agreement for the rectangular plate. The transverse shear stress is of good agreement with literature for various temperature loadings and a wide range of the power-law index p. Table 8 shows the effect of variating the power-law index and the elastic foundation parameters. The vertical displacement tends to increase with increasing the material index while it is decreasing when applying the two elastic foundation models. The nonlinear loading effect is more important than the linear one both in terms of vertical displacement, and vertical shear stress. Table 9 shows a comparison for the transverse deflection and stress of square FGM plates with various power indices while varying the viscoelastic damping effect. It is noticed that deflection decrease with increasing the viscous damping parameter. Furthermore, when considering thinner plates of high width to thickness ratios, the deflection decreases considerably due to distributing the mechanical load over a wider plate area.

Table 8 Effects of the power-law index and thermal loads on the stresses of FG plates on an elastic foundation ($a = 10h;\ k_w = k_p = 10;\ C = 0, q = 100$).

p	k_w	k_p	Linear hygro-thermomechanical loading				Non-linear hygro-thermomechanical loading			
			$\bar{w}$		$\bar{\tau}_{yz}$		$\bar{w}$		$\bar{\tau}_{yz}$	
			Zenkour and Radwan-2019	present	Zenkour and Radwan-2019	present	Zenkour and Radwan-2019	present	Zenkour and Radwan-2019	present
2	0	0	7.24370	7.24370	7.70266	7.70266	12.55015	12.55015	13.90145	13.90145
	10	0	6.97934	6.97934	7.89873	7.89873	12.09186	12.09186	14.24136	14.24136
	10	10	4.02358	4.02358	10.09100	10.09105	6.96771	6.96771	18.04191	18.04191
4	0	0	7.39848	7.39848	7.14317	7.14317	12.79973	12.79973	12.88316	12.88316
	10	0	7.11490	7.11490	7.33152	7.33152	12.30881	12.30881	13.20922	13.20922
	10	10	4.01347	4.01347	9.39149	9.39149	6.93976	6.93976	16.77533	16.77533
6	0	0	7.51587	7.51587	7.06804	7.06804	12.99452	12.99452	12.74417	12.74417
	10	0	7.21971	7.21971	7.25927	7.25927	12.48214	12.48214	13.07500	13.07500
	10	10	4.02196	4.02196	9.32399	9.32400	6.94982	6.94982	16.64711	16.64711
8	0	0	7.61549	7.61550	7.10113	7.10113	13.16176	13.16175	12.80253	12.80253
	10	0	7.30936	7.30936	7.29741	7.29740	12.63232	12.63232	13.14198	13.14198
	10	10	4.03496	4.03496	9.39677	9.39677	6.96953	6.96953	16.77266	16.77266
10	0	0	7.69887	7.69887	7.14639	7.14639	13.32513	13.30269	12.79746	12.88409
	10	0	7.38459	7.38459	7.34745	7.34745	12.78089	12.75929	13.14563	13.23173
	10	10	4.04779	4.04780	9.48213	9.48213	7.00257	6.98995	16.84224	16.92261

Table 9 Comparison of the dimensionless stresses and displacements of a FG square plate for linear hygro-thermomechanical loading ($k_w = k_p = 10, t_2 = 100, C_2 = 20\%, t_1 = t_3 = C_1 = C3 = 0, q = 100$).

P	*Ct*	*a/h*=10		*a/h*=100	
		$\bar{w}$	$\bar{\tau}_{xz}$	$\bar{w}$	$\bar{\tau}_{xz}$
0	**ct=0**	3.5264	-1.5940	0.2018	1.4698
	ct=0.05	3.3796	-1.7305	0.1936	1.3900
	ct=0.1	3.2445	-1.8560	0.1862	1.3163
	ct=1	1.8870	-3.1177	0.1098	0.5646
3	**ct=0**	3.9018	-1.7499	0.2464	1.1858
	ct=0.05	3.7022	-1.8741	0.2342	1.1051
	ct=0.1	3.5220	-1.9862	0.2231	1.0319
	ct=1	1.8772	-3.0094	0.1206	0.3538
5	**ct=0**	3.9316	-1.7636	0.2504	1.1615
	ct=0.05	3.7270	-1.8864	0.2378	1.0808
	ct=0.1	3.5425	-1.9970	0.2264	1.0079
	ct=1	1.8736	-2.9981	0.1215	0.3373

Table 11 shows the effect of varying the hygrothermal loads from linear to nonlinear on the FGM square plate deflection and stresses. The table shows the comparison for a range of the power-law index while changing the foundation parameters. The viscoelastic model reflects less deflection on the plate than the elastic models.

Table 10 shows the importance of the nonlinear hygrothermal loads on the bending of the FGM plate. The viscoelastic model gives lower deflection for high damping coefficients. The same trend is noticed for stresses, where the transverse stress decline by elevating the viscous parameter of the viscoelastic foundation.

Table 10 Comparison of the dimensionless stresses and displacements of a FG square plate resting on viscoelastic foundation under nonlinear hygro-thermomechanical loading ($k_w = k_p = 10,, t_2 = t_3 = 100, C_2 = C3 = 2, t_1 = C_1 = 0, q = 100$).

p	*Ct*	*a/h*=10		*a/h*=100	
		$\bar{w}$	τ_{xz}	$\bar{w}$	τ_{xz}
0	**ct=0**	6.0442	-2.9800	0.2275	1.3283
	ct=0.05	5.7925	-3.2139	0.2183	1.2383
	ct=0.1	5.5610	-3.4290	0.2099	1.1552
	ct=1	3.2342	-5.5915	0.1238	0.3077
3	**ct=0**	6.6649	-3.2207	0.2748	1.0346
	ct=0.05	6.3239	-3.4329	0.2612	0.9445
	ct=0.1	6.0160	-3.6244	0.2489	0.8630
	ct=1	3.2065	-5.3721	0.1345	0.1066
5	**ct=0**	6.7105	-3.2399	0.2791	1.0095
	ct=0.05	6.3611	-3.4495	0.2650	0.9196
	ct=0.1	6.0463	-3.6383	0.2523	0.8384
	ct=1	3.1979	-5.3469	0.1354	0.0912

Table 11 Effects of hygro-thermal parameters on the deflection and stresses of FG square plates resting on viscoelastic foundation ($a = 10h, q = 100$).

p	k_w	k_p	ct	Linear hygro-thermal loading		Non-linear hygro-thermal loading	
				$\bar{w}$	τ_{xz}	$\bar{w}$	τ_{xz}
0	10	0	**ct=0**	5.3675	0.1170	9.1998	-0.0474
			ct=0.05	5.0346	-0.1924	8.6292	-0.5777
			ct=0.1	4.7406	-0.4657	8.1252	-1.0460
			ct=1	2.3111	-2.7234	3.9612	-4.9158
	10	10	**ct=0**	3.5264	-1.5940	6.0442	-2.9800
			ct=0.05	3.3796	-1.7305	5.7925	-3.2139
			ct=0.1	3.2445	-1.8560	5.5610	-3.4290
			ct=1	1.8870	-3.1177	3.2342	-5.5915
3	10	0	**ct=0**	6.7952	0.0499	11.6073	-0.1463
			ct=0.05	6.2118	-0.3130	10.6108	-0.7662
			ct=0.1	5.7207	-0.6185	9.7718	-1.2881
			ct=1	2.3608	-2.7085	4.0326	-4.8582
	10	10	**ct=0**	3.9018	-1.7499	6.6649	-3.2207
			ct=0.05	3.7022	-1.8741	6.3239	-3.4329
			ct=0.1	3.5220	-1.9862	6.0160	-3.6244
			ct=1	1.8772	-3.0094	3.2065	-5.3721
5	10	0	**ct=0**	6.9420	0.0421	11.8485	-0.1579
			ct=0.05	6.3283	-0.3260	10.8011	-0.7862
			ct=0.1	5.8143	-0.6343	9.9238	-1.3124
			ct=1	2.3616	-2.7054	4.0308	-4.8473
	10	10	**ct=0**	3.9316	-1.7636	6.7105	-3.2399
			ct=0.05	3.7270	-1.8864	6.3611	-3.4495
			ct=0.1	3.5425	-1.9970	6.0463	-3.6383
			ct=1	1.8736	-2.9981	3.1979	-5.3469
10	10	0	**ct=0**	7.1570	0.0545	12.1885	-0.1038
			ct=0.05	6.4974	-0.3297	11.0653	-0.7580
			ct=0.1	5.9492	-0.6490	10.1316	-1.3018
			ct=1	2.3618	-2.7384	4.0223	-4.8602
	10	10	**ct=0**	3.9728	-1.8002	6.7657	-3.2623
			ct=0.05	3.7609	-1.9236	6.4048	-3.4725
			ct=0.1	3.5704	-2.0345	6.0805	-3.6614
			ct=1	1.8678	-3.0262	3.1809	-5.3503

4.8 Acknowledgement

This work is supported by the deanship of graduate studies (DSR) at King Fahd university of Petroleum and Minerals through project No. DF181032. The Civil and Environment Engineering department support is also acknowledged.

Chapter 5

Conclusions and Recommendations

5.1 Conclusions

5.1.1 Two-Dimensional Theory

This work investigated the hygro-thermo-mechanical bending behavior of advanced functionally graded ceramic-metal plates resting on a three-parameter viscoelastic foundation using an integral 2D higher-order shear deformation theory. The analytical solution is obtained using the Navier method. The impact of temperature and moisture concentration is shown to be important. The influence of the viscoelastic foundation on the plate deflection and stresses is critical. The presence of the viscoelastic foundation reduces the central deflection substantially. The parametric investigation emphasized the influence of various factors on the FGM plate bending response. Elevating the value of the gradient index causes an increase in the central deflection and a decrease in the longitudinal and shear stresses of the FGM plate. Furthermore, when increasing the viscoelastic foundation damping value (C_t), the deflection and stresses of the FGM plate declined noticeably. This fact shows that plate design capacity is greatly influenced by considering the viscoelastic foundation effect.

FGM plates with nonlinear hygrothermal loads and a high viscoelastic damping coefficient have a similar deflection to FGM plates with linear hygro-thermal loads but a small viscoelastic damping effect. For all kinds of loadings, deflection decreases by increasing the viscous damping coefficient. Finally, this research's findings should help enhance the design efficiency of the advanced FGM plates by considering the influence of the viscoelastic foundation.

5.1.2 Quasi-3D Theory

The work also investigated the bending response of a FG plate resting on a viscoelastic foundation subjected to mechanical loading in a hygrothermal environment using a quasi-3D theory. The trigonometric quasi-3D theory considered the thickness stretching effect to give more accurate results that were in good agreement with the literature. The theory has only four unknowns by incorporating an integral term in the displacement field which greatly reduces the computational cost. The parametric study showed that the effect of the viscoelastic foundation on the plate behavior is important. Deflection decreases by increasing the viscoelastic damping coefficient for all loading conditions; hence the findings of this work shall contribute to the design efficiency of FGM plates.

5.2 Recommendations

This work investigated the static response of FGM plates under various loading conditions and simple boundary conditions. Future work could address the behavior in the dynamic aspects. Future work could also study the following:

- Extending the work to mixed boundary conditions.
- Studying the effect of porosity distribution on the static response of FGM plates.
- Extending the work to the static response of beams in hygrothermal environments.

- Extending the work to the behavior of nano FGM plates.

References

[1] Z. Zhong, L. Wu, and W. Chen, *Mechanics of functionally graded materials and structures*. 2012.

[2] A. W. Leissa, “The free vibration of rectangular plates,” *J. Sound Vib.*, vol. 31, no. 3, pp. 257–293, 1973, doi: 10.1016/S0022-460X(73)80371-2.

[3] R. D. Mindlin, “Influence of Rotatory Inertia and Shear on Flexural Motions of Isotropic, Elastic Plates,” *Collect. Pap. Raymond D. Mindlin Vol. I*, vol. 18, no. 1951, pp. 225–232, 1989, doi: 10.1007/978-1-4613-8865-4_29.

[4] J. N. Reddy, “A simple higher-order theory for laminated composite plates,” *J. Appl. Mech. Trans. ASME*, vol. 51, no. 4, pp. 745–752, 1984, doi: 10.1115/1.3167719.

[5] B. Mokhtar, T. Abedlouahed, A. B. El Abbas, and Megueni, “Buckling Analysis of Functionally Graded Plates with Simply Supported Edges,” 2009.

[6] E. Reissner, “On the theory of bending of elastic plates,” *J. Math. Phys.*, vol. 23, no. 1–4, pp. 184–191, 1944.

[7] S. A. Ambartsumian, “On the theory of bending plates,” *Izv Otd Tech Nauk AN SSSR*, vol. 5, no. 5, pp. 69–77, 1958.

[8] M. Levinson, “An accurate, simple theory of the statics and dynamics of elastic plates,” *Mech. Res. Commun.*, vol. 7, no. 6, pp. 343–350, 1980, doi: 10.1016/0093-

6413(80)90049-X.

[9] M. Touratier, “An efficient standard plate theory,” *Int. J. Eng. Sci.*, vol. 29, no. 8, pp. 901–916, 1991, doi: 10.1016/0020-7225(91)90165-Y.

[10] K. P. Soldatos, “A transverse shear deformation theory for homogeneous monoclinic plates,” *Acta Mech.*, vol. 94, no. 3–4, pp. 195–220, 1992.

[11] J. N. Reddy and J.N. Reddy, *Mechanics of laminated composite plates and shells: theory and analysis*. CRC press, 2003.

[12] M. Karama, K. S. Afaq, and S. Mistou, “Mechanical behaviour of laminated composite beam by the new multi-layered laminated composite structures model with transverse shear stress continuity,” *Int. J. Solids Struct.*, vol. 40, no. 6, pp. 1525–1546, 2003.

[13] S. H. Chi and Y. L. Chung, “Mechanical behavior of functionally graded material plates under transverse load-Part I: Analysis,” *Int. J. Solids Struct.*, vol. 43, no. 13, pp. 3657–3674, 2006, doi: 10.1016/j.ijsolstr.2005.04.011.

[14] E. Winkler, *Die Lehre von der Elasticität und Festigkeit mit besonderer Rücksicht auf ihre Anwendung in der Technik*. 1867.

[15] J. K. Lee and S. Jeong, “Flexural and torsional free vibrations of horizontally curved beams on Pasternak foundations,” *Appl. Math. Model.*, vol. 40, no. 3, pp. 2242–2256, 2016, doi: 10.1016/j.apm.2015.09.024.

[16] A. D. Kerr, “Elastic and viscoelastic foundation models,” 1964.

[17] B. Saleh *et al.*, “30 Years of functionally graded materials : An overview of manufacturing methods , Applications and Future Challenges,” *Compos. Part B*, vol. 201, no. January, p. 108376, 2020, doi: 10.1016/j.compositesb.2020.108376.

[18] A. Edwin, V. Anand, and K. Prasanna, “SUSTAINABLE DEVELOPMENT THROUGH FUNCTIONALLY GRADED MATERIALS: AN OVERVIEW,” *Rasayan J. Chem*, vol. 10, no. 1, pp. 149–152, doi: 10.7324/RJC.2017.1011578.

[19] V. N. Van Do and C. H. Lee, “Nonlinear analyses of FGM plates in bending by using a modified radial point interpolation mesh-free method,” *Appl. Math. Model.*, vol. 57, pp. 1–20, 2018, doi: 10.1016/j.apm.2017.12.035.

[20] E. K. Njim, M. Al-Waily, and S. H. Bakhy, “A Critical Review of Recent Research of Free Vibration and Stability of Functionally Graded Materials of Sandwich Plate,” *IOP Conf. Ser. Mater. Sci. Eng.*, vol. 1094, no. 1, p. 012081, 2021, doi: 10.1088/1757-899x/1094/1/012081.

[21] A. Ali and A. Andriyana, “Properties of multifunctional composite materials based on nanomaterials: a review,” *RSC Adv.*, vol. 10, no. 28, pp. 16390–16403, 2020, doi: 10.1039/c9ra10594h.

[22] S. Zghal, S. Trabelsi, and F. Dammak, “Post-buckling behavior of functionally graded and carbon-nanotubes based structures with different mechanical loadings,” *Mech. Based Des. Struct. Mach.*, vol. 0, no. 0, pp. 1–43, 2020, doi:

10.1080/15397734.2020.1790387.

[23] Y. Ousset and F. Roudolff, “Numerical analysis of delamination in multilayered composite plates,” *Comput. Mech.*, vol. 20, no. 1–2, pp. 122–126, 1997, doi: 10.1007/s004660050227.

[24] M. Koizumi, “FGM activities in Japan,” *Compos. Part B Eng.*, vol. 28, no. 1–2, pp. 1–4, 1997.

[25] S. P. Sintering, A. Oxide, T. Stress, M. Property, and Y. Shinohara, “Functionally Grade Composite Materi- al Production,” 2014.

[26] S. Zghal, D. Ataoui, and F. Dammak, “Static bending analysis of beams made of functionally graded porous materials,” *Mech. Based Des. Struct. Mach.*, vol. 0, no. 0, pp. 1–18, 2020, doi: 10.1080/15397734.2020.1748053.

[27] A. R. E.-D. M. S. EL-Wazery, “A review on Functionally Graded Ceramic-Metal Materials A review on Functionally Graded Ceramic-Metal Materials,” no. January 2015, 2019.

[28] A. Gupta and M. Talha, “Recent development in modeling and analysis of functionally graded materials and structures,” *Prog. Aerosp. Sci.*, vol. 79, pp. 1–14, 2015, doi: 10.1016/j.paerosci.2015.07.001.

[29] D. K. Jha, T. Kant, and R. K. Singh, “A critical review of recent research on functionally graded plates,” *Compos. Struct.*, vol. 96, pp. 833–849, 2013, doi: 10.1016/j.compstruct.2012.09.001.

[30] S. Zghal, A. Frikha, and F. Dammak, “Mechanical buckling analysis of functionally graded power-based and carbon nanotubes-reinforced composite plates and curved panels,” *Compos. Part B Eng.*, vol. 150, no. June, pp. 165–183, 2018, doi: 10.1016/j.compositesb.2018.05.037.

[31] H. Mellouli, H. Jrad, M. Wali, and F. Dammak, “Meshless implementation of arbitrary 3D-shell structures based on a modified first order shear deformation theory,” *Comput. Math. with Appl.*, vol. 77, no. 1, pp. 34–49, 2019, doi: 10.1016/j.camwa.2018.09.010.

[32] S. Trabelsi, A. Frikha, S. Zghal, and F. Dammak, “Thermal post-buckling analysis of functionally graded material structures using a modified FSDT,” *Int. J. Mech. Sci.*, vol. 144, no. May, pp. 74–89, 2018, doi: 10.1016/j.ijmecsci.2018.05.033.

[33] P. L. Pasternak, “On a new method of an elastic foundation by means of two foundation constants,” *Gos. Izd. Lit. po Stroit. i Arkhitekture*, 1954.

[34] A. M. Zenkour, “A comprehensive analysis of functionally graded sandwich plates: Part 1-Deflection and stresses,” *Int. J. Solids Struct.*, vol. 42, no. 18–19, pp. 5224–5242, 2005, doi: 10.1016/j.ijsolstr.2005.02.015.

[35] S. Zghal, A. Frikha, and F. Dammak, “Static analysis of functionally graded carbon nanotube-reinforced plate and shell structures,” *Compos. Struct.*, vol. 176, pp. 1107–1123, 2017, doi: 10.1016/j.compstruct.2017.06.015.

[36] A. M. Zenkour, “Generalized shear deformation theory for bending analysis of

functionally graded plates," *Appl. Math. Model.*, vol. 30, no. 1, pp. 67–84, 2006, doi: 10.1016/j.apm.2005.03.009.

[37] M. Li, C. Guedes Soares, and R. Yan, "A novel shear deformation theory for static analysis of functionally graded plates," *Compos. Struct.*, vol. 250, p. 112559, 2020, doi: 10.1016/j.compstruct.2020.112559.

[38] T. M. Tu, T. H. Quoc, and N. Van Long, "Bending analysis of functionally graded plates using new eight-unknown higher order shear deformation theory," *Struct. Eng. Mech.*, vol. 62, no. 3, pp. 311–324, 2017, doi: 10.12989/sem.2017.62.3.311.

[39] T. M. Tu, T. H. Quoc, and N. Van Long, "Vibration analysis of functionally graded plates using the eight-unknown higher order shear deformation theory in thermal environments," *Aerosp. Sci. Technol.*, vol. 84, pp. 698–711, 2019, doi: 10.1016/j.ast.2018.11.010.

[40] J. M. Whitney and C. T. Sun, "A higher order theory for extensional motion of laminated composites," *J. Sound Vib.*, vol. 30, no. 1, pp. 85–97, 1973, doi: 10.1016/S0022-460X(73)80052-5.

[41] C. M. Wang, J. N. Reddy, and K. H. Lee, "Theories of Plate Bending," *Shear Deform. Beams Plates*, pp. 89–109, 2000, doi: 10.1016/b978-008043784-2/50006-x.

[42] T. H. Daouadji, B. Adim, and R. Benferhat, "Bending analysis of an imperfect FGM plates under hygro-thermo-mechanical loading with analytical validation,"

Adv. Mater. Res., vol. 5, no. 1, pp. 35–53, 2016, doi: 10.12989/amr.2016.5.1.035.

[43] A. S. Sayyad and Y. M. Ghugal, “Effects of nonlinear hygrothermomechanical loading on bending of FGM rectangular plates resting on two-parameter elastic foundation using four-unknown plate theory,” *J. Therm. Stress.*, vol. 42, no. 2, pp. 213–232, 2019.

[44] S. Zghal, A. Frikha, and F. Dammak, “Free vibration analysis of carbon nanotube-reinforced functionally graded composite shell structures,” *Appl. Math. Model.*, vol. 53, pp. 132–155, 2018, doi: 10.1016/j.apm.2017.08.021.

[45] S. Zghal, S. Trabelsi, A. Frikha, and F. Dammak, “Thermal free vibration analysis of functionally graded plates and panels with an improved finite shell element,” *J. Therm. Stress.*, vol. 44, no. 3, pp. 315–341, 2021, doi: 10.1080/01495739.2021.1871577.

[46] A. S. Sayyad and Y. M. Ghugal, *A Unified Shear Deformation Theory for the Bending of Isotropic, Functionally Graded, Laminated and Sandwich Beams and Plates*, vol. 9, no. 1. 2017.

[47] S. Zghal, A. Frikha, and F. Dammak, “Non-linear bending analysis of nanocomposites reinforced by graphene-nanotubes with finite shell element and membrane enhancement,” *Eng. Struct.*, vol. 158, no. April 2017, pp. 95–109, 2018, doi: 10.1016/j.engstruct.2017.12.017.

[48] B. Bouderba, “Bending of FGM rectangular plates resting on non-uniform elastic

foundations in thermal environment using an accurate theory," *Steel Compos. Struct.*, vol. 27, no. 3, pp. 311–325, 2018.

[49] N. Van Long, T. H. Quoc, and T. M. Tu, "Bending and free vibration analysis of functionally graded plates using new eight-unknown shear deformation theory by finite-element method," *Int. J. Adv. Struct. Eng.*, vol. 8, no. 4, pp. 391–399, 2016, doi: 10.1007/s40091-016-0140-y.

[50] J. H. Kim and G. H. Paulino, "Mixed-mode fracture of orthotropic functionally graded materials using finite elements and the modified crack closure method," *Eng. Fract. Mech.*, vol. 69, no. 14–16, pp. 1557–1586, 2002, doi: 10.1016/S0013-7944(02)00057-7.

[51] H. Hellal *et al.*, "Dynamic and stability analysis of functionally graded material sandwich plates in hygro-thermal environment using a simple higher shear deformation theory," *J. Sandw. Struct. Mater.*, 2019, doi: 10.1177/1099636219845841.

[52] A. M. A. Neves, A. J. M. Ferreira, E. Carrera, M. Cinefra, R. M. N. Jorge, and C. M. M. Soares, "Buckling analysis of sandwich plates with functionally graded skins using a new quasi-3D hyperbolic sine shear deformation theory and collocation with radial basis functions," *ZAMM Zeitschrift fur Angew. Math. und Mech.*, vol. 92, no. 9, pp. 749–766, 2012, doi: 10.1002/zamm.201100186.

[53] S. Trabelsi, S. Zghal, and F. Dammak, "Thermo-elastic buckling and post-buckling

analysis of functionally graded thin plate and shell structures," *J. Brazilian Soc. Mech. Sci. Eng.*, vol. 42, no. 5, pp. 1–22, 2020, doi: 10.1007/s40430-020-02314-5.

[54] A. Melaibari, R. M. Abo-bakr, S. A. Mohamed, and M. A. Eltaher, "Static stability of higher order functionally graded beam under variable axial load," *Alexandria Eng. J.*, vol. 59, no. 3, pp. 1661–1675, 2020, doi: 10.1016/j.aej.2020.04.012.

[55] M. Guellil *et al.*, "Influences of porosity distributions and boundary conditions on mechanical bending response of functionally graded plates resting on Pasternak foundation," *Steel Compos. Struct.*, vol. 38, no. 1, pp. 1–15, 2021.

[56] T. T. Tran, V. K. Tran, Q. H. Pham, and A. M. Zenkour, "Extended four-unknown higher-order shear deformation nonlocal theory for bending, buckling and free vibration of functionally graded porous nanoshell resting on elastic foundation," *Compos. Struct.*, vol. 264, no. December 2020, p. 113737, 2021, doi: 10.1016/j.compstruct.2021.113737.

[57] A. A. Daikh, M. S. A. Houari, and M. A. Eltaher, "A novel nonlocal strain gradient Quasi-3D bending analysis of sigmoid functionally graded sandwich nanoplates," *Compos. Struct.*, vol. 262, no. September 2020, p. 113347, 2021, doi: 10.1016/j.compstruct.2020.113347.

[58] S. K. Sah and A. Ghosh, "Free vibration and buckling analysis of FGM plates using inverse trigonometric shear deformation theory," *Aircr. Eng. Aerosp. Technol.*, vol. ahead-of-p, no. ahead-of-print, pp. 298–310, 2021, doi:

10.1108/aeat-01-2020-0001.

[59] S. Zghal, A. Frikha, and F. Dammak, “Large deflection response-based geometrical nonlinearity of nanocomposite structures reinforced with carbon nanotubes,” *Appl. Math. Mech. (English Ed.*, vol. 41, no. 8, pp. 1227–1250, 2020, doi: 10.1007/s10483-020-2633-9.

[60] F. El-Haina, A. Bakora, A. A. Bousahla, A. Tounsi, and S. R. Mahmoud, “A simple analytical approach for thermal buckling of thick functionally graded sandwich plates,” *Struct. Eng. Mech. An Int. J.*, vol. 63, no. 5, pp. 585–595, 2017.

[61] A. S. Sayyad and Y. M. Ghugal, “Effects of nonlinear hygrothermomechanical loading on bending of FGM rectangular plates resting on two-parameter elastic foundation using four-unknown plate theory,” *J. Therm. Stress.*, vol. 42, no. 2, pp. 213–232, 2019, doi: 10.1080/01495739.2018.1469962.

[62] R. G. Reid and R. Paskaramoorthy, “Analysis of functionally graded plates,” *Int. SAMPE Tech. Conf.*, vol. 684, no. June 1999, pp. 663–684, 2010.

[63] M. Zidi, A. Tounsi, M. S. A. Houari, E. A. Adda Bedia, and O. Anwar Bég, “Bending analysis of FGM plates under hygro-thermo-mechanical loading using a four variable refined plate theory,” *Aerosp. Sci. Technol.*, vol. 34, no. 1, pp. 24–34, 2014, doi: 10.1016/j.ast.2014.02.001.

[64] S. I. Tahir, A. Tounsi, A. Chikh, M. A. Al-Osta, S. U. Al-Dulaijan, and M. M. Al-Zahrani, “An integral four-variable hyperbolic HSDT for the wave propagation

investigation of a ceramic-metal FGM plate with various porosity distributions resting on a viscoelastic foundation," *Waves in Random and Complex Media*, 2021, doi: 10.1080/17455030.2021.1942310.

[65] Z. Zhang, X. Liu, and R. Mohammadi, "Impacts of the hygro - thermo conditions on the vibration analysis of 2D - FG nanoplates based on a novel HSDT," *Eng. Comput.*, no. 0123456789, 2021, doi: 10.1007/s00366-021-01443-2.

[66] A. S. Sayyad and S. M. Ghumare, "Thermomechanical Bending Analysis of FG Sandwich Plates Using a Quasi-Three-Dimensional Theory," vol. 34, no. 3, 2021, doi: 10.1061/(ASCE)AS.1943-5525.0001249.

[67] A. Belarouci and A. Fekrar, "A new quasi-3D theory for the study of the bending of thick FGM's plates on elastic foundation," *Smart Struct. Syst.*, vol. 27, no. 5, p. 847, 2021.

[68] A. M. Zenkour, M. H. Aljadani, A. M. Zenkour, and M. H. Aljadani, "Уточненная квазитрехмерная теория функционально - градиентных пористых пластин : исследование колебаний Quasi-3D refined theory for functionally graded porous plates :," vol. 2, pp. 56–70, 2021, doi: 10.24412/1683-805X-2021-2-56-70.

[69] J. N. Reddy, "Analysis of functionally graded plates," *Int. J. Numer. Methods Eng.*, vol. 47, no. 1-3, pp. 663–684, 2000.

[70] S. S. Akavci and A. H. Tanrikulu, "Static and free vibration analysis of

functionally graded plates based on a new quasi-3D and 2D shear deformation theories," *Compos. Part B Eng.*, vol. 83, pp. 203–215, Dec. 2015, doi: 10.1016/j.compositesb.2015.08.043.

[71] S. M. Hasheminejad and B. Gheshlaghi, "Three-dimensional elastodynamic solution for an arbitrary thick FGM rectangular plate resting on a two parameter viscoelastic foundation," *Compos. Struct.*, vol. 94, no. 9, pp. 2746–2755, Sep. 2012, doi: 10.1016/j.compstruct.2012.04.010.

[72] M. Naghavi, *Bending analysis of functionally graded sandwich plates using the refined finite strip method*. 2021.

[73] A. Hassan, A. Hassan, and N. Kurgan, "Engineering Science and Technology , an International Journal Bending analysis of thin FGM skew plate resting on Winkler elastic foundation using multi-term extended Kantorovich method," *Eng. Sci. Technol. an Int. J.*, vol. 23, no. 4, pp. 788–800, 2020, doi: 10.1016/j.jestch.2020.03.009.

[74] I. Mechab, H. A. Atmane, A. Tounsi, H. A. Belhadj, and E. A. A. Bedia, "A two variable refined plate theory for the bending analysis of functionally graded plates," *Acta Mech. Sin. Xuebao*, vol. 26, no. 6, pp. 941–949, 2010, doi: 10.1007/s10409-010-0372-1.

[75] S. Sahraee, "Bending analysis of functionally graded sectorial plates using Levinson plate theory," *Compos. Struct.*, vol. 88, no. 4, pp. 548–557, 2009, doi:

10.1016/j.compstruct.2008.05.014.

[76] M. S. Ahmed Houari, S. Benyoucef, I. Mechab, A. Tounsi, and E. A. Adda Bedia, “Two-variable refined plate theory for thermoelastic bending analysis of functionally graded sandwich plates,” *J. Therm. Stress.*, vol. 34, no. 4, pp. 315–334, 2011, doi: 10.1080/01495739.2010.550806.

[77] P. V Joshi, N. K. Jain, and G. D. Ramtekkar, “Thin-Walled Structures Effect of thermal environment on free vibration of cracked rectangular plate : An analytical approach,” *Thin Walled Struct.*, vol. 91, pp. 38–49, 2015, doi: 10.1016/j.tws.2015.02.004.

[78] H. Matsunaga, “Stress analysis of functionally graded plates subjected to thermal and mechanical loadings,” *Compos. Struct.*, vol. 87, no. 4, pp. 344–357, Feb. 2009, doi: 10.1016/j.compstruct.2008.02.002.

[79] B. Hadj, B. Rabia, and T. H. Daouadji, “Vibration analysis of porous FGM plate resting on elastic foundations: Effect of the distribution shape of porosity,” *Coupled Syst. Mech.*, vol. 10, no. 1, pp. 61–77, 2021.

[80] S. I. Tahir, A. Chikh, A. Tounsi, M. A. Al-Osta, S. U. Al-Dulaijan, and M. M. Al-Zahrani, “Wave propagation analysis of a ceramic-metal functionally graded sandwich plate with different porosity distributions in a hygro-thermal environment,” *Compos. Struct.*, vol. 269, no. May, p. 114030, 2021, doi: 10.1016/j.compstruct.2021.114030.

[81] A. Chikh, A. Tounsi, H. Hebali, and S. R. Mahmoud, “Thermal buckling analysis of cross-ply laminated plates using a simplified HSDT,” *Smart Struct. Syst.*, vol. 19, no. 3, pp. 289–297, 2017.

Vitae

Name	Ismail Mohammed Mudhaffar
Nationality	Yemen
Date of Birth	July 10, 1993
Email	ismailmmudhafar@gmail.com
Address	TV Street, Sana'a, Yemen. Zip code: 37970
Nationality	Yemen
Academic Background	B.Sc. Civil and Environmental Engineering, (2013-2018) KFUPM, Dhahran, Saudi Arabi M.S. Civil and Environmental Engineering, (2019-2021) KFUPM, Dhahran, Saudi Arabi
Published Papers	Ismail M. Mudhaffar, Abdelouahed Tounsi, Abdelbaki Chikh, Mohammed A. Al-Osta, Mesfer M. Al-Zahrani and Salah U. Al-Dulaijan, 2021. Hygro-Thermo-Mechanical Bending Behavior of Advanced Functionally Graded Ceramic Metal Plates Resting on a Viscoelastic Foundation
KFUPM Activities	CE-Club president of the scientific committee (2016) CE-Club president of the visiting committee (2017) Participants of several KFUP voluntary days
Courses Grading	Chemistry department for one semester Civil Engineering department for eight semesters Math department for two semesters
Software Skills	Mathematica STAAD Pro AutoCAD MS Office